

# Direct laser writing and structuring of functional polymers for electro-optical switches

**Citation for published version (APA):**

Versteeg, D. J. (2002). *Direct laser writing and structuring of functional polymers for electro-optical switches*. [Phd Thesis 1 (Research TU/e / Graduation TU/e), Chemical Engineering and Chemistry]. Technische Universiteit Eindhoven. <https://doi.org/10.6100/IR558148>

**DOI:**

[10.6100/IR558148](https://doi.org/10.6100/IR558148)

**Document status and date:**

Published: 01/01/2002

**Document Version:**

Publisher's PDF, also known as Version of Record (includes final page, issue and volume numbers)

**Please check the document version of this publication:**

- A submitted manuscript is the version of the article upon submission and before peer-review. There can be important differences between the submitted version and the official published version of record. People interested in the research are advised to contact the author for the final version of the publication, or visit the DOI to the publisher's website.
- The final author version and the galley proof are versions of the publication after peer review.
- The final published version features the final layout of the paper including the volume, issue and page numbers.

[Link to publication](#)

**General rights**

Copyright and moral rights for the publications made accessible in the public portal are retained by the authors and/or other copyright owners and it is a condition of accessing publications that users recognise and abide by the legal requirements associated with these rights.

- Users may download and print one copy of any publication from the public portal for the purpose of private study or research.
- You may not further distribute the material or use it for any profit-making activity or commercial gain
- You may freely distribute the URL identifying the publication in the public portal.

If the publication is distributed under the terms of Article 25fa of the Dutch Copyright Act, indicated by the "Taverne" license above, please follow below link for the End User Agreement:

[www.tue.nl/taverne](http://www.tue.nl/taverne)

**Take down policy**

If you believe that this document breaches copyright please contact us at:

[openaccess@tue.nl](mailto:openaccess@tue.nl)

providing details and we will investigate your claim.

**Direct Laser Writing and Structuring  
of Functional Polymers  
for Electro-Optical Switches**

Dit proefschrift is goedgekeurd door de promotoren:

prof.dr.ing. D.J. Broer

en

prof.dr. P.J. Lemstra

Copromotor:

dr.ing. C.W.M. Bastiaansen

The research presented in this thesis was financially supported by the Dutch Polymer Institute (DPI)

## **CIP-DATA LIBRARY TECHNISCHE UNIVERSITEIT EINDHOVEN**

Versteeg, Dennis J.

Direct laser writing and structuring of functional polymers for electro-optical switches / by Dennis J. Versteeg.  
– Eindhoven : Technische Universiteit Eindhoven, 2002.

Proefschrift. – ISBN 90-386-2604-5

NUR 971

Trefwoorden: vloeibaar-kristaldisplays ; oriëntatielaag / polyimide / LPP / laserschrijven / micro-patronering / vloeibaar-kristaluitlijning / foto-oriëntatie / optische eigenschappen / micro-elektronica / goud nanodeeltjes

Subject heading : liquid crystal displays ; orientation layer / polyimide / LPP / laser writing / micro-patterning / liquid crystal alignment / photo alignment / optical properties / micro-electronics / gold nanoparticles

An electronic copy of this thesis is available from the site of the Eindhoven University of Technology in PDF-format (<http://www.tue.nl/bib>).

© 2002, D.J. Versteeg

Cover painting © 2002, H. Hofstede

Cover design by J. Luiten and D.J. Versteeg

Cover credit:

The cover of this thesis is based on a painting by Henk Hofstede from Amsterdam, especially created for this thesis. Henk Hofstede is best known for being the singer and songwriter of Dutch pop band 'Nits', but he is also a respected artist, whose paintings and sculptures have been featured in several international exhibits.

Printed by: University Press Facilities, Eindhoven, the Netherlands.

# Direct Laser Writing and Structuring of Functional Polymers for Electro-Optical Switches

PROEFSCHRIFT

ter verkrijging van de graad van doctor aan de  
Technische Universiteit Eindhoven, op gezag van de  
Rector Magnificus, prof.dr. R.A. van Santen, voor een  
commissie aangewezen door het College voor  
Promoties in het openbaar te verdedigen  
op dinsdag 12 november 2002 om 14.00 uur

door

Dennis John Versteeg

geboren te Nunspeet



# Table of Contents

Summary .....	7
---------------	---

Samenvatting.....	11
-------------------	----

## Chapter 1 - Introduction

1.1 Nano- and microstructuring of polymers with replication techniques .....	15
1.2 Direct writing techniques for the patterning and structuring of polymers.....	16
1.3 Micro-patterning in anisotropic functional polymers .....	17
1.4 Objective and scope of the thesis .....	17
1.5 References .....	19

## Chapter 2 - Laser Writing Regimes in Polyimides

2.1 Introduction .....	21
2.2 Experimental.....	22
2.2.1 Materials.....	22
2.2.2 Direct focused laser writing.....	23
2.2.3 Characterisation .....	23
2.3 Results and discussion .....	23
2.3.1 Absorption of polyimide.....	23
2.3.2 The heating and melting regimes .....	24
2.3.3 The pyrolysis and ablation regimes.....	29
2.4 Conclusions.....	38
2.5 References .....	39

## Chapter 3 - Laser Melting of Rubbed Polyimide Orientation Layers

3.1 Introduction .....	41
3.2. Liquid crystal alignment .....	42
3.3 Experimental.....	47
3.3.1 Materials.....	47
3.3.2 Direct focused laser writing.....	47
3.3.3 Cell design .....	48
3.3.4 Characterisation.....	48
3.4 Results and discussion .....	48
3.4.1. Cell design .....	48

3.4.2 Liquid crystal orientation at laser-written surface patterns in non-rubbed polyimide ..	49
3.4.3 Liquid crystal orientation at laser-written surface patterns in rubbed polyimide.	50
3.4.4 Transmittance measurements .....	56
3.5 Conclusions .....	57
3.6 References .....	57

## **Chapter 4 - Laser-written Polyimides in Electro-Optical Switches**

4.1 Introduction .....	61
4.2 Electro-optical switches .....	62
4.2.1 Twisted nematic liquid crystal displays .....	62
4.2.2 Personalised security features .....	66
4.2.3 Cholesteric texture liquid crystal displays .....	67
4.3 Experimental.....	70
4.3.1 Direct focused laser writing .....	70
4.3.2 Materials.....	70
4.3.3 Cell design .....	71
4.3.4 Characterisation .....	71
4.4 Results and discussion .....	72
4.4.1 Twisted nematic liquid crystal displays .....	72
4.4.2 Personalised security features .....	76
4.4.3 Cholesteric texture liquid crystal displays .....	77
4.5 Conclusions .....	79
4.6 References .....	80

## **Chapter 5 - Laser Patterning in Linearly Photo-Polarisable Polymers**

5.1 Introduction .....	83
5.2. Linearly photo-polarisable polymers .....	84
5.3 Experimental.....	86
5.3.1 Direct focused laser writing and interferometry .....	86
5.3.2 Materials.....	86
5.3.3 Cell design and characterisation .....	87
5.4 Results .....	87
5.4.1 LPP materials and UV sensitivity.....	87
5.4.2 Masked illumination.....	89
5.4.3 Direct focused laser writing.....	91
5.4.4 Complex patterns by multiple scanning directions .....	93
5.4.5 Interferometry.....	95
5.5 Conclusions .....	97
5.6 References .....	98

## Chapter 6 - Laser Writing of Conductive Patterns Using Gold Nanoparticles

6.1 Introduction .....	99
6.2 Experimental.....	101
6.2.1 Materials.....	101
6.2.2 Synthesis .....	101
6.2.3 Coating.....	102
6.2.4 Direct focused laser writing.....	103
6.2.5 Development of conductive structures.....	103
6.2.6 Characterisation.....	104
6.3 Results.....	104
6.3.1 Synthesis and analysis of alkanethiol stabilised gold nanoparticles.....	104
6.3.2 Gold nanoparticle coatings .....	108
6.3.3 Thermal decomposition .....	109
6.3.4 Direct focused laser writing.....	110
6.3.5 Electrical conductivity .....	115
6.4 Discussion .....	116
6.5 Conclusions.....	116
6.6 References .....	117
<b>Technology Assessment.....</b>	<b>119</b>
<b>Appendix - Laser Patterning</b>	
A.1 Laser principles.....	123
A.2 Direct focused laser writing.....	124
A.3 Interferometry and holography.....	126
A.4 References .....	130
<b>Dankwoord.....</b>	<b>131</b>
<b>Curriculum Vitae.....</b>	<b>133</b>

## Summary

Nano- and micro-structuring of functional polymeric layers, using direct writing or replication techniques, has become an indispensable tool for designing novel and improved components and devices in the information and communication technology. Data generation, data transport, data storage, data processing and data display increasingly depend on nano- and micro-patterns in polymers and numerous techniques are available to produce these, often complex, patterns with the required resolution.

Typically, patterns are generated through replication techniques. Thereto, first a master is produced using techniques such as photo-, e-beam or ion-beam lithography, depending on the resolution and geometry of the pattern. The patterned master is then replicated into metallic copies, which are used to pattern polymeric substrates or films using techniques such as embossing, moulding or casting. This manner of patterning involves many steps and intermediate materials and often there is a need for extensive etching or other post-processing techniques. Direct writing of the patterns in polymeric substrates or films circumvents these steps. In the past, the disadvantages of direct writing, such as its relatively slow speed, were overcome and these techniques are increasingly used to produce unique structures, which are unavailable through any other technique. Direct patterning with lasers, with techniques such as direct focused laser writing and holography, are especially promising. A wide range of (photo-)chemical and physical (thermal) processes can be induced in polymers with a large freedom in design and nature of the patterns.

Usually, the polymer in which the pattern is written is only a carrier material with no additional functionality. However, recently new patterning techniques were developed for functional polymers in which several (electro-)optical functionalities originating from both the substrate and the written pattern are combined. Typical examples are the patterning of photosensitive alignment layers for liquid crystal displays and the solid state embossing of structured functional polymers for optical applications.

In this thesis, we used lasers to directly write micro-patterns in functional polymers to generate novel, unique patterns with special electrical or optical properties. More specifically, the wide range of possibilities that laser patterning offers with respect to chemical or physical processes is combined with anisotropic functional polymers. A large variety of novel patterns are formed, which can be used in applications such as flat panel displays.

Specifically, this thesis focuses on the direct laser patterning of liquid crystal orientation layers. We showed that several chemical and thermal processing regimes, such as melting, pyrolysis and ablation could be used to pattern polyimides. At low laser intensities, a fast, local melting of the substrate occurs during direct laser writing, which, after re-solidification, induces relief structures with a typical height of 50 to 200 nm. At intermediate laser intensities, pyrolysis occurs, which results in local carbonisation and graphitisation of the material. At high laser intensities, ablation starts to occur, resulting in relief structures with a typical width and height of several micrometers.

Subsequently, we investigated the alignment of liquid crystals (LC's) above the laser-written patterns in previously rubbed polyimide. Rubbed polyimide is known to align liquid crystals by a combination anisotropic dispersive interaction of the LC molecules with the oriented polyimide chains at the interface and by the induced nanogrooves. Local melting of the polyimide both removes the chain orientation by relaxation and the nanogrooves by surface tension effects. Therefore the alignment characteristics of these films is destroyed at the position of the molten laser-written lines. We constructed electro-optical cells using two rubbed polyimide alignment layers placed perpendicular to each other and in which one alignment layer was laser-written with a pre-designed pattern. After filling with a liquid crystal, high contrast, hybrid optical cells were obtained, consisting of uniaxially aligned regions in a twisted nematic environment. The liquid crystals align themselves in the direction imposed by the orientation layer of the opposite substrate. We also showed that the writing of patterns in alignment layers is potentially useful to add icons to the displays or, more importantly, in the manufacturing of novel security features with combinations of security levels or even personalised security items. These optical cells were adapted for use in electro-optical switches, such as liquid crystal displays (LCD's) and personalised security features.

Linearly photo-polarisable polymers (LPP) are a class of polymeric materials that obtain their aligning properties through linearly polarised UV irradiation. By performing direct focused laser writing and interferometry in the sub-melting regime with polarised UV light, we locally induced purely photochemical changes in LPP materials. This resulted in local changes in the LC aligning direction of the LPP material. These patterned orientation layers were used to construct high-resolution hybrid optical cells with alternating twisted and uniaxial liquid crystal orientations, similar to the hybrid cells with laser-melted polyimide layers. With direct focused laser writing, patterns of any design can be written with a minimum resolution of several microns. Smaller resolutions were obtained using interferometry.

Electrically conductive patterns (with a conductivity of  $0.1 - 10 \Omega^{-1}\text{cm}^{-1}$ ) were written in polyimide films in the pyrolysis regime. These lines were used for the addressing of

LCD's. Especially LCD's that need absorbing layers, such as cholesteric texture LCD's (CTLCD), benefit from the black electrode structure that is formed. The pyrolysed patterns have a depth of 10  $\mu\text{m}$  or more, which directly provides the cell gap for the display. The pyrolysed lines were able to switch the cholesteric liquid crystals from a reflective to the focal conic or homeotropic states, which appear black due to the black electrode.

Direct writing of conductive patterns on thin coatings was achieved with direct focused laser writing in the (organic) ablation regime on polymer-inorganic layers, consisting of a model system of alkanethiol stabilised gold nanoparticles blended with poly(methyl methacrylate). The organic material is removed completely with direct focused laser writing, leaving behind gold particles, which are fused into electrically conductive pathways (with a conductivity of  $0.001 - 0.1 \Omega^{-1}\text{cm}^{-1}$ ) upon a second pass of the focused laser beam. If desired, the patterns can be developed by rinsing the non-exposed sections of the coatings with a solvent. The conductive gold pattern that remains on the substrate might be applied for the addressing of liquid crystal displays or for microelectronic applications, such as integrated circuits.

In conclusion, the structuring of functional polymers used for liquid crystal alignment with direct laser writing in all the main laser writing regimes may form patterns that are not accessible by other liquid crystal orientation techniques. These patterned functional polymers may be considered for new designs of electro-optical devices for displays and security applications.



## Samenvatting

Het nano- en microstructureren van dunne functionele polymere films met behulp van directe schrijf- en replicatietechnieken is een bijzonder belangrijk proces voor het ontwerpen van nieuwe en verbeterde componenten en apparaten voor de informatie- en communicatietechnologie. Het transport, de opslag, de generatie, de verwerking en de weergave van data hangen in toenemende mate af van patronen in polymeren in het nanometre- of micrometerregime. Vele technieken zijn beschikbaar om deze, vaak complexe, patronen met de gewenste resolutie te produceren.

Normaal gesproken worden dergelijke patronen gegenereerd met behulp van replicatietechnieken. Met lithografische technieken (bijvoorbeeld foto- of elektronenlithografie, afhankelijk van de resolutie en geometrie van het patroon) wordt een 'master' geproduceerd, die vervolgens wordt gerepliceerd in metallische kopieën. Deze worden gebruikt om, met technieken als embossen of spuitgieten, polymere substraten of films te patroneren. Het aantal tussenstappen en gebruikte materialen is erg hoog en vaak is het nodig nabewerkingen (zoals etsen) uit te voeren voordat het patroon bruikbaar is. Het aantal processtappen kan gereduceerd worden door de patronen direct te schrijven. De traditionele nadelen van directe schrijftechnieken, waaronder de relatief langzame bewerkingsnelheid, zijn inmiddels grotendeels verbeterd. Daardoor worden deze technieken steeds vaker toegepast om unieke patronen te genereren die niet op een andere wijze toegankelijk zijn. Direct patroneren met behulp van gefocuseerde lasers of interfererende laserbundels (holografie) is derhalve een veelbelovende industriële technologie. Temeer daar met lasers een grote hoeveelheid (foto-)chemische en (thermisch-)fysische processen kunnen worden geïnduceerd in polymeren met grote vrijheid in het ontwerp van het patroon en met de mogelijkheid om het snel in een nieuw product in te voeren.

Normaal gesproken heeft het polymeer waarin geschreven wordt geen (elektro-)optische functionaliteit. Recentelijk zijn er echter nieuwe patroneringstechnieken ontwikkeld voor het patroneren van polymeren die al wel een dergelijke functionaliteit hebben. Door middel van nano- en micropatronering worden verschillende (elektro-)optische eigenschappen, afkomstig van zowel het oorspronkelijke polymeer, alsmede het geschreven patroon, gecombineerd. Een typische voorbeeld is het patroneren van fotogevoelige vloeibare kristaloriëntatielagen voor vloeibare kristalschermen ('liquid crystal displays', LCD's). Een ander voorbeeld is het embossen in de vaste fase van gestructureerde functionele polymeren voor optische toepassingen.



In dit proefschrift zijn lasers gebruikt om direct te schrijven in functionele polymeren met als doel het genereren van nieuwe, unieke patronen met specifieke elektrische en optische eigenschappen. Het grote aantal mogelijkheden die laserschrijven biedt met betrekking tot chemische en fysische processen is gecombineerd met anisotrope functionele polymeren. Een grote variëteit in dimensies, geometrie en ontwerp van patronen is gevormd voor toepassing in bijvoorbeeld platte beeldschermen en gepersonaliseerde beveiligingskenmerken voor waardedocumenten.

In dit proefschrift hebben we ons gefocuseerd op twee voorbeelden van lasergeïnduceerde modificatie/vormgeving van functionele polymeren, namelijk het direct laserpatroneren van vloeibare kristaloriëntatielagen en het laserschrijven van elektrodes voor het elektro-optisch schakelen van vloeibare kristallen. We lieten zien dat het mogelijk is om polyimides te patroneren in verschillende chemische en thermische regimes, zoals smelten, pyrolyse en ablatie. In het smeltregime treedt een zeer snel smelt- en resolidificatieproces in het substraat op. Dit resulteert in reliëfstructuren met een typische hoogte van 50 tot 200 nm. Bij hogere laserintensiteiten wordt het polymeer gepyrolyseerd. Hierdoor treden processen als carbonisatie en grafitisatie op. Bij verdere verhoging van de laserintensiteit vindt ablatie plaats, wat resulteert in reliëfstructuren van enkele micrometers.

We hebben vervolgens de uitlijning van vloeibare kristallen boven lasergesmolten patronen in gewreven polyimides onderzocht. Dit werd gedaan met behulp van (elektro-) optische cellen, bestaande uit twee gewreven en gekruist geplaatste polyimide oriëntatielagen met op één van de oriëntatielagen een laser gesmolten patroon. We lieten zien dat in dergelijke gepatroneerde cellen lokaal de uitlijningseigenschappen (verankering) van het polyimide vernietigd worden. Boven de patronen oriënteren de vloeibare kristallen zich hierdoor in de richting die opgelegd wordt door de oriëntatielaag aan het tegenoverliggende substraat. Het resultaat is een hybride optische cel, bestaande uit gebieden met vloeibare kristallen met een uniaxiale oriëntatie in een omgeving met een getwiste nematische oriëntatie. Deze hybride, gepatroneerde cellen zijn potentieel interessant voor verschillende toepassingen, zoals bijvoorbeeld het aanbrengen van pictogrammen in displays. Een ander voorbeeld is het vervaardigen van nieuwe beveiligingselementen in waardedocumenten en credit cards met combinaties van veiligheidsniveaus en zelfs gepersonaliseerde beveiligingsonderdelen.

Lineair foto-polariseerbare polymeren ('linearly photo-polarisable polymers', LPP) zijn een klasse van polymere materialen die hun vloeibare kristaluitlijningseigenschappen verkrijgen door middel van belichting met gepolariseerd UV licht. Direct gefocuseerd laserschrijven en holografie in het lage-intensiteit sub-smelt regime met het gepolariseerde licht van de UV laser resulteerden in lokale, puur fotochemische veranderingen in LPP materialen. Dit veranderde lokaal de uitlijning van het vloeibare kristal dat op het LPP

materiaal werd aangebracht. Deze gepatroneerde oriëntatielagen werden gebruikt om hoge resolutie, hybride optische cellen te maken met afwisselende getwiste en uniaxiale vloeibare kristaluitlijning, vergelijkbaar met de laser gesmolten polyimidelagen. Met direct gefocuseerd laserschrijven kunnen patronen met een grote ontwerpvrijheid geproduceerd worden met een minimum resolutie van enkele microns. Met holografie was het mogelijk om deze resolutie verder te verkleinen.

Door middel van laser schrijven in het pyrolysereregime hebben we direct elektrisch geleidende structuren (met een geleiding van  $0.1 - 10 \Omega^{-1}\text{cm}^{-1}$ ) geschreven in vrijstaande polyimide films. Deze lijnen werden toegepast voor het elektrisch aansturen van LCD's. Dit gebeurde specifiek in LCD's die gebruik maken van absorberende lagen, zoals 'cholesteric texture' LCD's (CTLCD's). Deze LCD's profiteren van de zwarte electrodestructuur die gevormd wordt door middel van laserpyrolyse. De gepyrolyseerde patronen hebben een diepte van  $10 \mu\text{m}$  of meer. Dit vormt direct de lege ruimte binnen de cel die gevuld kan worden met het vloeibare kristal. De cholesterische vloeibare kristallen konden elektrisch worden geschakeld met de gepyrolyseerde lijnen tussen een (gekleurde) reflectieve en een zwarte toestand.

Met behulp van direct gefocuseerd laserschrijven in het (organische) ablatieregime konden direct geleidende patronen worden geschreven in dunne coatings die bestonden uit een modelsysteem van alkaanthiol gestabiliseerde goud nanoparticles gemengd met poly(methyl methacrylaat). Met laserschrijven werd het organische materiaal volledig verwijderd. De gouddeeltjes bleven achter en met behulp van een tweede passage van de laser werden deze gefuseerd tot een elektrisch geleidend patroon (met een geleiding van  $0.001 - 0.1 \Omega^{-1}\text{cm}^{-1}$ ). Indien gewenst was het mogelijk om de lijnen verder te ontwikkelen door middel van het wegspoelen van de niet-belichte delen van de coating. De geleidende goudpatronen kunnen eventueel gebruikt worden voor het aansturen van LCD's of voor micro-elektronische toepassingen, zoals geïntegreerde circuits.

Afsluitend kunnen we concluderen dat het direct laserstructureren in alle laserschrijfregimes van functionele polymeren voor vloeibare kristaluitlijning resulteert in patronen die niet toegankelijk zijn met andere vloeibare kristaluitlijningstechnieken. De gepatroneerde polymeren kunnen overwogen worden voor toepassing in nieuwe ontwerpen van elektro-optische componenten en apparaten voor display- en beveiligingstoepassingen voor documenten en credit cards.



# Chapter 1

## Introduction

### 1.1 Nano- and microstructuring of polymers with replication techniques

Polymeric components and devices with nano- and micro-patterned surfaces play a dominant role in information and communication technology. For instance, nano- and micro-structured components are nowadays used in data generation, data transport, data processing, data display and data storage systems where they perform a wide range of optical, electronic and opto-electronic functions<sup>1-6</sup>. A variety of techniques was developed to generate complex patterns with resolutions on a micrometer scale or far below. Typically, with the most common nano- and micropatterning techniques<sup>7,8</sup>, a master is generated via photo-lithography, e-beam lithography, x-ray lithography, micro-machining, direct writing or holography. The dimensions and the geometry of the desired pattern determine the actual choice for a specific technique. A first generation master is subsequently replicated into larger metallic copies using advanced lithographic and etching techniques. The actual transfer of the nano- or microstructure into polymers is performed with techniques such as casting, moulding<sup>9</sup>, micro-contact printing<sup>10</sup> or embossing<sup>11</sup>.

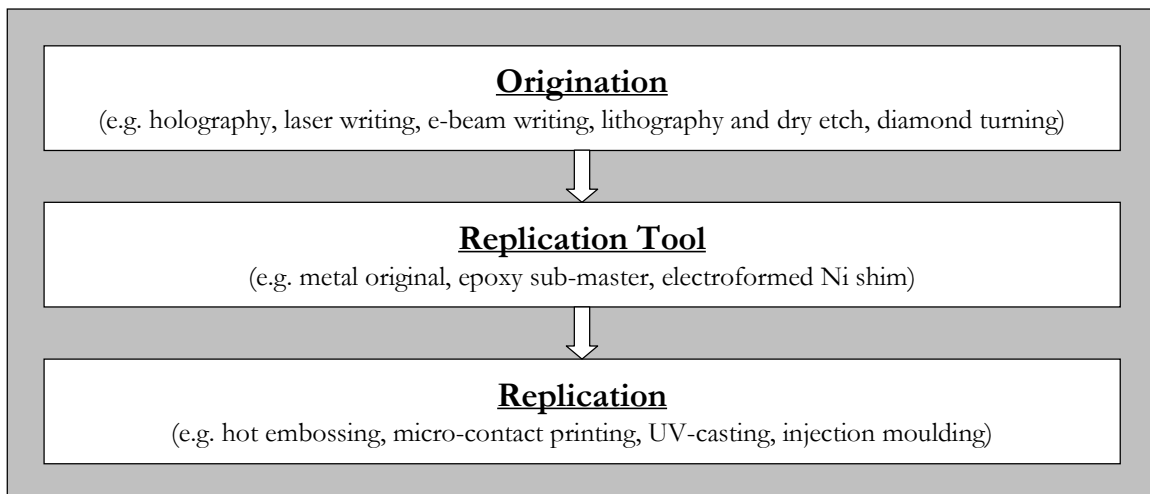


Figure 1.1 Common procedures and techniques to micro-pattern materials<sup>7,8</sup>

## 1.2 Direct writing techniques for the patterning and structuring of polymers

Some of the techniques that are used for the production of masters can also be used to directly write patterns in a polymeric component or end product to circumvent the extensive multi-step replication procedure<sup>12</sup>. Direct writing is especially interesting for the production of unique and/or specialised patterns, while replication with masters is the preferred choice for the mass production of the same pattern in high quantities. In principle all sources of radiation used in the production of masters, such as x-rays<sup>13</sup>, photons<sup>14</sup>, electrons<sup>15,16</sup>, ions<sup>17</sup>, atoms<sup>18</sup> and atomic interactions (scanning probes)<sup>19-23</sup>, can be applied to pattern polymers by direct writing. However, these direct writing techniques often require rather bulky, expensive equipment in order to focus and steer the beam. In practice, direct patterning techniques are therefore restricted to light in the ultra-violet, visible or near-infrared wavelength range of the spectrum, predominantly in the form of laser light. Another disadvantage of direct writing of patterns is that the processes tend to be comparatively slow. However, these disadvantages were overcome to a large extent and direct writing techniques are nowadays extensively used for the mass-production of patterns in polymeric materials<sup>14</sup>.

The most common techniques for direct patterning of polymers are direct focused laser writing<sup>14,24</sup> and holography<sup>24-26</sup>. With direct focused laser writing the radiation is delivered in the form of a coherent, focused beam. By scanning the beam over the sample, patterns are directly generated in the surface of the sample because of chemical or physical changes that occur upon absorption of the irradiation energy. With interferometry (a special type of holography) the pattern is formed through interference of two laser beams. In principle, these techniques eliminate the need for masks and laborious etching procedures and complex patterns can be directly written with a large design freedom.

Direct focused laser writing is nowadays extensively used for the encoding of consumer products with barcodes and date-of-last-use indicators on food packaging.<sup>27</sup> Special polymers or additives are used to transfer the laser light into written information. Moreover, more complex patterns, full colour patterns and even images are written on products. This important advantage of direct writing is also increasingly used to create unique and personalised patterns for applications such as personalised security features.

Interferometry and holography are techniques that are used to generate high-resolution holographic diffraction gratings often based on photo-induced refractive index modulations. By varying the grating geometry and depending on the material, these gratings can be used for different optical functions<sup>28-30</sup>, such as lenses, reflectors, colour filters or light guides. A more extensive description of both direct focused laser writing and interferometry is given in the appendix.

### 1.3 Micro-patterning in anisotropic functional polymers

Besides their function as product or component materials, the polymeric substrates used in most replication and direct writing techniques are usually only isotropic carriers and supports for the pattern, which is usually a relief structure formed through a physical or chemical process. However, recently several new techniques were developed for the patterning of anisotropic polymeric layers with additional optical, electrical and/or electro-optical functionalities. First, an anisotropic structure is introduced in a polymer, e.g. by mechanical, chemical or physical processes, to obtain an (electro-optical) functionality (e.g. the rubbing of polyimides to obtain liquid crystal alignment properties). Finally, a micro-patterning step locally alters or removes this functionality or adds a new one on top.

An example of this is the micro-patterning of photosensitive liquid crystal alignment layers<sup>1,31-33</sup>. In these techniques, a special class of photopolymers is used, which is aligned on a molecular scale using linearly polarised light. A second micro-pattern is super-imposed on the alignment layer using photolithography or micro-contact printing. The end result is a micro-structured material with a different molecular director and alignment in the separate microscopic domains. These patterned substrates can be applied for use in liquid crystal displays with enhanced viewing angle characteristics<sup>31</sup>.

Another example for the micro-patterning of anisotropic functional polymers is the use of anisotropic polymeric substrates, which are combined with surface relief structures. Typically, a high birefringence is generated in these polymer substrates by stretching. Relief structures are induced in the oriented polymers with techniques such as solid state embossing<sup>34,35</sup>, direct laser writing<sup>30,36</sup> or micro-machining<sup>30,36</sup>. The oriented film is attached on top of a side-lit substrate with a refractive index between the ordinary and extraordinary refractive index of the oriented film. One of the polarisation directions of the in-coupled light is totally internally reflected at the interface. The other enters the oriented layer and is coupled out at the patterned structures. In this way, wave-guides are generated with a capability to produce linearly polarised light with a high efficiency for display illumination.

### 1.4 Objective and scope of the thesis

The nano- and micro-structuring of anisotropic functional polymers offers a range of possibilities to create unique patterns with different length scales and functionalities. In this thesis, we investigate direct writing techniques, such as focused laser writing and interferometry (holography), in (anisotropic) functional polymers, such as orientation layers for liquid crystals. The main objective is to expand the range of patterns in polymeric substrates and to generate design freedom in substrates and components for demanding

applications in areas such as flat panel displays, personalised security features and microelectronic pathways for use in LCD addressing or integrated circuits.

The thesis is subdivided into six main chapters and an appendix. In **Chapter 2** we investigated the direct laser writing in polyimides. This chapter focuses on laser writing regimes (e.g. heating, melting, ablation, pyrolysis and ablation) that are induced in polyimides. The chapter aims to reveal information on the influence of laser writing parameters such as the light intensity and laser spot dimensions.

In **Chapter 3** we studied direct focused laser writing of rubbed polyimide in the melting regime. The influence of this laser writing process on the alignment of liquid crystals is investigated in an attempt to induce hybrid liquid crystal alignment properties in a single substrate.

In **Chapter 4**, laser-patterned polyimide is applied in electro-optical switches, such as liquid crystal displays. Laser-melted rubbed polyimide orientation layers are applied in twisted nematic displays and personalised security features. Electrically conductive pathways written in polyimide in the pyrolysis regime are applied for the addressing of liquid crystal display systems. Moreover, we investigated whether the high optical absorption of the conductive carbon patterns on polyimide substrates can be further exploited for a specific type of flexible flat panel displays (cholesteric texture LCD's).

In **Chapter 5**, photochemical changes induced by direct focused laser writing and holography in photosensitive liquid crystal orientation layers are used to generate micro-patterns. In this chapter, the use of rubbed polyimide layers is avoided in an attempt to generate super-imposed patterns in alignment layers with non-mechanical techniques. With this technique, we investigated novel types of patterned liquid crystal orientation layers with unique patterns, which can only be made in this type of materials.

In **Chapter 6**, we present a laser writing technique to produce conductive micro-patterns. A relatively simple three-step procedure based on direct focused laser writing is used to generate the patterns on a hybrid organic-inorganic material consisting of a polymer carrier and stabilised metallic nanoparticles. In this chapter, the complete route to produce the patterns is investigated, including the synthesis of the materials, coating procedures, direct laser writing and the properties of the resulting patterns.

Concluding remarks and evaluations of the objectives of this thesis are presented in the **Technology Assessment**. Also, the possibilities for potential further research into materials, processes and applications are discussed there. The **Appendix** gives a technical and theoretical background about the laser writing techniques used in this thesis: direct focused laser writing and interferometry (holography).

## 1.5 References

- [1] M. Schadt, *Annu. Rev. Mater. Sci.* **27**, 305, (1997).
- [2] R. L. v. Renesse, *Optical Document Security*, Artech House, Boston, (1998).
- [3] R. W. Phillips, A. F. Bleikolm, *Appl. Opt.* **35**, 5529, (1996).
- [4] P. W. McOwan, W. J. Hossack, R. E. Burge, *Opt. Commun.* **83**, 21, (1991).
- [5] R. Staub, W. R. Tompkin, A. Schilling, *Opt. Eng.* **38**, 89, (1999).
- [6] Anonymous, *Microelectron. Reliab.* **37**, 1865, (1997).
- [7] Y. N. Xia, G. M. Whitesides, *Annu. Rev. Mater. Sci.* **28**, 153, (1998).
- [8] Y. N. Xia, J. A. Rogers, K. E. Paul, G. M. Whitesides, *Chem. Rev.* **99**, 1823, (1999).
- [9] H. C. Haverkorn van Rijsewijk, P. E. J. Legierse, G. E. Thomas, *Philips Technol. Rev.* **40**, 287, (1982).
- [10] A. Kumar, G. M. Whitesides, *Appl. Phys. Lett.* **63**, 2002, (1993).
- [11] M. Emmelius, G. Pawlowski, H. W. Vollmann, *Angew. Chem., Int. Ed. Engl.* **28**, 1445, (1989).
- [12] L. R. Harriott, *Proc. IEEE* **89**, 366, (2001).
- [13] P. Hoffmann, G. Benassayag, J. Gierak, J. Flicstein, M. Maarstumm, H. Vandenberg, *J. Appl. Phys.* **74**, 7588, (1993).
- [14] D. Bäuerle, *Laser Processing and Chemistry, second edition*, Springer, Berlin, (1996).
- [15] J. Lohau, S. Friedrichowski, G. Dumpich, E. F. Wassermann, *J. Vac. Sci. Technol. B* **16**, 77, (1998).
- [16] A. N. Broers, W. Molzen, J. Cuomo, N. Wittels, *Appl. Phys. Lett.* **29**, 596, (1976).
- [17] J. M. Gibson, *Phys. Today* **1997**, 56, (1997).
- [18] K. S. Johnsson, K. K. Berggren, A. J. Black, A. P. Chu, N. H. Dekker, D. C. Ralph, J. H. Thywissen, R. Youkin, M. Prentiss, M. Tinkham, G. M. Whitesides, *Appl. Phys. Lett.* **69**, 2773, (1996).
- [19] R. S. Becker, J. A. Golovchenko, B. S. Swartzentruber, *Nature* **325**, 419, (1987).
- [20] N. Kramer, H. Birk, J. Jorritsma, C. Schonenberger, *Appl. Phys. Lett.* **66**, 1325, (1995).
- [21] J. A. Dagata, *Science* **270**, 1625, (1995).
- [22] A. J. Bard, G. Denault, R. A. Friesner, B. C. Dornblaser, L. S. Tuckerman, *Anal. Chem.* **63**, 1282, (1991).
- [23] E. Betzig, K. Trautman, *Science* **257**, 189, (1992).
- [24] W. M. Steen, *Laser Material Processing*, Springer-Verlag, London, (1998).
- [25] S. S. Charschan, *Guide To Laser Materials Processing*, CRC Press, Boca Raton, (1993).
- [26] W. E. Kock, *Lasers and Holography - An Introduction to Coherent Optics, Second, Enlarged Edition*, Dover Publications Inc., New York, (1981).
- [27] <http://www.dsm.com/solutions/applications/laser/~en/index.pl?f=dlcr98-2.htm>
- [28] L. Solymar, D. J. Cooke, *Volume Holography and Volume Gratings*, Academic Press, London, (1981).
- [29] J. Wilson, J. F. B. Hawkes, *Lasers Principles and Applications*, Prentice Hall, New York, (1987).
- [30] H. J. B. Jagt, *Polymeric Polarisation Optics for Energy Efficient Liquid Crystal Display Illumination (PhD thesis)*, Technische Universiteit Eindhoven, Eindhoven, (2001).
- [31] M. Schadt, H. Seiberle, A. Schuster, *Nature* **381**, 212, (1996).



- 
- [32] M. Schadt, H. Seiberle, *Patent WO 9852077*, (1998).
- [33] J. T. A. Wilderbeek, *Liquid Crystalline Driven Morphology Control of In-Situ Formed Polymers (PhD thesis)*, Technische Universiteit Eindhoven, Eindhoven, (2001).
- [34] N. Stutzmann, T. A. Tervoort, C. W. M. Bastiaansen, K. Feldman, P. Smith, *Adv. Mater.* **12**, 557, (2000).
- [35] N. Stutzmann, *Microstructuring of Polymers and Polymer-Supported Matter - Process and Applications (PhD Thesis)*, ETH, Zurich, (2001).
- [36] H. J. B. Jagt, H. J. Cornelissen, D. J. Broer, C. W. M. Bastiaansen, *IDRC (Palm Beach, USA)*, 92, (2000).

## Chapter 2

### Laser Writing Regimes in Polyimides

#### 2.1 Introduction

The direct laser patterning of polymers is usually performed in various physical and chemical regimes depending on the power density of the laser. In this chapter, the physical, structural and chemical changes that are induced in polyimides are studied for these different laser writing regimes. In subsequent chapters, these laser writing regimes are further investigated, often in combination with (anisotropic) functional polymers for specific applications. First, a general overview of the different laser writing regimes in polymers is presented.

Upon irradiation of a polymer with a laser, part of the light is absorbed, part is transmitted and part is reflected<sup>1</sup>. The ratio in which absorption, reflection and transmission occurs depends on the type of polymer, the wavelength, the power density, the type of laser and the surface properties of the material. A wide variety of chemical or physical processes can take place upon absorption of laser light<sup>1-3</sup>. In general, the laser absorption introduces (sub)- molecular vibrations, which manifest themselves eventually as thermal energy. Four main laser processing regimes are distinguished with an increasing laser power density and/or absorbed energy, i.e. heating, melting, pyrolysis and ablation<sup>1,2</sup>.

In the heating regime, at low laser intensities, the electronic vibrations in the polymer do not have sufficient energy<sup>1</sup> to cause changes in the polymers other than local expansion and contraction. However, a local temperature increase induced by a laser can be used in specific processes, such as local thermal activation of the surface for chemical reactions or physical processes<sup>1-3</sup>. In the melting regime, the vibrational energy induced by the absorbed laser beam is stronger than intermolecular forces within the polymer and deformation and/or breakage of secondary bonds occurs. The polymeric material loses its semi-crystalline nature or is heated above the glass transition temperature and the polymer starts to exhibit flow behaviour<sup>1</sup>. Often the resulting patterns are relief structures due to an extremely fast melting and re-solidification of the polymer. At higher absorbed energy, pyrolysis starts to occur in the polymer. Pyrolysis is a chemical process in which organic molecules exhibit carbonisation and/or graphitisation, depending on the power density<sup>4,5</sup>.

Finally, in the ablation regime, at very high absorbed energies, the vibrational energy breaks both inter- and intramolecular bonds and the polymer will effectively vaporise. This results in a local removal of material. Of course, the described regimes often overlap and several of the described chemical and/or physical processes can occur in consecutive order or even simultaneously.

In this chapter, we attempted to create patterns in polyimides in all four laser writing regimes using direct focused laser writing and the geometry and morphology of these patterns is investigated. Polyimides are selected as model materials because they are a versatile class of engineering polymers that are also extensively used in various electrical and optical applications (to be discussed in later chapters of this thesis).

## 2.2 Experimental

### 2.2.1 Materials

A solution of polyimide precursor polyamic acid AL1051 in N-methyl-2-pyrrolidone, was obtained from JSR Electronics. The polyimide precursor was spin-coated (5 s at 1000 rpm, 40 s at 5000 rpm) on 2.5 x 2.5 cm glass substrates. After a pre-bake at 100 °C, the coating was placed in a vacuum oven at 170 °C for 90 minutes to produce a polyimide coating with a thickness of 200 nm, determined by profilometry. Freestanding polyimide films (Kapton) were obtained from Dupont. Kapton is a PMDA-ODA polyimide film. Various film thicknesses were used (Kapton 200HN: 120 μm, Kapton 300HN: 180 μm, Kapton 500HN: 300 μm). Kapton is highly coloured; the thinnest films were bright yellow, the thickest films were deep orange. Figure 2.1 gives the chemical structures of polyimide AL1051 and Kapton.

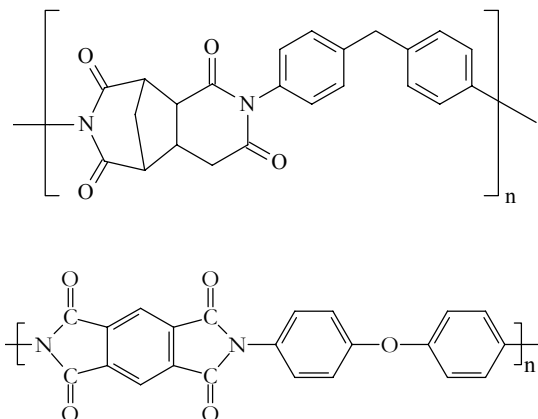


Figure 2.1 Chemical structures of polyimides AL1051 (top) and Kapton (bottom)

### 2.2.2 Direct focused laser writing

Laser writing was performed using a continuous wave Argon Ion laser (Spectra-Physics Beamlok 2050), operating at 351 nm in TEM<sub>00</sub> mode. The beam was frequency stabilised using a Spectraphysics Z-Lok system. The beam was focused using a UV grade, plano-convex, fused silica lens (Melles-Griot 01 LQP 001) to a diameter of approximately 10  $\mu\text{m}$  (defined at the  $1/e^2$  position, see appendix). The focal distance of the lens was 50 mm. Ultra-precision, computer controlled translation stages (Newport PM-500) supported the sample holder to position the sample through the laser beam. The writing speed and the laser power density were varied. The power was measured internally, at the head of the laser, but due to losses on the optics, this resulted to a power of 55% (measured after the focusing lens) of the set power. The power density of the focused beam (in  $\text{W}/\text{m}^2$ ) was used to compare different values.

### 2.2.3 Characterisation

Coating thickness was determined using a Tencor P-10 Profilometer. Light absorption of the polyimide layer was determined by UV-VIS-NIR scanning spectroscopy (Shimadzu UV-3102 PC). The dimensions of the lines were studied by light microscopy (Zeiss Universal), Environmental Scanning Electron Microscopy (Philips XL30 FEG-ESEM, operating at low voltage mode, the samples were not stained with a staining agent) and Atomic Force Microscopy (Digital Instruments Dimension 3100). Cross-sections of samples were made by cold fracture.

## 2.3 Results and discussion

### 2.3.1 Absorption of polyimide

Polyimides were used as model materials because of their potential usefulness in optical and electro-optical applications. Initially, thin ( $\sim 200$  nm), spin-coated polyimide layers on a glass substrate were predominantly used. Figure 2.2 gives a UV-VIS spectrum of the polyimide coatings after baking.

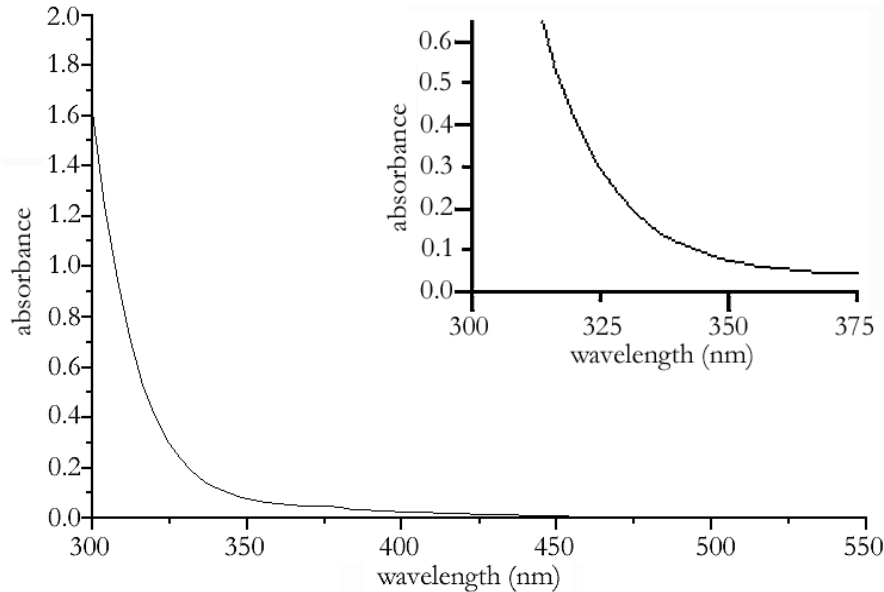


Figure 2.2 UV-VIS spectrum of spin-coated polyimide. Insert: enlargement of 300-375 nm area

The spectrum shows that thin polyimide layers are highly transparent in the visible wavelength range (400 – 700 nm) and that absorption occurs in the near ultra-violet range. Therefore, a continuous  $\text{Ar}^+$  laser with an operating wavelength of 351 nm was used for subsequent laser writing experiments. The absorption at this wavelength appeared to be, in some cases, sufficient for direct laser patterning (to be discussed later).

### 2.3.2 The heating and melting regimes

In a first set of laser writing experiments, the laser beam was focused to a diameter of 10  $\mu\text{m}$ . The influence of the laser power density at a writing velocity of 0.1 mm/s was investigated. At low laser intensities ( $< 1.0 \times 10^{11} \text{ W/m}^2$ ), it is impossible to observe any pattern with optical microscopy (figure 2.3a). This indicates that a threshold exists in minimum absorbed laser energy below which there is insufficient energy to induce a permanent structural change in the polyimide. At somewhat higher laser intensities ( $\sim 1.2 \times 10^{11} \text{ W/m}^2$ ), discontinuous structures start to appear which resemble the pattern formed by a thrown rock that skips over water (figure 2.3b). At higher laser intensities ( $> 1.4 \times 10^{11} \text{ W/m}^2$ ), continuous line patterns are observed in the polyimide (figure 2.3a, 2.3b and 2.3c). The line width of the written patterns increases with increasing laser power density (compare 2.3c and 2.3d). At the highest laser intensities ( $> 4.2 \times 10^{11} \text{ W/m}^2$ ), dark discolourations start to appear in the optical micrographs (figure 2.3f), which indicates that chemical changes start to occur during laser writing. The writing of patterns in this regime is discussed more extensively in the next paragraph.

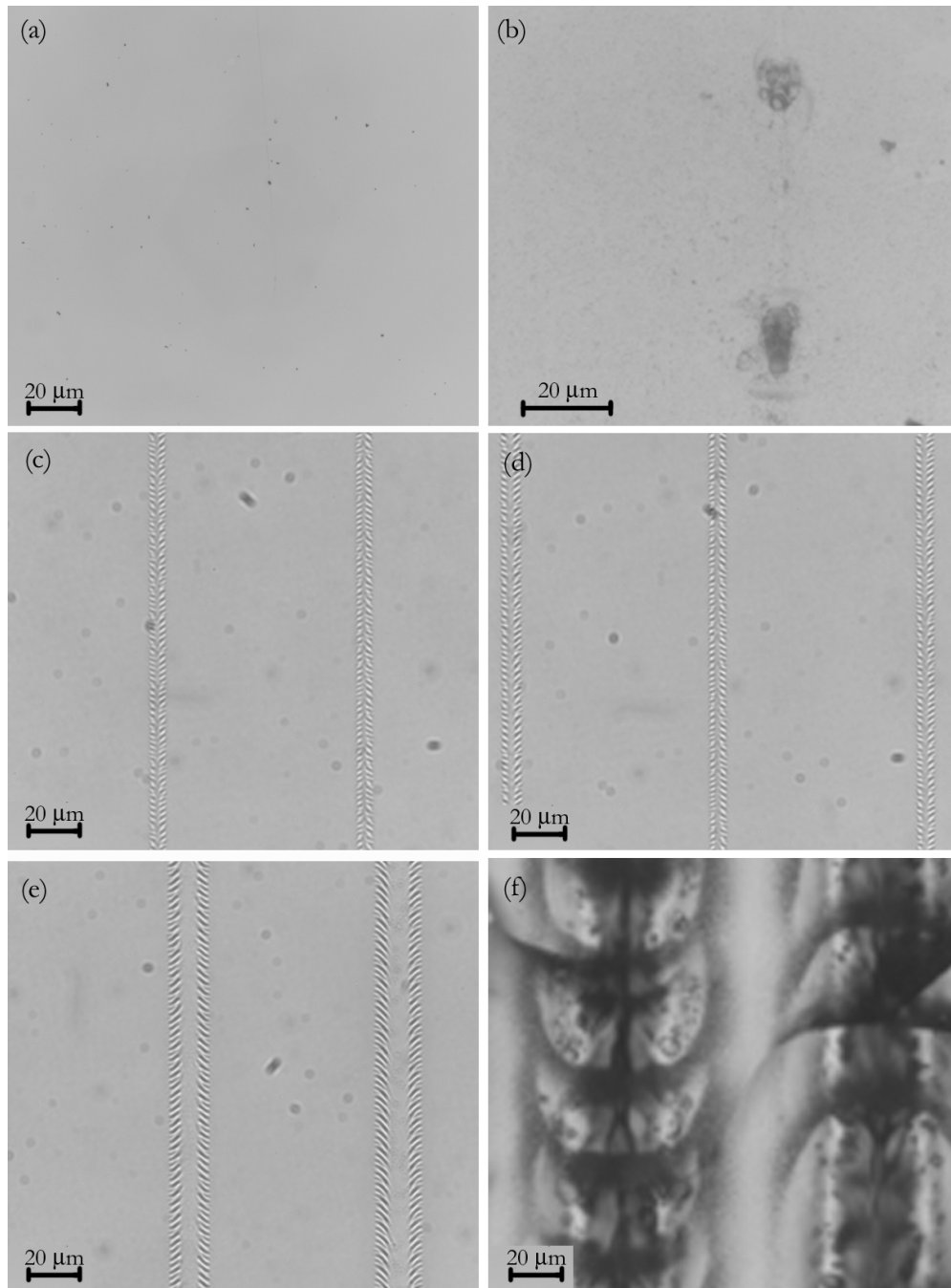


Figure 2.3 Optical micrographs of laser-written polyimide films ( $v = 0.1$  mm/s) at a laser power density of:  
(a)  $0.8 \times 10^{11}$  W/m<sup>2</sup>, (b)  $1.2 \times 10^{11}$  W/m<sup>2</sup>, (c)  $1.4 \times 10^{11}$  W/m<sup>2</sup>, (d)  $2.1 \times 10^{11}$  W/m<sup>2</sup>, (e)  $3.5 \times 10^{11}$  W/m<sup>2</sup>,  
(f)  $4.5 \times 10^{11}$  W/m<sup>2</sup>

Figure 2.4 shows the line width of the patterns as a function of the laser power density at a constant writing velocity of 0.1 mm/s and 1.0 mm/s. The graphs show that a more or less linear relationship exists between the laser power density and line width in the melting regime.

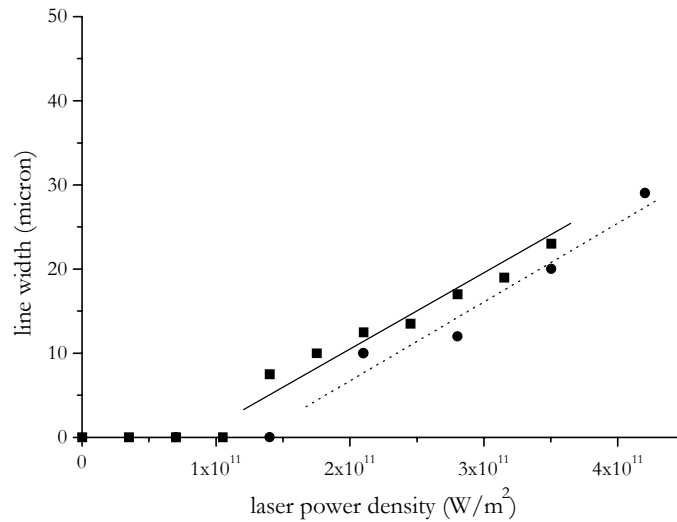


Figure 2.4 Line width of laser-written patterns as a function of laser power density; (■, continuous line)  $v = 0.1$  mm/s, (●, dotted line)  $v = 1.0$  mm/s

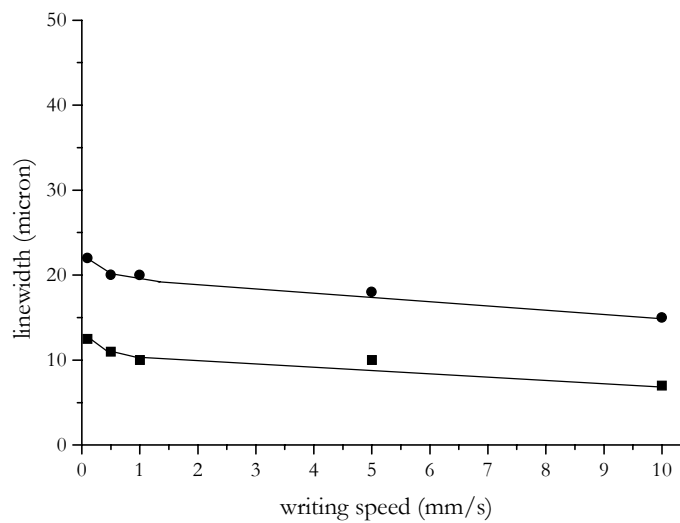


Figure 2.5 Line width of laser-written patterns as a function of writing velocity (■)  $2.1 \times 10^{11}$   $W/m^2$ , (●)  $3.5 \times 10^{11}$   $W/m^2$

Figure 2.5 presents a plot of the line width of laser-melted patterns as a function of the writing velocity. This graph illustrates that the writing velocity has a minor influence on the resulting line width. Apparently, even with relatively short interaction times due to high scanning speeds (e.g.  $v = 10$  mm/s), the width of the structures is mainly determined by the laser power density.

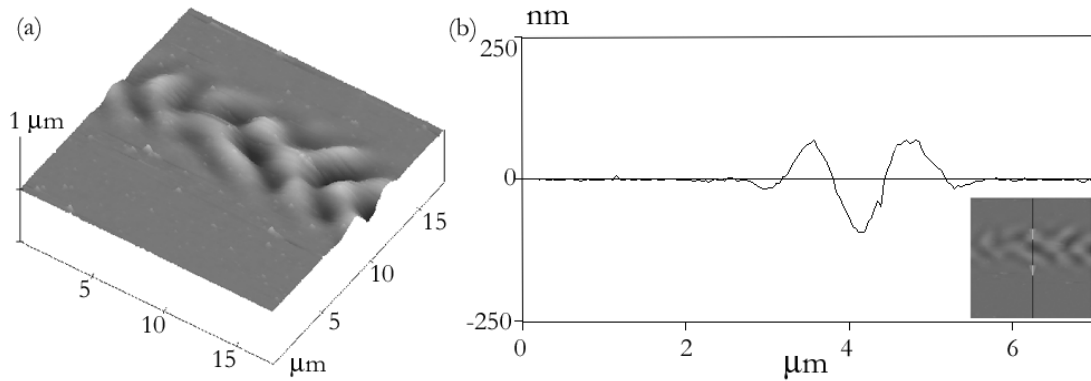


Figure 2.6 Scanning probe micrographs of laser-written line patterns at a low absorbed power density.

Height profiles: (a) three dimensional view, (b) cross-section

In a subsequent set of experiments, the written patterns were investigated more closely with scanning probe microscopy. Figure 2.6 shows a typical relief structure of the written patterns. In this particular case, a laser power density of  $1.4 \cdot 10^{11} \text{ W/m}^2$  was used in combination with a writing velocity of  $0.1 \text{ mm/s}$  which corresponds to writing conditions just above the absorbed energy threshold for laser melting (see figure 2.4). The pattern in figure 2.6a is rather irregularly shaped both in the writing direction and perpendicular to it. A cross-section of the pattern (figure 2.6b) illustrates that a relief structure is obtained with a typical height and depth of approximately  $60 - 70 \text{ nm}$ .

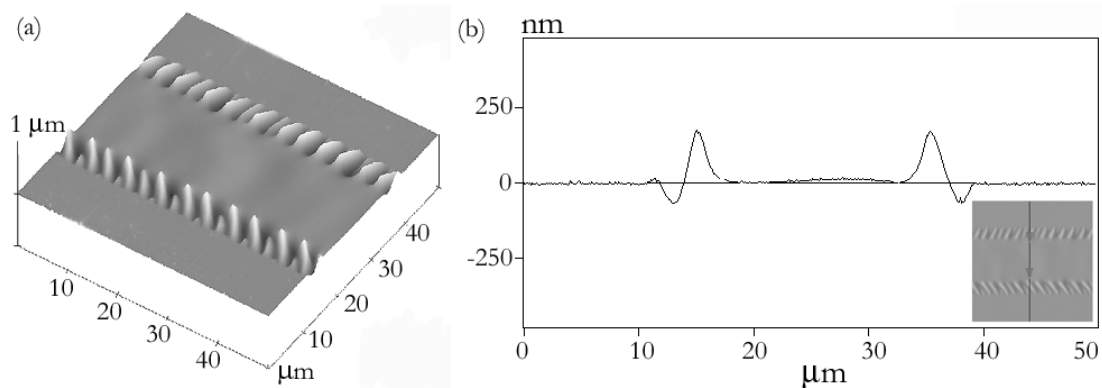


Figure 2.7 Scanning probe micrographs of laser-written line patterns at a high-absorbed energy level

Height profiles: (a) three dimensional view (b) cross-section

Figure 2.7a and 2.7b show scanning probe micrographs of laser-written patterns that were generated at a higher laser power density ( $3.5 \cdot 10^{11} \text{ W/m}^2$ ). In this particular case, a wide central plateau is observed with irregular edges. The cross-sections at high and low laser energies appear similar if one assumes that the central part of the relief structure is widened upon increasing the absorbed laser energy.



The appearance of the observed irregular relief structures is typical of laser-melted structures and was previously reported in literature<sup>1,2</sup>. The process that occurs is sketched in figure 2.8. The Gaussian beam intensity profile of the beam results in a rather large temperature distribution gradient within the polymer film (see the appendix for some theoretical background on the temperature increase of a surface irradiated by a moving Gaussian beam). The irradiated sections with a sufficient temperature rise form a so-called meltpool (figure 2.8b). Marangoni flows occur in the meltpool due to the temperature dependence of the surface tension and fast convective flows are induced by the temperature gradient itself. Due to these flows, near the edges of the laser beam, material is pushed up from the surface, while in the middle a depression is formed (a ‘keyhole’). In principle no material is removed during laser melting, but due to the fast flows, some material may be ejected from the surface. After the laser beam passed the irradiated spot or if the laser irradiation is discontinued, the material quickly resolidifies. The meltpool is effectively frozen in, causing relief structures in the form of elevations and depressions on the surface (see figure 2.8c).

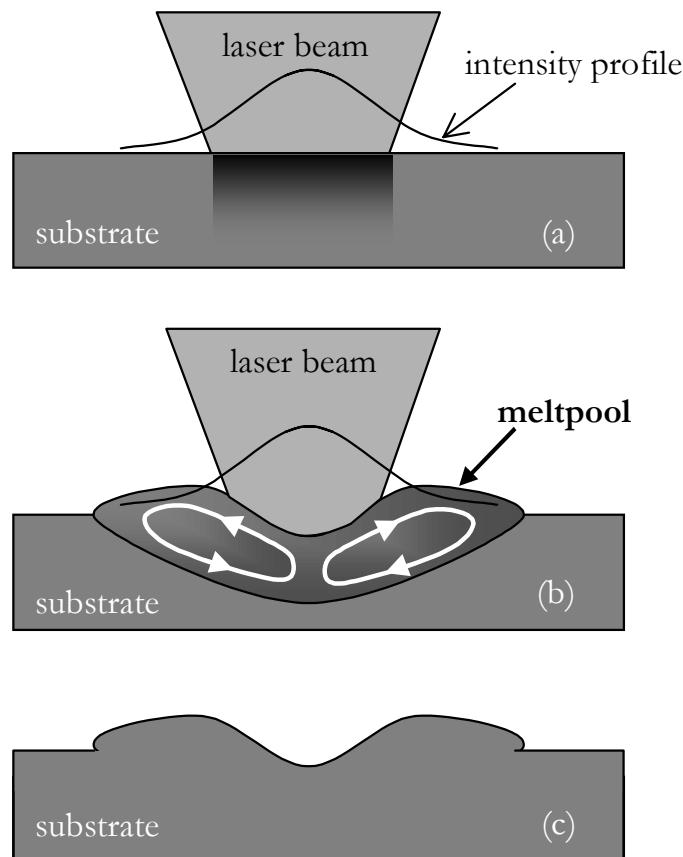


Figure 2.8 Formation of relief structures during laser melting: (a) initial laser contact, (b) flows within the meltpool, (c) solidified relief structures

The shape of the meltpool and the subsequent relief structures is determined by material properties such as thermal conductivity and surface tension, as well as laser beam properties such as beam spot size, focusing depth and laser power density. Also, the thickness of the laser-written substrate is of importance. The temperature profile in thin layers extend more easily throughout the thickness of the film than in thicker films. Heat might be absorbed by the back substrate or diffuse sideways, resulting in a different shape and size of the meltpool and the subsequent relief structures. Of course, this writing mechanism results in a regular relief structure along the length of a written line if the writing velocity is truly constant. The stepper motor characteristics of the used translation stages cause short periods in which some small areas are irradiated slightly longer than others, resulting in subsequent holes and humps, most visible in the structures on the edges, but also present, though less clearly visible, in the central plateau.

Since polyimides have a high glass transition temperature of several hundreds of degrees, which often lies even above the degradation temperature of the polyimide, it is surprising that melting flow effects are observed without degradation. Probably, this is caused by kinetic effects, the short interaction time and the type of polyimide.

In this paragraph, we showed that relief structures with a wide range of geometries, width (5-25  $\mu\text{m}$ ) and height (50-150 nm) were written in thin polyimide layers without inducing chemical changes in the polymer. In chapter 3, the alignment of liquid crystals in the presence of these relief structures is studied.

### 2.3.3 The pyrolysis and ablation regimes

Figure 2.3f already showed that black discolourations start to occur in thin polyimide layers upon irradiation with high intensity laser beams. In general, this discolouration is associated with pyrolysis, a chemical process, in the polymer related to carbonisation or graphitisation, resulting in glassy carbon<sup>4</sup> and/or graphite-like<sup>6,7</sup> structures. In this paragraph, the writing of patterns in polyimides, at these high laser intensity levels ( $> 4.0 \times 10^{11} \text{ W/m}^2$ ) is examined further. The laser light absorption process becomes rather uncontrolled in thin polyimide layers at high laser intensity levels. Irregular black lines start to appear already just above the melting regime originating from pyrolysis (figure 2.9a). The film shows cracks and an inhomogeneous line quality. When the intensity is further increased (above approximately  $6.0 \times 10^{11} \text{ W/m}^2$ ), laser ablation starts to play an important role and polymeric material is removed. This results in even more irregular patterns (figure 2.9b).

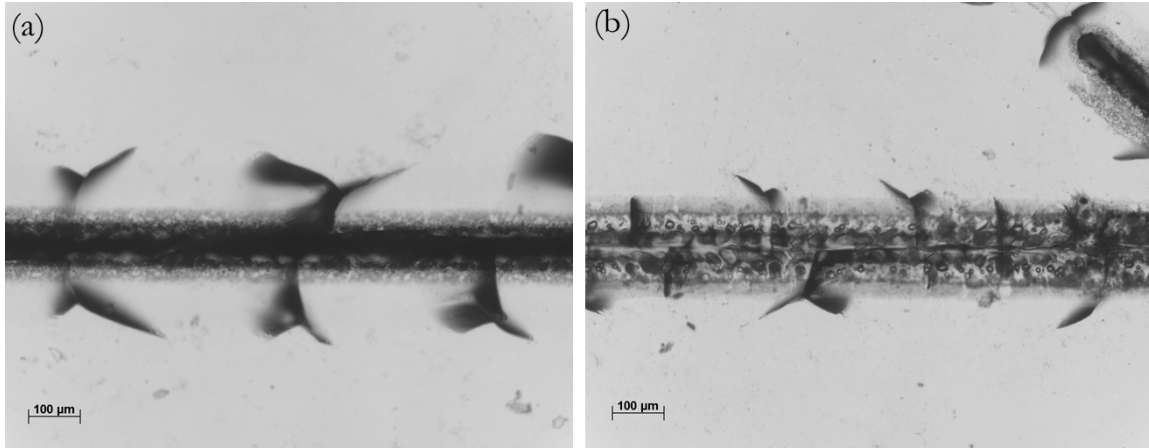


Figure 2.9 Optical micrograph of written patterns in thin polyimide layers. Laser power density:  
(a)  $5.0 \times 10^{11} \text{ W/m}^2$ , (b)  $6.4 \times 10^{11} \text{ W/m}^2$

The thin polyimide films are not suitable to accurately describe the pyrolysis and ablation regimes. Therefore, a second set of writing experiments was performed in an attempt to improve the quality of the written patterns. In this particular case, thick (100-300  $\mu\text{m}$ ), freestanding polyimide films were used (see experimental section). Figure 2.10 shows UV-VIS spectra of these freestanding polyimide films. These films are strongly yellow or orange coloured, depending on the thickness. Compared to the spin-coated polyimide films, the larger thickness of the films and the different chemical structure of the polyimide result in a higher absorption in the UV wavelength range (above the detection maximum of the UV-VIS spectrometer). Due to this high absorption, the laser intensity to reach the pyrolysis and ablation regimes are much lower than for spin-coated films.

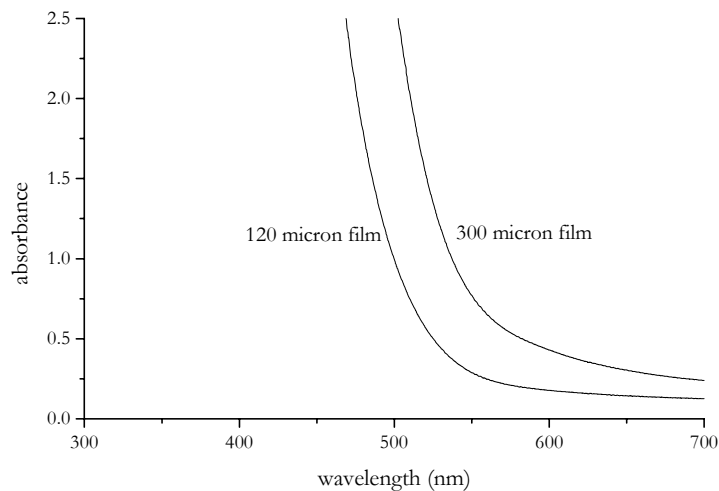


Figure 2.10 UV-VIS spectra of free-standing polyimide films

Figure 2.11 shows a series of lines written with increasing laser power density on a 120  $\mu\text{m}$  thick film. Above a laser power density of  $0.19 \times 10^{11} \text{ W/m}^2$  discontinuous lines start to form. Below this level no effect is observed (no melting regime was observed; for this type of polyimide the degradation temperature is reached before the glass transition temperature). From  $0.32 \times 10^{11} \text{ W/m}^2$  continuous black lines are formed due to carbonisation and/or graphitisation of the polyimide.

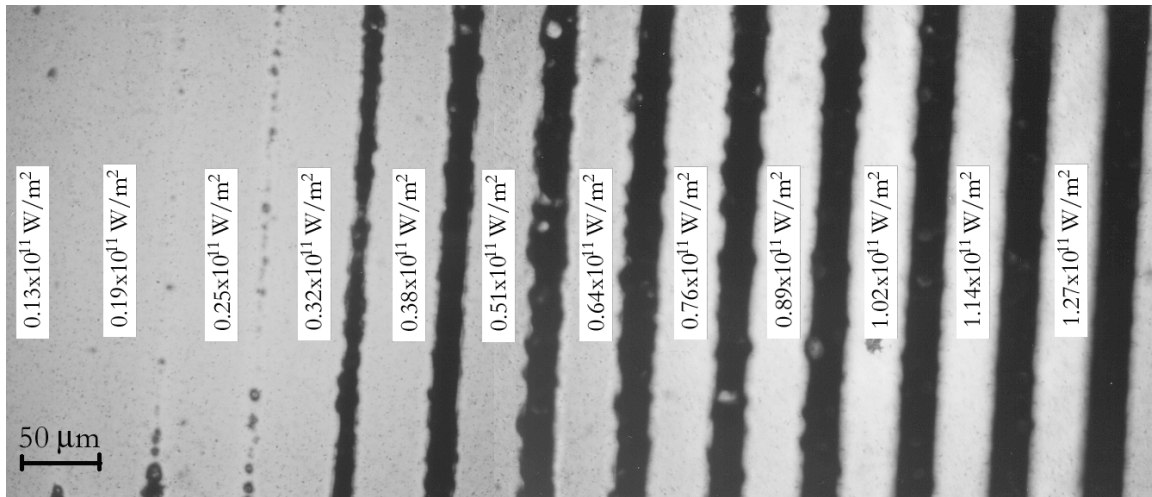


Figure 2.11 Optical micrograph of laser-written lines at increasing power density, writing speed: 1 mm/s

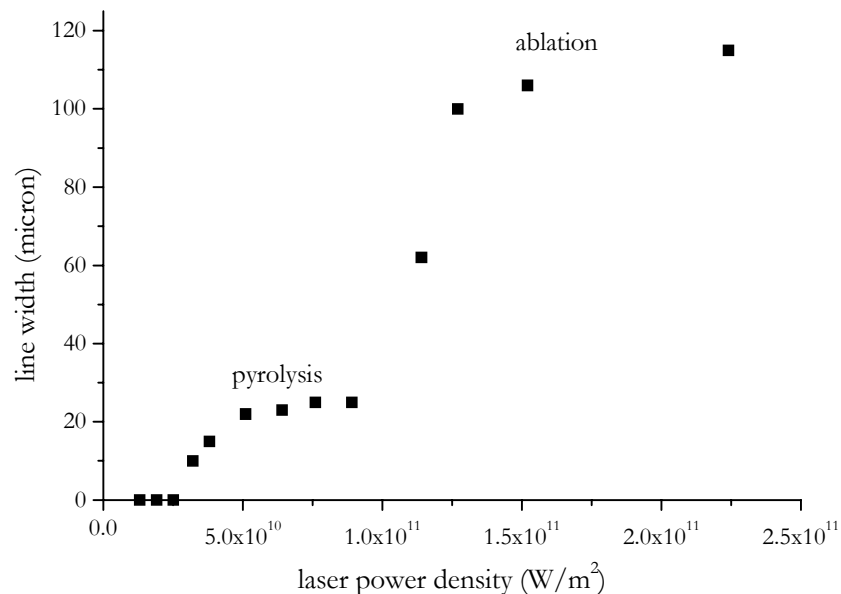


Figure 2.12 Line width of laser-written patterns on a 120  $\mu\text{m}$  thick polyimide film as a function of laser power density,  $v = 1 \text{ mm/s}$

Figure 2.12 gives a plot of the line width as a function of the laser power density, determined by optical microscopy. Below  $3.0 \times 10^{10} \text{ W/m}^2$ , no continuous lines are formed. At the pyrolysis threshold, a quick increase occurs until the line width reaches a plateau level of approximately 20-25  $\mu\text{m}$ . From laser intensities higher than approximately  $1.0 \times 10^{11} \text{ W/m}^2$ , ablation threshold is reached and the line width strongly increases again. This indicates the transition from pyrolysis to ablation. At  $1.5 \times 10^{11} \text{ W/m}^2$  the line width reaches another plateau of 110-120  $\mu\text{m}$ , indicating that ablation determines the line width. Figure 2.13 presents the line width as a function of the writing speed at two laser power densities ( $1.27 \times 10^{11} \text{ W/m}^2$  and  $2.54 \times 10^{11} \text{ W/m}^2$ ). The transition from pyrolysis to ablation is less sharp than in figure 2.12, but occurs for both intensities approximately between writing speeds of 1 mm/s and 5 mm/s.

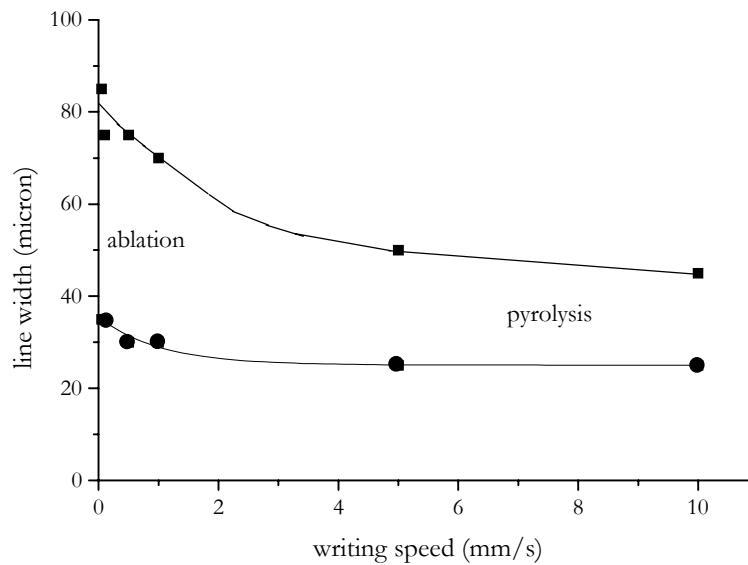


Figure 2.13 Line width as a function of the writing speed for two laser power densities.

(●)  $1.27 \times 10^{11} \text{ W/m}^2$ , (■)  $2.54 \times 10^{11} \text{ W/m}^2$

The lines were further studied using Environmental Scanning Electron Microscopy (ESEM), which shows the morphology of laser-written patterns on a 120  $\mu\text{m}$  thick film. Figure 2.14 shows top views and cross-sections of the written patterns at constant velocity (1 mm/s) and variable power density ( $0.38 \times 10^{11} \text{ W/m}^2$ ,  $1.14 \times 10^{11} \text{ W/m}^2$  and  $2.28 \times 10^{11} \text{ W/m}^2$ ). The debris visible in the lines, mainly consisting of loose carbon flakes, is partially caused by the pyrolysis and ablation processes, but also by the cold fracture of samples.

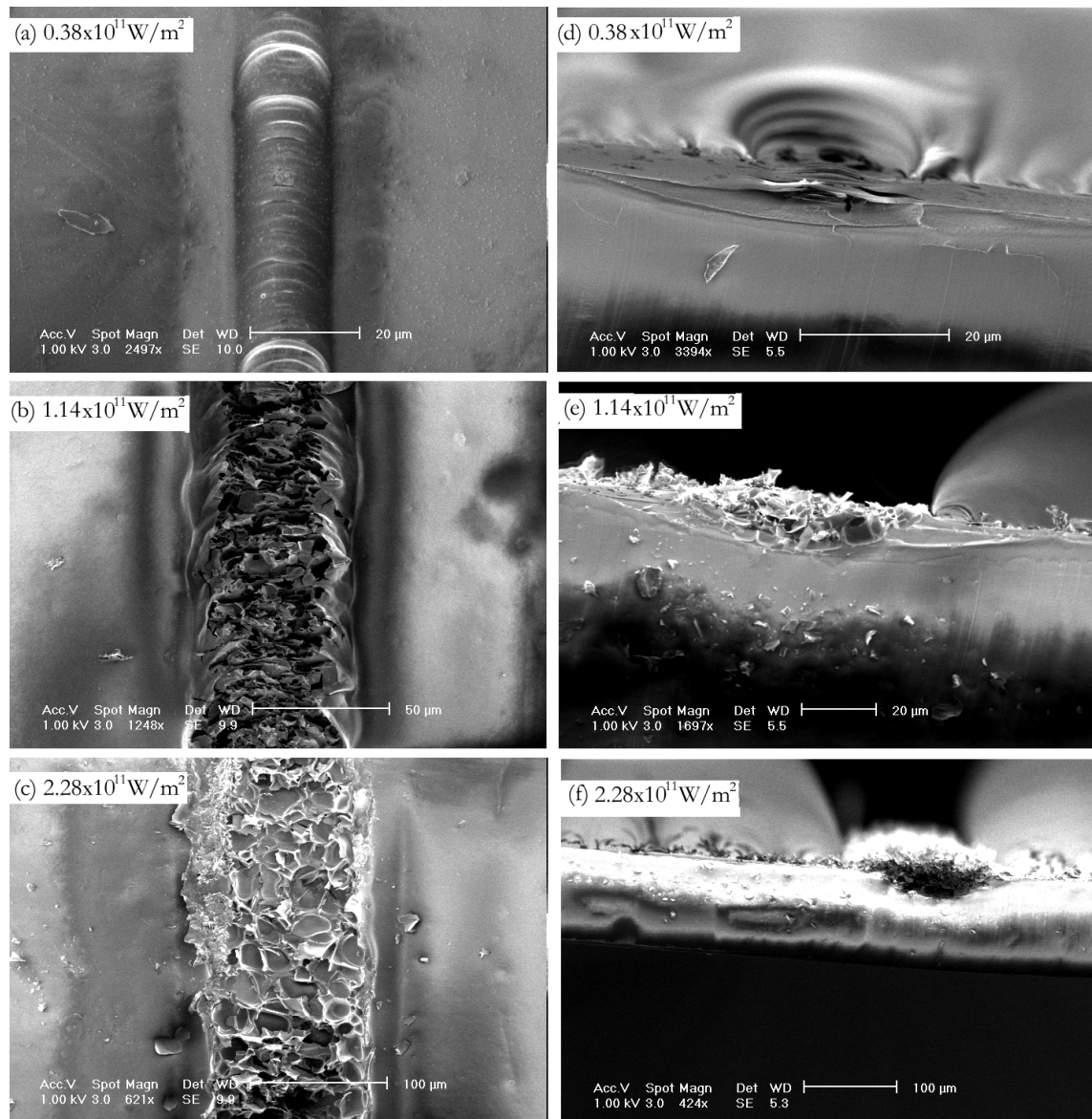


Figure 2.14 ESEM images of laser-written lines on a 120  $\mu\text{m}$  thick polyimide film with a writing speed of 1 mm/s and varying laser power density, which is indicated on the images; (a), (b), (c) top view, (d), (e), (f), cross-section

The dimensions of the lines correspond with the line width measured by optical microscopy and plotted in figure 2.12. The line written at  $0.38 \times 10^{11} \text{ W/m}^2$  (figures 2.14a and 2.14d) shows a continuous, undamaged pyrolysed pattern. Writing a grid pattern at these settings results in structures as shown in figure 2.15. The pattern consists of undamaged lines, but they do show an overlaying pattern of arc-like structures, which point in the laser writing direction. Consecutive lines were written in the opposite direction, as is clearly shown in figure 2.15b. If the first line was written from left to right, the next one is written in the opposite direction. At higher power density levels the pattern gets increasingly porous and

damaged, which indicates that the pyrolysis becomes more extreme and surface break-up occurs due to violent releases of gaseous products, such as  $\text{CO}_2$ ,  $\text{CO}$ ,  $\text{HCN}$ ,  $\text{C}_2\text{H}_2$ ,  $\text{H}_2\text{O}$  and small amounts of more complex molecules<sup>4</sup>. Also, initial ablative material removal is expected. This is clearly visible in figures 2.14b and 2.14e, which shows lines written at a power density level of  $1.14 \times 10^{11} \text{ W/m}^2$ . Still, pyrolysis structures similar to figure 2.14a are present near the edges of the line. In the center of the line the pattern is broken up due to the higher intensity in the middle of the Gaussian beam. At higher intensities (figure 2.14c and 2.14f), ablation is the main process and the damage extends over the whole line width. At these high intensities, the ablative process is quite violent and material might be ejected from the surface during the writing, which can form a halo of contaminations around the laser-written structures. This should be kept to a minimum or be removed (e.g. by sufficient ventilation). At very high laser power density ( $> 6.5 \times 10^{11} \text{ W/m}^2$ ), the laser beam cuts through the sample.

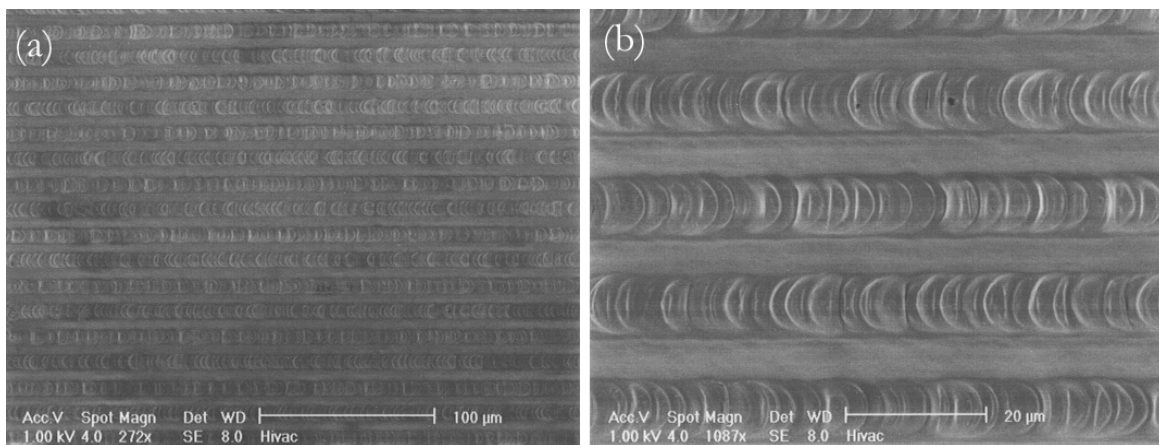


Figure 2.15 ESEM images of laser-pyrolysed lines on a  $120 \mu\text{m}$  thick polyimide film ( $0.38 \times 10^{11} \text{ W/m}^2$ ,  $1 \text{ mm/s}$ )

Next, the influence of the writing speed at constant power density ( $2.54 \times 10^{11} \text{ W/m}^2$ ) was investigated. Figure 2.16 shows ESEM images of lines written at  $0.05 \text{ mm/s}$ ,  $1 \text{ mm/s}$  and  $10 \text{ mm/s}$ , each in top-view and cross-section. These correspond with the line width plot in figure 2.13. At  $10 \text{ mm/s}$  (figures 2.16c and 2.16f) the line is almost undamaged and comparable in structure to the pyrolysed line in figure 2.14a, which was written at both lower speed and power density ( $0.38 \times 10^{11} \text{ W/m}^2$  and  $1 \text{ mm/s}$ ), although the width is about 3 times as large as that line. The width of undamaged pyrolysed lines can therefore only be set by varying both the laser power density and writing speed. At lower writing speeds ( $1 \text{ mm/s}$ ), the lines become damaged and broken up due to ablation (figures 2.16b and 2.16e). In the patterns loose carbon flakes are present, which are easily blown off the polyimide surface. At very low writing speeds ( $0.05 \text{ mm/s}$ ), ablation becomes the predominant effect, resulting in

steep grooves (figure 2.16a and 2.16d), while along the edges pyrolysis still takes place. The material removal mainly seems to be directed into the depth of the material, while the line widths are not drastically increased.

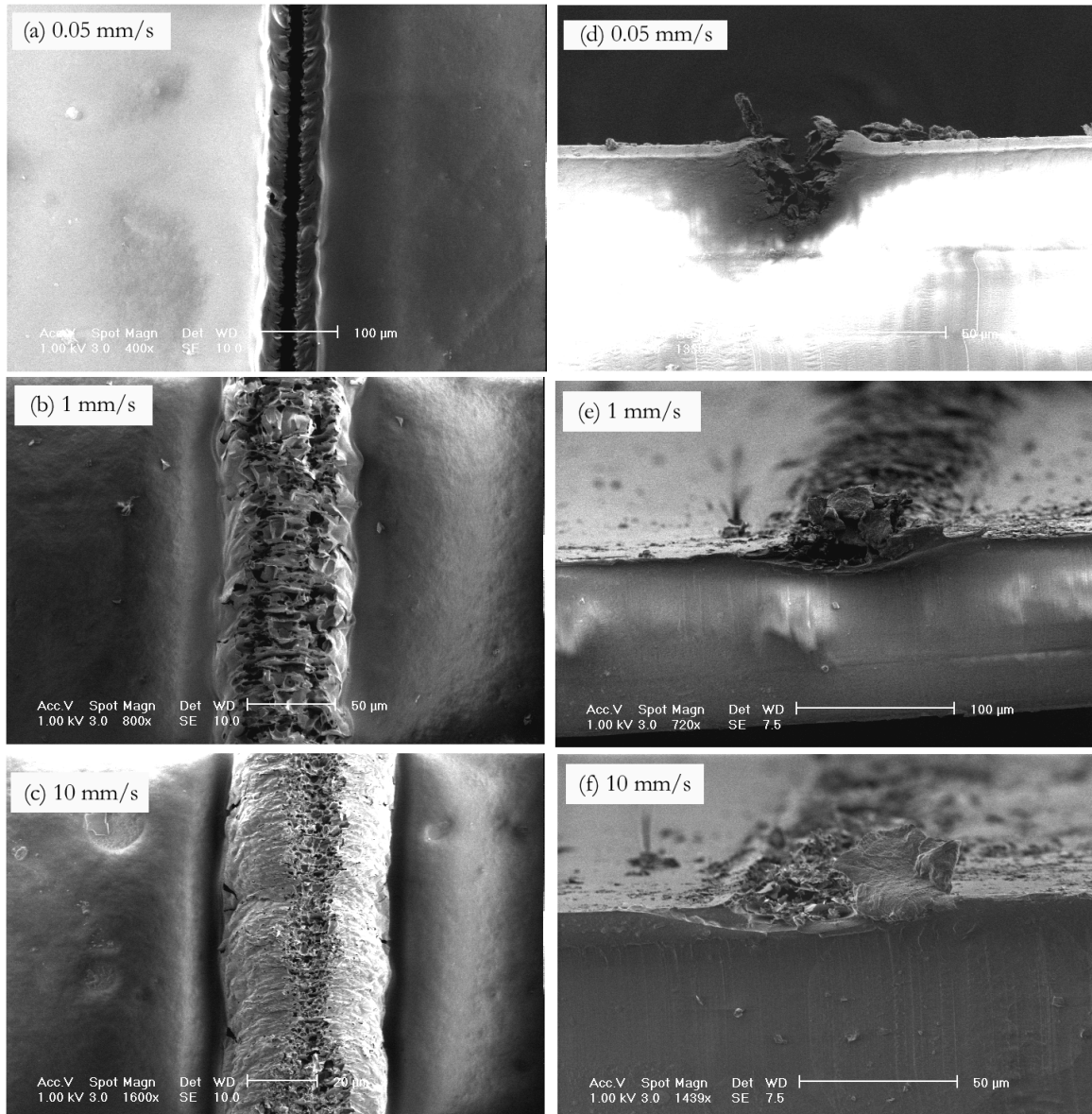


Figure 2.16 ESEM images of laser-written 120  $\mu\text{m}$  thick polyimide film with an intensity of  $2.54 \times 10^{11}$   $\text{W}/\text{m}^2$  and varying writing speeds, which are indicated on the images; (a), (b), (c) top view, (d), (e), (f), cross-section

Depending on the power density and velocity settings, carbon fibres are ‘scraped’ off the surface at high writing speeds (e.g. power density =  $1.6 \times 10^{11}$   $\text{W}/\text{m}^2$  and speed > 25 mm/s or power density =  $3.8 \times 10^{11}$   $\text{W}/\text{m}^2$  and speed > 5 mm/s). Figure 2.17 shows optical micrographs of the polyimide surface and the fibres. This effect was previously reported in



literature<sup>4</sup>. The length of the fibres ranges from several millimetres to two or three centimetres. The thickness is approximately 50 to 100  $\mu\text{m}$ . These fibres are extremely brittle and disintegrate into powder quite easily.

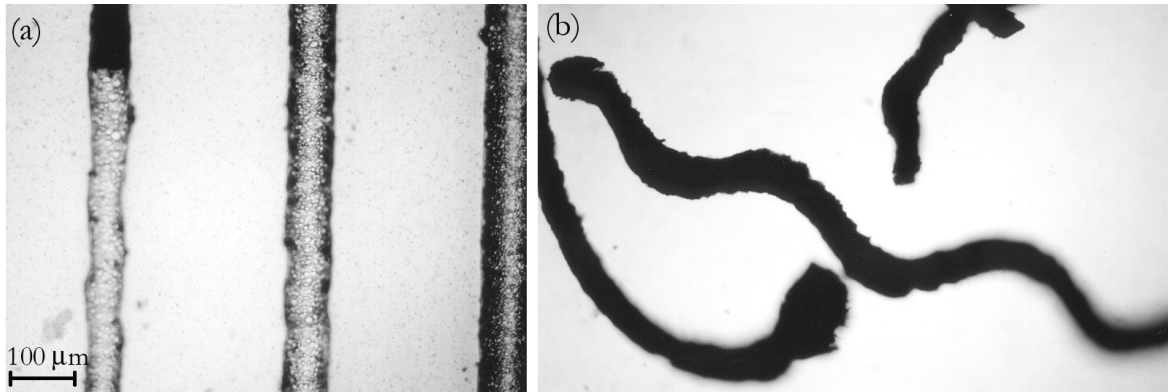


Figure 2.17 Optical micrographs of carbon fibres scraped off the polyimide surface during laser writing at  $3.8 \times 10^{11} \text{ W/m}^2$  and 10 mm/s. (a) surface after laser scraping, (b) fibres, same scale as (a)

The above-mentioned results show that it is relatively easy to generate pyrolysed patterns of varying geometry and morphology in polyimides using direct focused laser writing. There is a large freedom in the design of the geometry and length scale of the structures (figure 2.18). It is possible to pattern lines or structures with larger sizes by writing lines with a spacing similar to the line width, thus creating touching lines that can form larger areas.

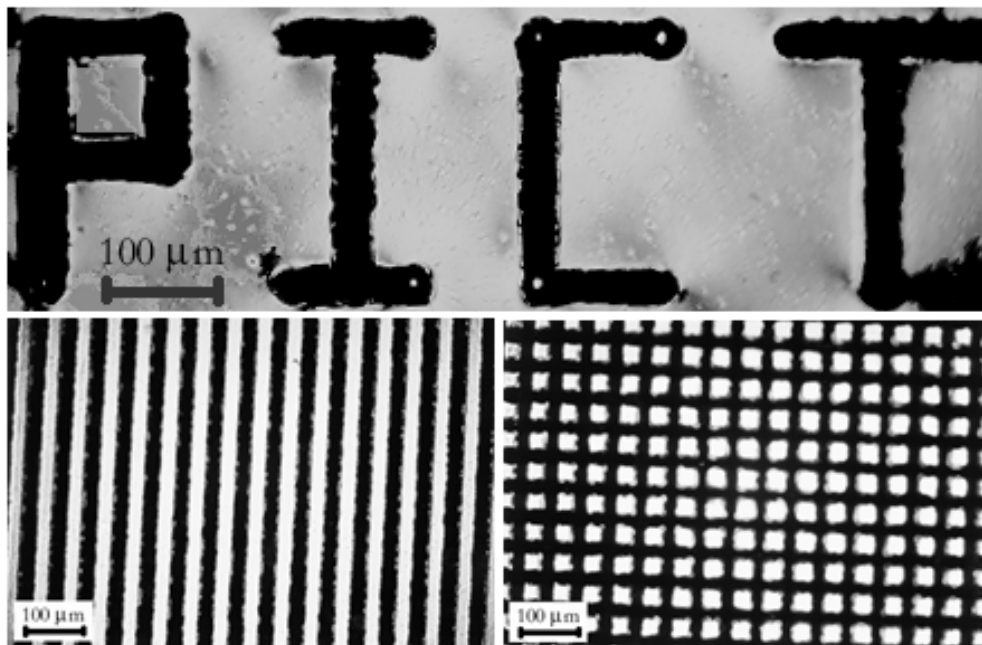


Figure 2.18 Optical micrographs of examples of various laser-pyrolysed patterns

The laser-pyrolysed structures on the polyimide surface mainly consist of carbon, which is an electrically conductive material<sup>8-13</sup>. Electrical conductivity ranging between 1 to  $10 \Omega^{-1} \text{ cm}^{-1}$ , depending on the thickness of the polyimide film and the laser writing process, has been reported<sup>5,14</sup>. The conductivity is attributed to a phonon-assisted variable range hopping mechanism<sup>15</sup>.

Most laser-pyrolysed lines described in this chapter did not show conductivity due to discontinuities in the lines (caused by defects formed during the laser writing process and/or damage due to handling of the very fragile patterns). Therefore 200  $\mu\text{m}$  wide large patterns, consisting of 5 overlapping lines with a width of 60  $\mu\text{m}$  and written with a line spacing of 50  $\mu\text{m}$ , were chosen as model patterns to investigate the conductivity. These patterns were written with an intensity of  $2.54 \times 10^{11} \text{ W/m}^2$  and 1 mm/s (similar to the structures shown in figures 2.16b and 2.16e). These laser writing settings result in patterning in the intermediate regime between pyrolysis and ablation and both processes take place simultaneously. The overlapping lines homogenize the patterns by eliminating edge effects of the lines, but also cause slightly more debris than in single lines. Figure 2.19 shows a cross-section of such a pattern.

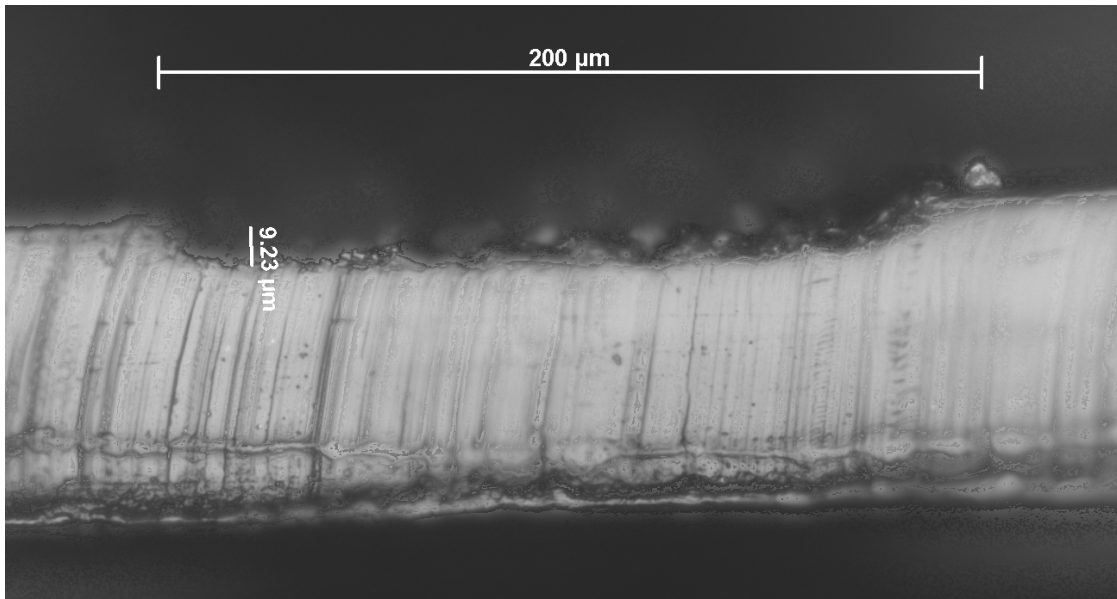


Figure 2.19 Optical micrograph of a laser-pyrolysed pattern consisting of 5 lines in polyimide (cross-section)

As opposed to single lines, these wider patterns consisting of 5 lines usually did show conductivity. The conductivity was measured, resulting in values ranging from 0.1 to  $10 \Omega^{-1} \text{ cm}^{-1}$ . This range in the value for conductivity is caused by several effects, such as the amount of debris lying on the lines, the sensitivity to damage of the lines and the fact that the effective electrical path length is determined by the amount of defects in the pattern.

Removing the carbon flakes from the lines with a strong nitrogen flow reduced the conductivity with approximately 5-10 %. Decreasing the laser writing intensity resulted in non-overlapping and therefore non-conductive patterns. Reducing the line spacing can of course solve this. Decreasing the intensity further resulted in discontinuous lines without any conductivity. Increasing the intensity above the used settings gradually decreases the conductivity, due to breaking up of the lines due to increased ablation.

Laser pyrolysis was in all cases mentioned in this paragraph performed in a normal nitrogen/oxygen atmosphere. If the pyrolysis would be performed in an oxygen-free atmosphere, the chemical processes change and the dependence of line width on the writing speed and power density, as well as the electrical conductivity are expected to be different.

## 2.4 Conclusions

In this chapter it was shown that direct focused laser writing on polyimide in several regimes induces unique patterns with different structural, compositional characters and length scales on polyimides. Figure 2.20 gives a typical overview of the laser writing regimes and their boundaries for spin-coated polyimide. The line width is given as a function of the energy flux (see appendix). This range of patterns can be applied for various purposes, as will be shown in the following chapters of this thesis.

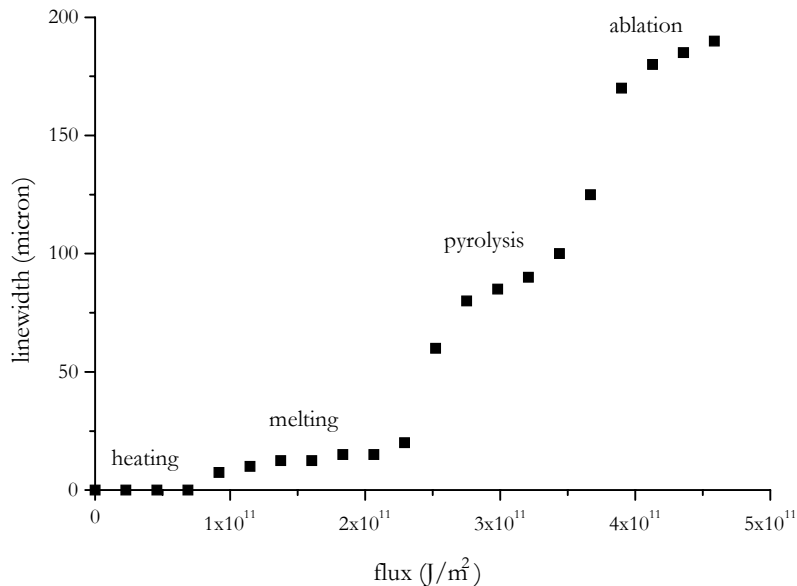


Figure 2.20 Overview of laser writing regimes in spin-coated polyimide films

In the heating regime no permanent patterns are formed. The melting regime induces relief structures with a typical height ranging from 50-150 nm and a width of 5-25  $\mu\text{m}$ . In specific cases, a large central plateau is observed between two relief structures at the side of the plateau. Laser pyrolysis results in black patterns due to the carbonisation and/or graphitisation of the polyimide. Undamaged lines with line widths ranging between 15-50  $\mu\text{m}$  were obtained, depending on the laser power density and writing speed. Continuous laser-pyrolysed patterns show electrical conductivity with a conductivity ranging from 0.1-10  $\Omega^{-1}\text{cm}^{-1}$ . Ablation leads to porous and damaged structures and, usually, debris in the form of carbon flakes is found on the patterns.

## 2.5 References

- [1] W. M. Steen, *Laser Material Processing*, Springer-Verlag, London, (1998).
- [2] D. Bäuerle, *Laser Processing and Chemistry, second edition*, Springer, Berlin, (1996).
- [3] S. S. Charschan, *Guide To Laser Materials Processing*, CRC Press, Boca Raton, (1993).
- [4] R. Srinivasan, R. R. Hall, W. D. Loehle, W. D. Wilson, D. C. Allbee, *J. Appl. Phys.* **78**, 4881, (1995).
- [5] H. M. Philips, S. Wahl, R. Sauerbrey, *Appl. Phys. Lett.* **62**, 2572, (1993).
- [6] H. B. Brom, Y. Tomkiewicz, A. Aviram, A. Broers, B. Sunners, *Solid State Commun.* **35**, 135, (1980).
- [7] J. B. Cooper, B. Julian, H. Morrison, P. Song, S. Albin, J. L. Zhen, *Thin Solid Films* **303**, 180, (1997).
- [8] T.F. Mendenhall jr, R.N. Quick, C.W. Wilkins jr, M.A. Lyons, M. Robbins, *Patent US 4691091*, (1987).
- [9] J. Davenas, *Appl. Surf. Sci.* **36**, 539, (1989).
- [10] J. I. Raffel, J. F. Freidin, G. H. Chapman, *Appl. Phys. Lett.* **42**, 705, (1983).
- [11] G. H. Wynn, A. W. Fountain, *J. Electrochem. Soc.* **144**, 3769, (1997).
- [12] Ramos, R.A., Chartash, K.E., Suh, N.P., *Patent US 4159414*, (1979).
- [13] M. Eckart, *Patent US 4496607*, (1985).
- [14] M. Schumann, R. Sauerbrey, M. C. Smayling, *Appl. Phys. Lett.* **58**, 428, (1991).
- [15] T. Feurer, R. Sauerbrey, M. C. Smayling, B. J. Story, *Applied Physics A* **56**, 275, (1993).



## Chapter 3

### Laser Melting of Rubbed Polyimide Orientation Layers\*

#### 3.1 Introduction

The molecular alignment of liquid crystals in contact with polymeric and non-polymeric substrates was investigated extensively in the past<sup>1-3</sup>. Especially the alignment of liquid crystals (LC) by rubbed polyimide layers was studied in detail. This is related to its technological relevance for liquid crystal display (LCD) applications. Rubbed polyimides are mechanically, thermally and chemically very stable materials and have excellent transparency in the visible wavelength region. Therefore, rubbed polyimides are the industrial standard for LC alignment layer materials. However, there are certain disadvantages to the use of rubbed polyimides<sup>4</sup>, e.g. the build-up of electro-static charges during rubbing and the subsequent damage of the electrical components at the active plate of the LCD. Also, small dust particles are generated during the rubbing process, which interfere with the manufacturing of LCD's under extreme clean conditions. To overcome these disadvantages, a variety of other alignment techniques was also developed, based on, for instance, surface relief structures<sup>5-8</sup>, photo-aligned polymers<sup>9</sup> and other non-contact techniques<sup>10</sup>. Recently, the micro-patterning of these orientation layers has attracted worldwide attention. This originates predominantly from the possibility to produce wide viewing angle liquid crystal displays through multi-domain formation<sup>11,12</sup>. This subscribes the need for still new patterning techniques for alignment layers for liquid crystals used in displays. But also other applications of liquid crystals may make use of new alignment techniques with a higher control over the local order, such as future generations of advanced and personalised security features<sup>13</sup>. These security features operate on the principle of a reflective twisted nematic (TN) optical cell filled with an LC layer, which has a fixed orientation above a patterned alignment layer (e.g. by using curable liquid crystal monomers). Contrast occurs due to alignment differences inside and outside the patterns. By using a single polariser the image is made visible.

In this chapter, we describe the patterning of rubbed polyimides by direct focused laser writing and the influence of these patterns on LC alignment. It is known from literature

---

\* Part of this work has been published: D.J. Versteeg, C.W.M. Bastiaansen, D.J. Broer, *Proceedings ID/IDW'01* (Nagoya, Japan), 65, (2001); D.J. Versteeg, C.W.M. Bastiaansen, D.J. Broer, *J. Appl. Phys.* **91**, 4191, (2002).

that relief structures can induce LC alignment<sup>5,14</sup> and this effect is used to construct TN LCD cells by writing these relief structures using a laser<sup>7</sup>. However, these patterns were formed by ablation, using a pulsed high-energy laser, while in this chapter we report on direct laser writing in the melting regime at intensities below the pyrolysis and ablation threshold and therefore no material is removed from the substrate. Laser melting might influence the orientation at the rubbed polyimide surface without generating discolorations or large relief structures that are the result of laser writing in degradation regimes, such as pyrolysis and ablation.

In chapter 2, we showed that laser writing in polyimides resulted in structures with a wide range of dimensions and structural properties that are dependent on the laser writing regime that was used. This chapter focuses on laser processing in the melting regime, since it results in small relief structures without discoloration. The resulting liquid crystal orientation is studied in transmissive and reflective optical cells in various configurations.

### 3.2. Liquid crystal alignment

Due to their anisotropic shape, liquid crystals have a tendency to align themselves into ordered structures. The type and amount of order depends on several parameters, such as temperature (e.g. nematic or smectic ordering) and the presence of surfaces or external fields. The director ( $\mathbf{n}$ ) represents the local orientation of a liquid crystal, a vector, which is determined by the average direction of all the single molecules, specified by the tilt (polar) angle ( $\theta_0$ ) and the twist (azimuthal) angle ( $\Phi_0$ ), see also figure 3.1. The director is given by:

$$\mathbf{n} = (\cos\theta_0\cos\Phi_0, \cos\theta_0\sin\Phi_0, \sin\theta_0) \quad (3.1)$$

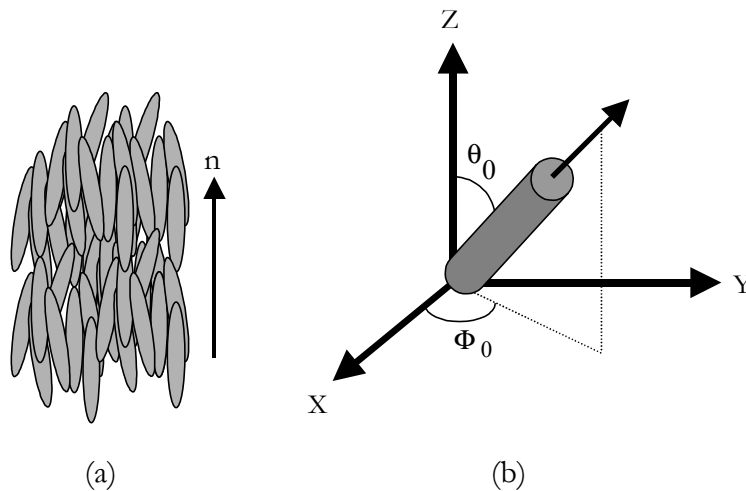


Figure 3.1 The most important variables in liquid crystal alignment. (see text for explanation of the symbols)

External influences cause deformations within a liquid crystal, such as bend, twist and splay (see figure 3.2). The deformation free energy is determined by the (spatial) director orientation and is given by the deformation free energy density function (in which  $K_1$ ,  $K_2$  and  $K_3$  are the elastic constants for splay, twist and bend)<sup>15-17</sup>:

$$f_{\text{elast}} = \frac{1}{2}K_1(\vec{\nabla} \cdot \vec{n})^2 + \frac{1}{2}K_2(\vec{\nabla} \times \vec{n})^2 + \frac{1}{2}K_3[\vec{n} \times (\vec{\nabla} \times \vec{n})]^2 \quad (3.2)$$

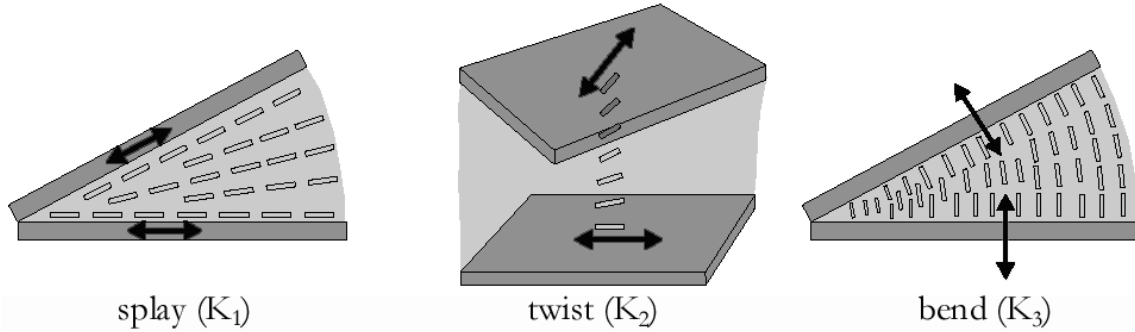


Figure 3.2 Splay, twist and bend deformations in liquid crystals<sup>18</sup>

Alignment of liquid crystals by surfaces has been known and studied for a long time<sup>1,3,19-21</sup>. If a liquid crystal is placed in contact with another (liquid or solid) phase, the nematic ordering is influenced close to the surface. Due to anisotropic interactions and minimisation of the interfacial energy between the LC and molecules at the surface of the other phase, certain orientations are favoured over others. This surface alignment is referred to as anchoring<sup>3,22</sup>. The anchoring direction and angle depends on the type of surface, liquid crystal and on the presence of external fields. When a surface induces an orientation in which the LC molecules are aligned with their long axis parallel to the surface, it is called the homogeneous planar configuration. If the LC molecules are aligned with their long axis perpendicular to the surface, this is referred to as the homeotropic configuration. Situations in between these two configurations are characterized by a tilt angle (the angle between the director of the LC and the surface). On a macroscopic scale the LC aligns itself in multiple domains, each with a different anchoring direction. If an oriented surface is used (e.g. rubbed polyimides or materials, such as silicon oxides, deposited under an angle), a single domain with a homogeneous LC alignment over the complete area is obtained<sup>23</sup>. The anchoring energy is defined as the energy needed to change the director from  $\theta_0$  (polar angle) or  $\Phi_0$  (azimuthal angle). Often, a distinction is made between strong and weak anchoring<sup>22</sup>. With strong anchoring the alignment of LC molecules at the surface is fixed (e.g. in the parallel or homeotropic state). With weak anchoring there is a balance between the energy



arising from the torque of the liquid crystal and the interfacial energy ( $\gamma_s$ ). The polar and azimuthal anchoring strength are given by the Rapini-Papoular equations for respectively constant azimuthal and polar angle<sup>24</sup>:

$$\begin{aligned} W_p &= \frac{1}{2} \left( \frac{\partial^2 \gamma_s}{\partial \theta^2} \right)_{\varphi} (\theta_s, \varphi_s) \\ W_a &= \frac{1}{2} \left( \frac{\partial^2 \gamma_s}{\partial \varphi^2} \right)_{\theta} (\theta_s, \varphi_s) \end{aligned} \quad (3.3)$$

$W_p$  is usually one or two orders of magnitude smaller than  $W_a$ .  $\gamma_s$  consists of a surface term and an absorption term, since wetting and absorption should be taken into account as well<sup>19,25,26</sup>. However, this absorption term is not an intrinsic property and depends on the history of the surface<sup>27,28</sup>.

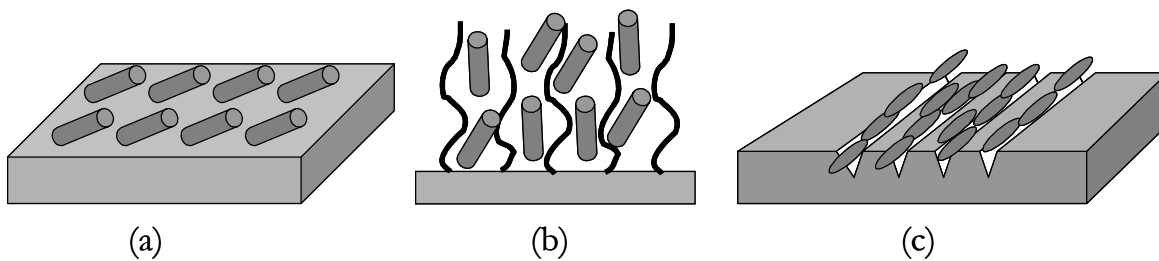


Figure 3.3 Main classes of surface anchoring: (a) smooth surfaces, (b) interpenetrable layers, (c) topographic alignment

Three main classes of surface anchoring are distinguished: alignment by smooth surfaces, alignment by interpenetrable layers and topographic alignment<sup>19</sup>. In the case of smooth surfaces, the alignment stems from dispersive interactions near the surface between the LC molecules and the molecules in the alignment layer<sup>29-31</sup>. Alignment by interpenetrable layers is obtained when long molecules are grafted on a surface and if those molecules extend themselves perpendicular to the surface penetrating into the LC layer. The liquid crystal molecules trapped between these grafts align themselves in the direction of the grafted molecules, usually resulting in a homeotropic alignment<sup>32-34</sup>. With topographic alignment, the LC molecules align themselves according to a surface relief structure that is present on the substrate (e.g. grooves or humps). The geometry and topography of the relief structures determine the exact nature and direction of the LC alignment<sup>5,7,29,35,36</sup>.

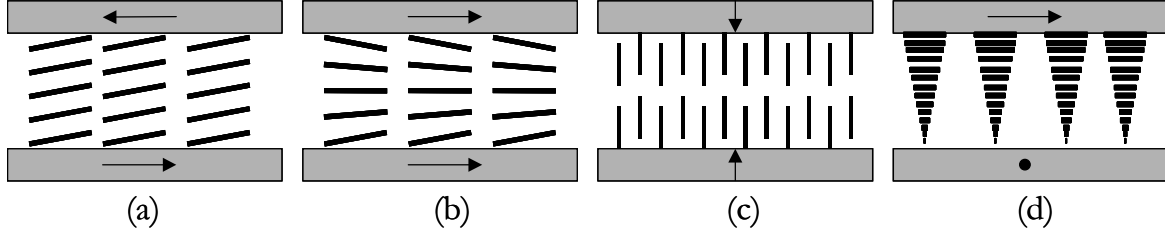


Figure 3.4 LC alignment configurations: (a) anti-parallel, (b) parallel, (c) homeotropic, (d) twisted

If an LC layer is sandwiched between two (equally strong) orientation layers, the LC aligns itself according to the effect of both. Figure 3.4 shows some of the most common LC alignment configurations. Figure 3.4a and 3.4b show planar configurations. In the anti-parallel configuration (figure 3.4a) the tilt angle of both orientation layers is in the opposite direction. This facilitates the stacking of the liquid crystals in a homogeneous planar configuration. In a parallel configuration (figure 3.4b), the tilt angles are in the same direction, resulting in a splayed LC alignment. The homeotropic alignment (figure 3.4c) induces an LC orientation with the director of the molecules perpendicular to the surface. In a twisted configuration (figure 3.4d), the orientation layers are placed with the direction of their aligning axis under an angle. Due to the elastic forces described previously in this paragraph, the LC molecules align themselves with their director rotating over the thickness of the cell. Two orientation layers placed perpendicular to each other induce a  $90^\circ$  twist angle over the thickness of the LC layer. These twisted LC layers can be used to modulate the polarisation direction of light<sup>37</sup>. Simply stated, the polarisation of light entering the twisted cell direction closely follows the director profile of the liquid crystal and is therefore rotated over  $90^\circ$ . If the cell is placed between crossed polarisers, the linearly polarised light entering the cell is rotated and transmitted through the second polariser (the analyser) and the cell appears transparent. Between parallel polarisers, the analyser blocks the light and the cell appears dark. Planar and homeotropic configurations show the opposite behaviour. Due to the absence of a twist, the polarisation direction is not modulated and the cells appear dark between crossed polarisers and bright between parallel polarisers. The rotation of the polarisation direction in twisted cells is more accurately described when the ellipticity ( $\chi$ ) of the light is taken into account<sup>38,39</sup>. This can be analytically represented as<sup>40</sup>:

$$\begin{aligned}
 \chi(z) &= u(z)e^{i2\varphi z/d} \\
 u(z) &= \frac{[\beta - i \tan(\varphi\beta z/d)]u_0 - i\alpha \tan(\varphi\beta z/d)}{-i\alpha \tan(\varphi\beta z/d)u_0 + \beta + i \tan(\varphi\beta z/d)} \\
 \beta &= \sqrt{1 + \alpha^2}, \alpha = \frac{\pi d \Delta n}{\varphi \lambda}
 \end{aligned}
 \tag{3.4}$$

In this equation,  $\varphi$  is the twist angle,  $d$  is the cell thickness,  $z$  is the position in the LC layer,  $u(z)$  is the ellipticity at distance  $z$ ,  $u_0$  is the ellipticity of the polarisation state at the beginning of the cell.  $\Delta n$  is the birefringence (liquid crystal are birefringent, due to their anisotropic shape they have a different refractive index for the ordinary polarisation direction ( $n_o$ , perpendicular to the director) and the extraordinary polarisation direction ( $n_e$ , parallel to the director) of light). The birefringence is given by:

$$\Delta n = n_e - n_o \quad (3.5)$$

When the cell thickness is not chosen right, the outgoing light does not remain linearly polarised inside the twisted LC layer, but becomes elliptically polarised. With the right cell thickness, the polarisation modulation can be tuned, so that the outgoing light remains linearly polarised and the cell behaves as described above. These optimised cells are said to be in the Mauguin limit, which is described by:

$$\frac{\pi d \Delta n}{\varphi \lambda} \gg 1 \quad (3.6)$$

Optimising the cell thickness (by optimising  $d\Delta n/\lambda$ ) for a  $90^\circ$  in equation 3.4 should result in  $u_{z=d} = u_0$ . The result of this optimisation results in a  $d\Delta n/\lambda$  series with maximum transmission:

$$\begin{aligned} \frac{d\Delta n}{\lambda} &= \sqrt{N^2 - \frac{1}{4}} \\ N &= 1, 2, 3, \dots \end{aligned} \quad (3.7)$$

This equation is valid for all for all values of  $u_0$ . Cells agreeing with this condition are at the  $N^{\text{th}}$  Gooch-Tarry maximum<sup>41</sup>. Practically, this means that these optimised cells have a maximum transmission between crossed polarisers:

$$\begin{aligned} T_{90^\circ \text{ twisted}} &= \frac{I}{I_0} = 1 - \frac{\sin^2\left(\frac{1}{2}\pi\sqrt{1+u^2}\right)}{1+u^2} \\ u &= \frac{d\Delta n}{\lambda} \end{aligned} \quad (3.8)$$

For uniaxial planar cells, the Gooch-Tarry maximums are usually determined in the case of a cell placed between crossed polarisers under an angle of  $45^\circ$  to the optical axes of the polarisers (this is related to switching characteristics of these cells, see chapter 4)<sup>42,43</sup>. The transmitted intensity as a function of the (corrected) thickness ( $d\Delta n/\lambda$ ) for this situation is<sup>41,43,44</sup>:

$$T_{\text{planar}} = \frac{I}{I_0} = \sin^2\left(\frac{\pi d\Delta n}{\lambda}\right) \quad (3.9)$$

### 3.3 Experimental

#### 3.3.1 Materials

Polyimide precursor AL1051 was obtained from JSR Electronics (see paragraph 2.2.1). The coating and curing was performed as described in paragraph 2.2.1. The LC material used was E7 ( $T_{N-I} = 59.8^\circ\text{C}$ ,  $\epsilon_{\perp} = 5.2$ ,  $\epsilon_{\parallel} = 19$ ,  $\Delta n = 0.2246$ ), a mixture of one cyanoterphenyl and three cyanobiphenyl components (see figure 3.5), obtained from Merck Ltd.

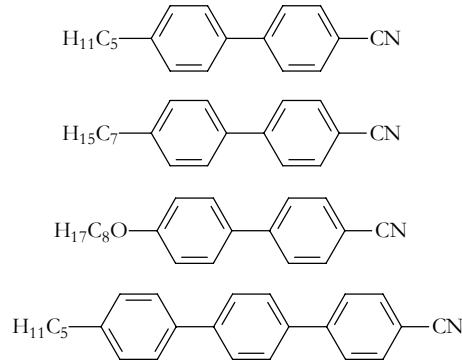


Figure 3.5 The chemical structures of the components in liquid crystal mixture E7

#### 3.3.2 Direct focused laser writing

The direct focused laser writing was performed with the same setup as described in chapter 2.2.2. The laser power (measured internally, at the head of the laser) was set to 500 mW. Due to losses on the optics, this resulted to a power of 212 mW after the focusing lens. The writing speed was set to 1 mm/s. With these settings the laser writing was performed in the melting regime at a power density of  $2.1 \times 10^{11} \text{ W/m}^2$ .

### 3.3.3 Cell design

Electro-optical cells were constructed with several configurations, which are extensively described in paragraph 3.4. Rubbed orientation was induced by uniaxial rubbing of the polyimide coated substrates with a cloth. After rubbing, this polyimide induces uniaxial alignment with strong anchoring. Two 2.5 x 2.5 cm plates of (patterned or non-patterned) polyimide on glass were attached to each other by application of a UV curable glue (Norland UV Sealant 91) at the edges and cured under pressure. The sealant is provided with 6  $\mu\text{m}$  cylindrical glass spacer particles, which determines the cell gap. This cell gap is optimised to be in the Mauguin limit ( $d = 6 \mu\text{m}$ ,  $\Delta n = 0.2246$  and  $\lambda = 550 \text{ nm}$ , resulting in  $d\Delta n/\lambda = 2.5$ ). The cells were capillary filled with LC material at 80 °C, 20 °C above the nematic – isotropic transition temperature of LC material E7.

### 3.3.4 Characterisation

Polyimide layer thickness was determined using a Tencor P-10 Profilometer. Light absorption of the polyimide layer was determined by UV-VIS-NIR scanning spectroscopy (Shimadzu UV-3102 PC). The dimensions of the lines were studied by light microscopy (Zeiss Universal), Environmental Scanning Electron Microscopy (Philips XL30 FEG-ESEM) and Atomic Force Microscopy (Digital Instruments Dimension 3100). The optical properties of the cells were examined by placing them between crossed and planar polarisers. Visual inspection and a digital photo camera were used to study macroscopic effects. Microscopic effects were studied by polarised light microscopy (Zeiss Universal, mounted with a photcamera and Zeiss Axioplan 2 mounted with a CCD camera). Contrasts between the written and non-written sections of the cell between crossed polarisers were measured using a HeNe laser (Melles Griot, model 05-LHP-991, 30 mW, 633.8 nm), an integrating sphere (Newport, model 819) and a power meter and detector (Newport, models 1815 C and 818-UV).

## 3.4 Results and discussion

### 3.4.1. Cell design

The influence of laser-melted patterns on the alignment of LC in the system is studied in optical cells that consist of a twisted nematic LC layer aligned by two (usually rubbed) polyimide orientation layers. The rubbing process induces a uniaxial alignment with near-zero pre-tilt and strong anchoring on the used polyimide. The  $d\Delta n/\lambda$  value of these

cells is 2.5 ( $d = 6 \mu\text{m}$ ,  $\Delta n = 0.2246$  and  $\lambda = 550 \text{ nm}$ ). These cells are in the Mauguin limit (equation 3.6) and are optimised for the planar configuration. Patterns are generated on one or both orientation layers by laser melting. The effects of the laser melting on the anchoring strength (equation 3.3) and the deformation free energy (equation 3.2) are described in this chapter and are illustrated by polarised optical micrographs that show the LC alignment in these cells.

### 3.4.2 Liquid crystal orientation at laser-written surface patterns in non-rubbed polyimide

Chapter 2 showed that laser melting induces relief structures into polyimides. The geometry of these relief structures depends on the laser power density used and on the writing velocity i.e. both structures with and without a large central plateau are generated (see figure 2.6 and 2.7). Flow patterns during and relief structures after the melting process might cause a molecular orientation of the polyimide, which could result in a change in LC alignment properties. To study the LC aligning properties of laser-melted patterns on polyimide substrates cells were constructed (with a cell thickness of  $6 \mu\text{m}$ ). These cells contained two non-rubbed polyimide layers, one of which with a laser-melted pattern (20-30 lines, each with a width of  $20 \mu\text{m}$ , per millimetre). Using polarised optical microscopy, the LC alignment within the optical cell was visualised. Great care was taken to ensure that cell construction and filling are done properly, to avoid features originating from the sheer flow during the capillary flow process.

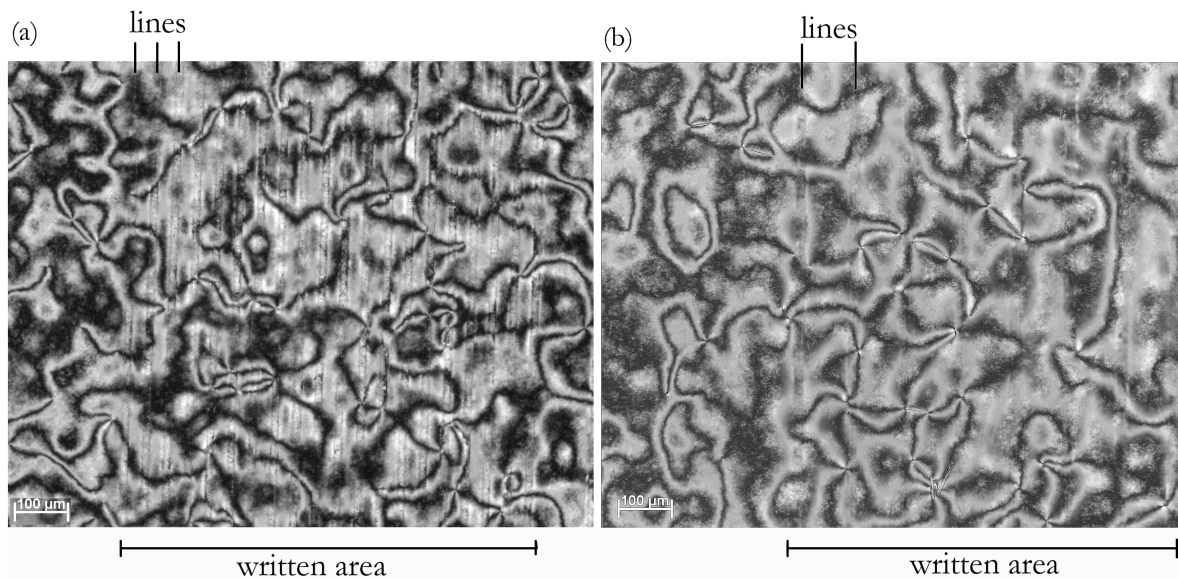


Figure 3.6 Optical micrographs between crossed polarisers of cells with two non-rubbed orientation layers; laser-melted lines written at: (a)  $2.1 \times 10^{11} \text{ W/m}^2$  and  $1 \text{ mm/s}$ , no central plateau, (b)  $3.5 \times 10^{11} \text{ W/m}^2$  and  $1 \text{ mm/s}$ , with central plateau

Figure 3.6 shows polarised optical micrograph of non-rubbed, laser-written cells. Because the polyimide was not rubbed, the LC molecules do not have a preferred orientation, as can be seen by the disclination lines, which indicate a typical non-aligned macroscopic nematic order. Above the laser-melted lines the disclinations are not disturbed, indicating that the lines themselves do not influence the LC alignment. Lines were written in different directions with respect to each other (horizontal, vertical and diagonal). No effect on the LC alignment was observed for any of the writing directions. Also, the width of the laser-melted lines or the presence of a central plateau (figure 3.6b) in the lines did not have an influence on the LC alignment. Multi-domain birefringent behaviour was observed in the cell. This indicates that the liquid molecules predominantly have an inhomogeneous planar orientation with varying director orientation. However, also tilt angle variations might be present in the different domains.

It was reported in literature that regular, homogeneously shaped, grooved relief structures (depth of tens of nanometres, width and line spacing of several microns) induce liquid crystal alignment in isotropic polymers<sup>3,6,7,36,45-47</sup>. However, the patterns described in this paragraph seem to indicate that these specific patterns do not influence the LC alignment. This is very likely due to the inhomogeneous shape (humps and holes) and the different dimensions (depth and height of 50-100 nm and a width of tens of microns) of the relief structures and the low line density of the patterns.

### 3.4.3 Liquid crystal orientation at laser-written surface patterns in rubbed polyimide

In chapter 2 and in the previous paragraph laser melting was performed on non-rubbed polyimide. The dependence of the line width on the writing speed and laser power density did not change when rubbed polyimides were used. The rubbed surface or the rubbing direction did not influence the regime boundaries and the resulting line geometry.

Figure 3.7 shows an interesting aspect of the laser-melted structures. This structure was written at slow speed (0.1 mm/s) and at a power density high in the melting regime ( $3.5 \times 10^{11}$  W/m<sup>2</sup>) to form an extended central plateau. The small depressions outside and perpendicular to the laser-melted line are several nanometre sized grooves that are caused by the rubbing process that might contribute to topographic LC aligning properties of the polyimide<sup>5,14</sup>. In the central plateau in figure 3.7 the rubbing grooves have disappeared, which indicates that the surface of the polyimide was indeed melted and subsequently resolidified, losing its original surface texture and, most probably, its molecular orientation.

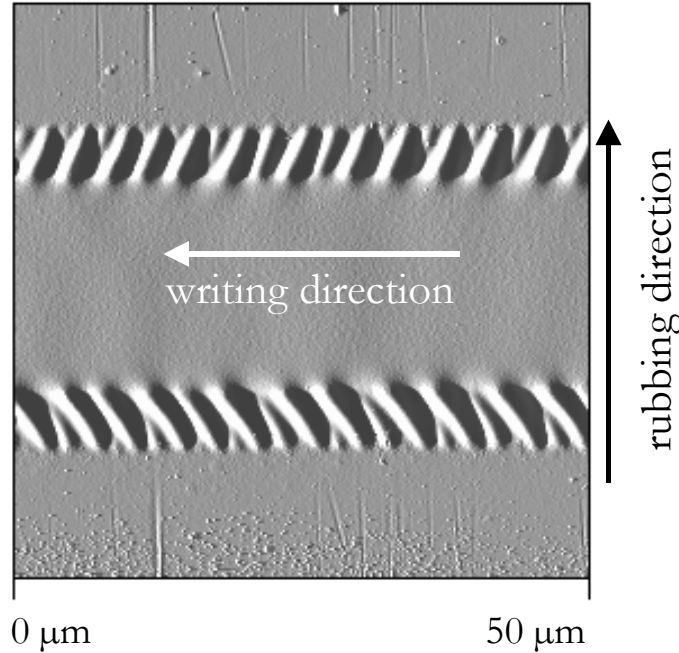


Figure 3.7 AFM height image of laser-melted patterns ( $3.5 \times 10^{11} \text{ W/m}^2$ ,  $0.1 \text{ mm/s}$ ) in rubbed polyimide

To investigate if laser-melted patterns influence the aligning properties of rubbed polyimides, optical cells were constructed with two rubbed polyimide layers perpendicular to each other ( $d\Delta n/\lambda = 2.5$ ). This causes the liquid crystals that are added to the cell to align in a  $90^\circ$  twist over the thickness of the cell, the twisted nematic (TN) configuration. A laser-melted pattern (written with a power density of  $2.1 \times 10^{11} \text{ W/m}^2$  and a speed of  $1 \text{ mm/s}$ ) was present on one orientation layer.

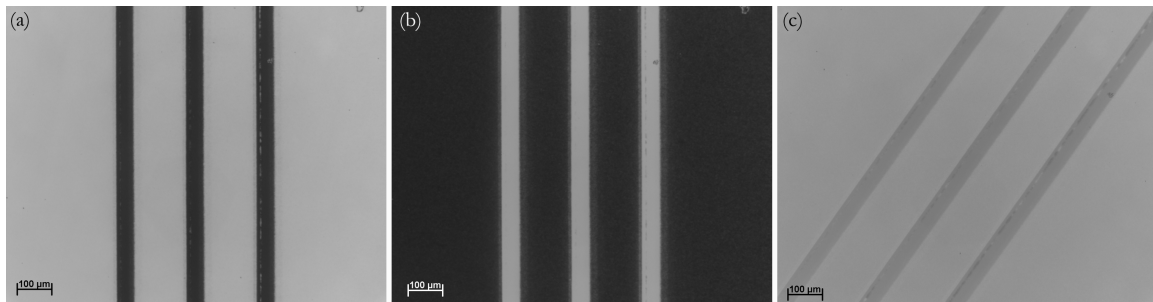


Figure 3.8 Polarised optical micrographs of a cell with a one side written configuration. (a) crossed polarisers, (b) parallel polarisers, (c) sample turned  $45^\circ$  between crossed polarisers

Figure 3.8 shows polarised optical micrographs of this configuration. The non-written sections of the cell show normal TN behavior: transparent between crossed polarisers (figure 3.8a). However, the written sections ( $100 \mu\text{m}$  spaced parallel lines) are dark. The optical contrast, measured in transmission between crossed polarisers, between the



patterned and non-patterned sections of the cell ranged between 40 and 50. Figure 3.8b shows that between parallel polarisers exactly the opposite occurs, the laser-melted lines are transparent, while the non-written sections are dark. By rotating the polarisers the appearance of the whole cell is inverted. If the cell is placed under an angle of  $45^\circ$  between crossed polarisers, contrast between the lines and the non-written area is still present (figure 3.8c). The patterned lines show birefringent behaviour, indicating that a planar orientation is present (and not a homeotropic state). Optically, the liquid crystals above the patterned lines behave the same as a homogeneously planar oriented system. The writing direction of the lines with respect to the rubbing direction does not have an influence. No difference in the LC alignment was observed above lines that were written perpendicular and parallel to the rubbing direction.

As was determined in the previous paragraph, the lines themselves do not induce an LC alignment (due to the shape and dimensions of the lines and the low line density of the pattern). We hypothesise that at the laser-melted patterns the strong anchoring is broken, reducing the azimuthal anchoring strength ( $W_a$  in equation 3.3). With two equally strong anchoring orientation layers placed with their aligning axes perpendicular to each other, the twist contribution ( $K_2$ ) of the deformation free energy density function (equation 3.2) is high and the liquid crystals are stacked in a twisted configuration. When the anchoring of one of the substrates is lowered or removed, the twist constant becomes negligible and the liquid crystal director follows the direction imposed by the opposite, non-treated orientation layer. Therefore, in our case, the LC molecules align themselves homogeneously planar (with a near-zero tilt angle) above the laser-melted patterns in the aligning direction of the (strong anchoring) opposite orientation layer (see figure 3.9). This hypothesis accurately describes the observed phenomena, since there is no twist at the laser-melted patterns (but the patterns do show birefringent behaviour), the polarisation direction of the light is not changed and the second polariser, in the case of crossed polarisers, blocks the light. Placing the polarisers with their optical axes parallel to each other, results in transmission through the second polariser at the laser-melted sections of the cell, while the second polariser blocks the light guided through the twisted, non-written surroundings.

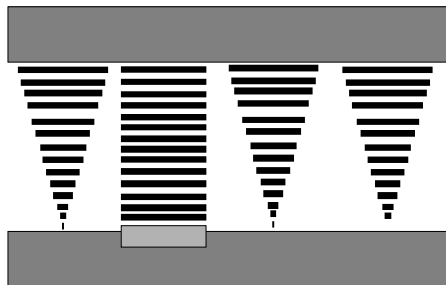


Figure 3.9 Schematic representation of a one-side written cell

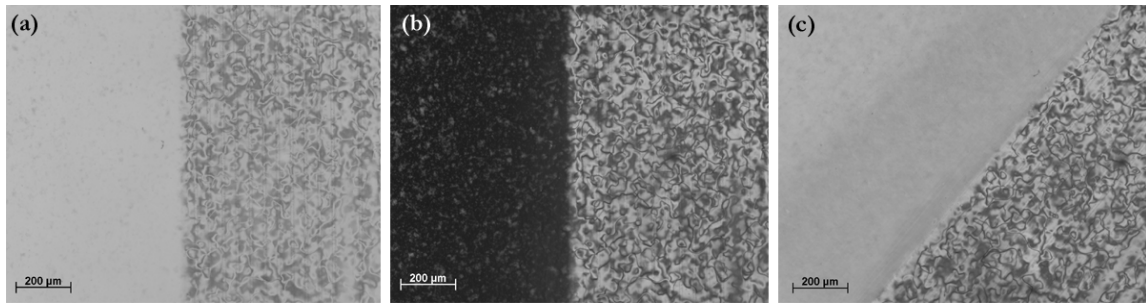


Figure 3.10 Laser-written rubbed – non-rubbed configuration. The right sides of the micrographs are the laser-written areas. (a) parallel polarisers, (b) crossed polarisers, (c) sample under  $45^\circ$  between crossed polarisers

To check the hypothesis, a cell was constructed with on one side a rubbed and on the other side a non-rubbed polyimide. Laser-melted patterns were written on the rubbed side. Figure 3.10 demonstrates that at the location of the written lines (right side of the micrographs), the multidomain nematic texture of the LC layer is clearly visible. Next to the written lines, where the orientation layer is still unaffected, a planar orientation is observed. The rubbed area of the polyimide imposes uniaxial alignment to the liquid crystal, although still containing some imperfections and defects because of strong anchoring at the opposite side. Where the surface anchoring in the polyimide was broken by the melting process, the liquid crystal layer was not directed at both sides, leading to the multidomain Schlieren texture.

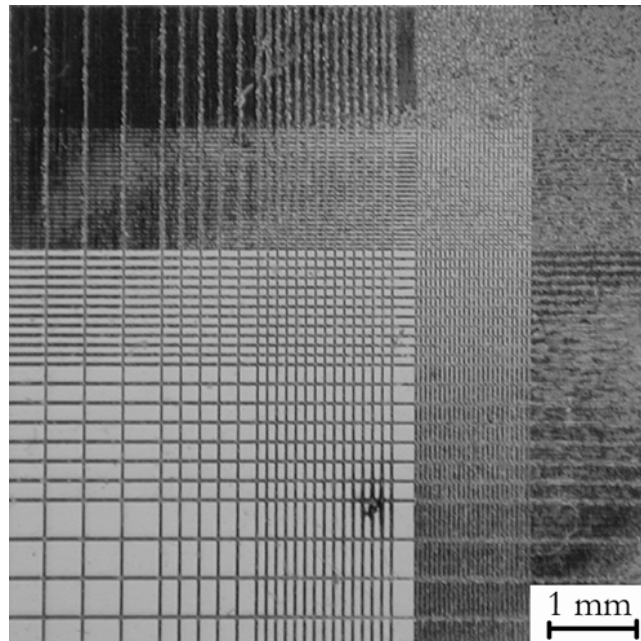


Figure 3.11 Photograph of a cell with on both side a rubbed polyimide with a laser-written pattern, between crossed polarisers

The next cell that was constructed consisted of two rubbed polyimide orientation layers, which both had an identical laser-melted pattern on them. The patterns consisted of parallel lines, with varying series line spacings (defined as the distance between the centre of two adjoining parallel lines; in this case: 800  $\mu\text{m}$ , 400  $\mu\text{m}$ , 200  $\mu\text{m}$ , 100  $\mu\text{m}$  and 50  $\mu\text{m}$ ). The two orientation layers were placed with their rubbing directions perpendicular to each other, creating a TN configuration in the non-written areas of the cell. The two overlapping line patterns formed a grid structure with combinations of all line spacings with each other (e.g. 200x200, 400x100, 800x50, 100x100, 50x50, etc.). Figure 3.11 shows the complete grid pattern within the cell. Several areas can be distinguished: non-written sections, sections with on one side a laser-written pattern and sections with on both sides a laser-written pattern. These sections are clearer in figure 3.12, which zooms in on some sections of this cell.

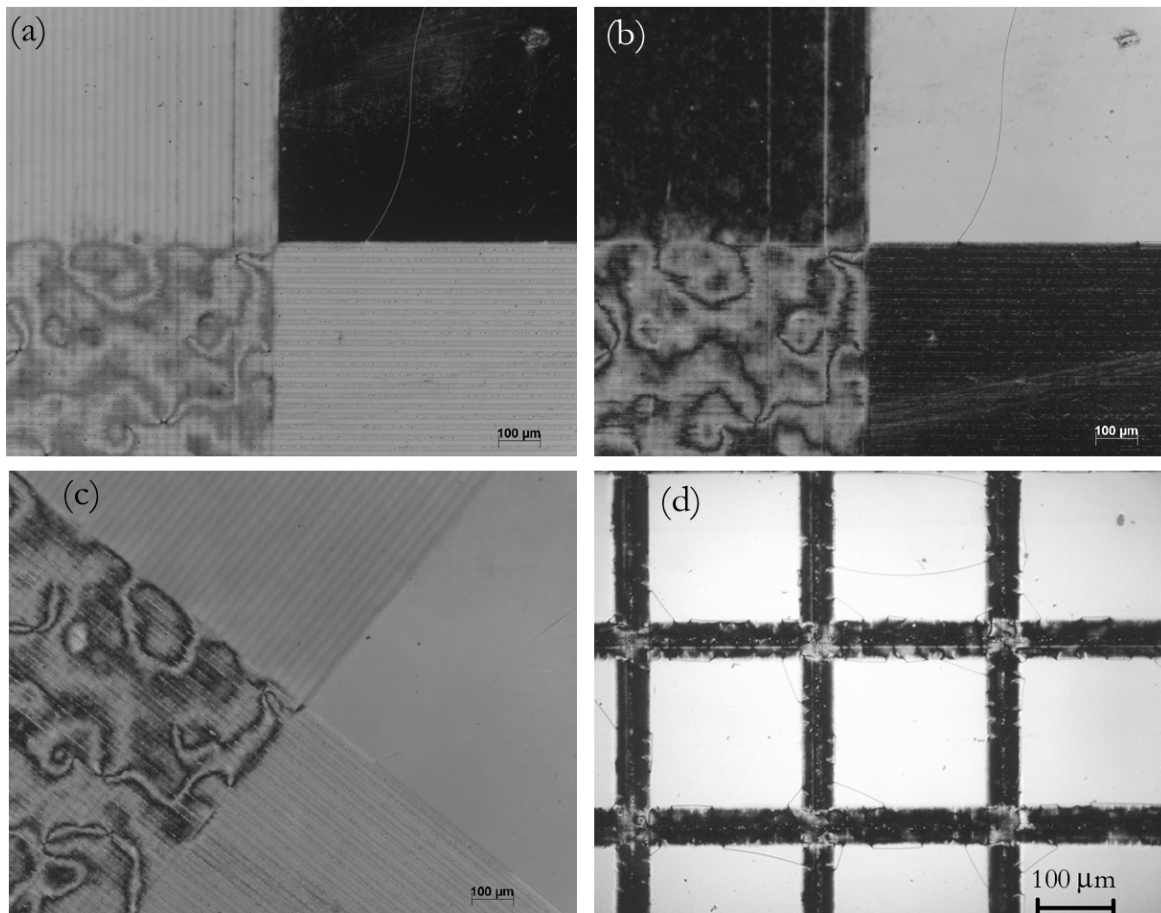


Figure 3.12 Polarised optical micrographs of a two-sides laser-written hybrid TN-cell. 50x50  $\mu\text{m}$  grid: (a) parallel polarisers, (b) crossed polarisers, (c) sample turned 45°, crossed polarisers, (d) 400x400  $\mu\text{m}$  grid: crossed polarisers

In the non-written sections the LC layer retained its 90° twist, these are the top right areas in figures 3.12a and 3.12b and the bright areas in figure 3.12d. The sections with only on one

side a laser-melted pattern show the same effect as mentioned before: due to lowering of the anchoring at the written areas, the LC molecules orient themselves according to the still strong anchoring, unaffected opposite orientation layer. The result is that at these sections the LC layer has a homogeneously planar configuration in the direction of the aligning axis of the rubbed polyimide. There are two different homogeneously planar configurations present within the cell. These two areas have an alignment perpendicular to each other, depending on the side on which the laser-melted pattern is present, but are visually indistinguishable from each other. In figure 3.12a, the two regions are the bright areas at the top left and bottom right of the micrograph. In figure 3.12d, the dark horizontal and vertical lines represent the homogeneously planar aligned areas. The third area within this type of cell is in the sections where there the laser-melted patterns on both sides overlap. This situation is very similar to the non-rubbed configuration described earlier. On both orientation layers the strong anchoring is broken and therefore, the LC layer is not aligned from either side, resulting in a typical nematic texture. This is visible in figure 3.12: in figures 3.12a and 3.12b, the nematic texture is clearly visible in the bottom left region of the micrographs. If the sample is turned 45°, as is shown in figure 3.12c, the nematic texture remains clearly visible. In figure 3.12d, the non-aligned areas are the places where the horizontal and vertical lines cross each other. Figure 3.13 shows a schematic overview of all the different regions that were obtained within one hybrid cell of this type.

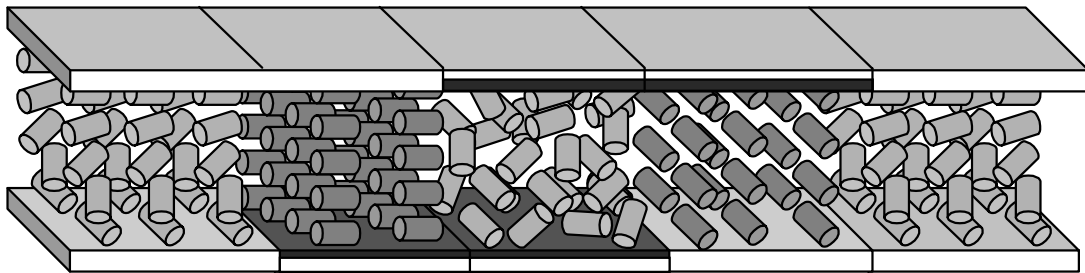


Figure 3.13 Schematic representation of a hybrid TN cell with on both sides a rubbed polyimide with a laser melted pattern. From left to right: TN, planar-1, non-aligned, planar-2, TN

The lines start touching each other below a line spacing of 50  $\mu\text{m}$  and larger continuous areas are formed where the orientation is removed. At these sections the LC exhibits a homogeneously planar orientation, except if on the other side also melted lines or zones are present. There, the LC alignment breaks up in domains with uncontrolled director patterns (e.g. the top right area in figure 3.11 or the lower left areas in figures 3.12a and 3.12b). By writing touching or overlapping lines, larger patterns up to millimetres or centimetres are obtained.

The laser melting process is not reversible for any of the above-mentioned configurations. The relief structures and other chemical or physical changes are permanent. This eliminates the possibility that this type of patterning can be used for rewritable optical data storage. Laser-melted, rubbed polyimide orientation layers can potentially be used in liquid crystal displays and for personalised security features, which is discussed in the next chapter.

#### 3.4.4 Transmittance measurements

The transmitted intensity as a function of the corrected thickness ( $d\Delta n/\lambda$ ) for a planar and a  $90^\circ$  twisted cell is given in equations 3.8 and 3.9 and plotted in so-called Gooch-Tarry curves<sup>41,43,44</sup> for the used  $d\Delta n/\lambda$  value of 2.5 (figure 3.14). Several maximums and minimums are present, which indicates that there is maximum transmission for several values of  $d\Delta n/\lambda$ . All the cells were constructed with  $d\Delta n/\lambda$  value of 2.5, which means they are optimised for the planar situation and are in the 3<sup>rd</sup> Gooch-Tarry maximum. As a result, the transmitted intensity is not optimised at these values for a  $90^\circ$  twisted configuration.

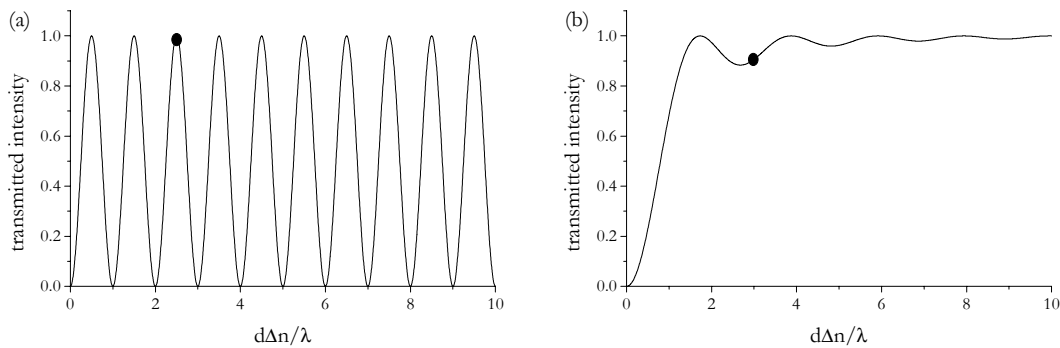


Figure 3.14 Gooch-Tarry curves (a) planar cell placed  $45^\circ$  between crossed polarisers, (b)  $90^\circ$  twisted cell between crossed polarisers (the dots indicate the position that are valid for the cells used in this chapter)

The Gooch-Tarry curves (figure 3.6) predict the transmitted intensity for the planar and twisted configuration. Therefore, the transmittance was experimentally determined on a TN cell with on one polyimide layer a laser-melted pattern. The pattern consisted of 50 touching lines (each with a width of  $50 \mu\text{m}$  and a length of  $2.5 \text{ mm}$ ) that form a  $2.5 \times 2.5 \text{ mm}$  area that covered the full measuring spot. The maximum transmittance through the brightest area in the cells between polarisers was determined as a reference ( $100 \%$  transmittance), followed by transmittance measurements inside and outside the laser-written patterns. The transmittance of the homogeneously planar aligned areas was determined in two ways. The first was between parallel polarisers, which resulted in a transmittance of  $91 \pm 3 \%$ . This

value is not 100 %, due to reflectance and/or some ‘leakage’ through the small spaces between the lines, which have a twisted configuration. The second measurement was conducted with the cell placed under an angle of  $45^\circ$  between crossed polarisers. In this case the transmittance was  $89 \% \pm 3 \%$ . The calculated value was 100 % (transmitted intensity = 1, indicated by the black dot in figure 3.14a). Again, the difference between the measured and the calculated values can be explained by reflectance and leakage through the spaces between the lines in the pattern. The transmittance of the twisted areas was measured with the cell placed between crossed polarisers. The resulting transmittance was  $86 \pm 3 \%$ , which agrees with the calculated transmitted intensity of 0.89 (see the black dot in figure 3.14b). The measured and calculated transmittance are in agreement for all configurations.

### 3.5 Conclusions

With direct focused laser writing in rubbed polyimide orientation layers in the melting regime, it is possible to locally remove the LC alignment properties of the material. We hypothesised that breaking the azimuthal anchoring strength (equation 3.3) of one orientation layer, liquid crystal areas with a locally different configuration are created. In cells where the liquid crystal is confined between two alignment layers, due to the elastic free energy (equation 3.2), the liquid crystals orient themselves uniaxially at the location where one of alignment layers is inactivated by laser writing. The liquid crystal director follows the direction imposed by the opposite orientation layer. If the opposite orientation layer itself does not induce an orientation (e.g. because it was not rubbed or there are laser-melted patterns on the opposite side), the LC material does not show homogeneous alignment but breaks up into a multi-domain texture. Polarised optical microscopy and transmittance measurements showed that this hypothesis explains the observed behaviour in all investigated cell configurations.

### 3.6 References

- [1] C. Mauguin, *B. Soc. Franc. Miner.* **34**, 71, (1911).
- [2] T. Uchida, *SID 96 Digest*, 31, (1996).
- [3] B. Jerome, *Rep. Prog. Phys.* **54**, 391, (1991).
- [4] H. Matsuda, D.-S. Seo, N. Yoshida, K. Fujibayashi, S. Kobayashi, *Mol. Cryst. Liq. Cryst.* **264**, 23, (1995).
- [5] D. W. Berreman, *Phys. Rev. Lett.* **28**, 1863, (1972).
- [6] H. Niino, Y. Kawabata, A. Yabe, *Jpn. J. Appl. Phys.* **28**, L2225, (1989).

- [7] C. J. Newsome, M. O'Neill, R. J. Farley, G. P. Bryan-Brown, *Appl. Phys. Lett.* **72**, 2078, (1998).
- [8] M. Ishiyama, T. Tanaka, M. Sato, T. Uchida, H. Seki, *IDW'00*, 97, (2000).
- [9] M. Schadt, H. Seiberle, A. Schuster, *Nature* **381**, 212, (1996).
- [10] P. Chaudhari, J. Lacey, J. Doyle, E. Galligan, S. C. A. Lien, A. Callegari, G. Hougham, N. D. Lang, P. S. Andry, R. John, K. H. Yang, M. H. Lu, C. Cai, J. Speidell, S. Purushothaman, J. Ritsko, M. Samant, J. Stohr, Y. Nakagawa, Y. Katoh, Y. Saitoh, K. Sakai, H. Satoh, S. Odahara, H. Nakano, J. Nakagaki, Y. Shiota, *Nature* **411**, 56, (2001).
- [11] K. H. Yang, *Jpn. J. Appl. Phys.* **31**, L1603, (1992).
- [12] J. Chen, P. J. Bos, D. R. Bryant, D. L. Johnson, S. H. Jamal, J. R. Kelly, *Appl. Phys. Lett.* **67**, 1990, (1995).
- [13] M. Schadt, H. Seiberle, *Patent WO 9852077*, (1998).
- [14] D. W. Berreman, *Mol. Cryst. Liq. Cryst.* **23**, 215, (1973).
- [15] C. W. Oseen, *Trans. Farad. Soc.* **29**, 883, (1933).
- [16] P. G. de Gennes, *The Physics of Liquid Crystals*, Clarendon Press, Oxford, (1974).
- [17] G. Vertogen, W. H. de Jeu, *Thermotropic Liquid Crystals, Fundamentals, Vol. 45*, Springer, Berlin, (1987).
- [18] image taken from: J. van Haaren, *Course Display Techniques, Basic Physics and New Developments in Liquid Crystal Displays (syllabus)*, (2001)
- [19] B. Jerome, in D. Demus, J. W. Goodby, G. W. Gray, H. W. Spies, V. Vill (Eds.): *Handbook of Liquid Crystals, vol. 1: Fundamentals*, Wiley-VCH, Weinheim, (1998).
- [20] T. J. Sluckin, A. Poniewierski, in C. A. Croxton (Ed.): *Fluid Interfacial Phenomena*, p. 215 , Wiley, New York, (1986).
- [21] A. A. Sonin, *The Surface Physics of Liquid Crystals*, Gordon and Breach, Amsterdam, (1995).
- [22] F. M. Leslie, in D. Demus, J. Goodby, G. W. Gray (Eds.): *Handbook of Liquid Crystals, Vol. 1: Fundamentals*, p. 25 , Wiley-VCH Verlag GmbH, Berlin, (1998).
- [23] J. Cognard, *Molec. Cryst. Liq. Cryst. Suppl.* **1**, 1, (1982).
- [24] A. Rapini, M. Papoular, *Journal de Physique (Paris), Colloque* **30**, 54, (1969).
- [25] Y. Ouchi, M. B. Feller, T. Moses, Y. R. Shen, *Phys. Rev. Lett.* **68**, 3040, (1992).
- [26] G. P. Crawford, D. K. Yang, S. Zumer, D. Finotello, J. W. Doane, *Phys. Rev. Lett.* **66**, 720, (1991).
- [27] B. O. Myrvold, *Liq. Cryst.* **18**, 287, (1995).
- [28] N. A. Clark, *Phys. Rev. Lett.* **55**, 292, (1985).
- [29] M. B. Feller, W. Chen, Y. R. Shen, *Phys. Rev. A* **43**, 6778, (1991).
- [30] M. Barmantlo, R. W. J. Hollering, N. A. J. M. van Aerle, *Phys. Rev. A* **46**, 4490, (1982).
- [31] P. G. de Gennes, *Mol. Cryst. Liq. Cryst.* **12**, 193, (1971).
- [32] J. Y. Huang, Y. R. Superfine, Y. R. Shen, *Phys. Rev. A* **42**, 3660, (1990).
- [33] K. Hiltrop, H. Stegemeyer, *Ber. Bunsenges. Phys. chem.* **85**, 582, (1981).

- [34] G. Porte, *J. Phys. France* **37**, 1245, (1976).
- [35] W. Chen, M. Feller, Y. R. Shen, *Phys. Rev. Lett.* **63**, 2665, (1989).
- [36] M. Nakamura, M. Ura, *J. Appl. Phys.* **52**, 210, (1981).
- [37] M. Schadt, W. Helfrich, *Appl. Phys. Lett.* **18**, 127, (1971).
- [38] E. Hecht, *Optics, 2nd edition*, Addison-Wesley, Reading, (1987).
- [39] E. E. Wahlstrom, *Optical Crystallography, 5th edition*, Wiley, New York, (1979).
- [40] R. M. A. Azzam, N. M. Bashara, *J. Opt. Soc. Am.* **62**, 222, (1972).
- [41] C. H. Gooch, H. A. Tarry, *J. Phys. D* **8**, 1575, (1975).
- [42] J. van Haaren, *Course Display Techniques, Basic Physics and New Developments in Liquid Crystal Displays (syllabus)*, (2001)
- [43] I. C. Sage, in D. Demus, J. Goodby, G. W. Gray (Eds.): *Handbook of Liquid Crystals, Vol. 1: Fundamentals*, p. 731, Wiley-VCH Verlag GmbH, Berlin, (1998).
- [44] P. Yeh, *Optical Waves in Layered Media*, Wiley, New York, (1988).
- [45] J. B. Cooper, B. Julian, H. Morrison, P. Song, S. Albin, J. L. Zhen, *Thin Solid Films* **303**, 180, (1997).
- [46] M. H. Kim, J. D. Kim, T. Fukuda, H. Matsuda, *Liq. Cryst.* **27**, 1633, (2000).
- [47] M. Nishikawa, J. L. West, *Jpn. J. Appl. Phys.* **38**, 5183, (1999).





## Chapter 4

# Laser-written Polyimides in Electro-Optical Switches\*

### 4.1 Introduction

Electro-optical switches, such as liquid crystal displays (LCD's) are extensively used for the display of electronic data. Liquid crystal orientation layers are a crucial component of LCD's. Rubbed polyimides are the material that is the current industry standard for aligning the liquid crystals. In this chapter we will give two examples of laser-written patterns in polyimides that are used to control liquid crystal alignment in some specific LCD designs. In addition, we will demonstrate the use of this technology for personalised security features.

In the previous chapter we showed how LC alignment is affected by laser melting and the resulting effects on the polarisation optics. Now we elaborate these principles further such that they can be successfully applied in actual LCD designs based on twisted nematic (TN) LC effects. Thereto, we constructed cells with laser-melted patterns and that can be electrically switched and we studied the effects of the switching on the liquid crystal alignment above the laser-melted patterns. The patterned TN cells are also adapted and evaluated for use as personalised security features for e.g. credit cards. Moreover, chapter 2 showed how electrically conductive patterns are directly written in polyimide films in the pyrolysis regime. By laser patterning a rubbed polyimide orientation layer in the pyrolysis regime, the electrical pathways can be directly written in the orientation layer. Now, we also investigate whether the combination of electrical conductivity and high optical absorption of the conductive carbon patterns on polyimide substrates can be further exploited for use in flexible cholesteric texture liquid crystal displays (CTLCD's). In this specific reflective LCD design, the black colour of the lines is an advantage. Also, we attempt to reduce several inorganic and organic functional layers to a single polymeric substrate. The next paragraph gives an overview about the operation of the types of LCD's relevant to this chapter; such as TN LCD's and cholesteric texture LCD's (CTLCD).

---

\* Part of this work has been published: D.J. Versteeg, C.W.M. Bastiaansen, D.J. Broer, *Proceedings ID/IDW'01* (Nagoya, Japan), 65, (2001); D.J. Versteeg, C.W.M. Bastiaansen, D.J. Broer, *J. Appl. Phys.* **91**, 4191, (2002).

## 4.2 Electro-optical switches

### 4.2.1 Twisted nematic liquid crystal displays

In the early 1970s, the discovery and development of the twisted nematic (TN) effect in liquid crystals<sup>1</sup> revolutionised the display technology. TN displays proved to be cheap, convenient and versatile devices for use in small area, flat and low-energy consuming applications, such as calculator screens, mobile phone displays and other simple information displays on numerous electronic devices. Since then, TN displays have been developed further and currently the majority of commercially applied liquid crystal displays (LCD's) still make use of improved versions of the original TN concept<sup>2</sup>. Also, liquid crystal displays operating on alternative principles have been successfully introduced<sup>3-8</sup>. The popularity of liquid crystal display devices has increased beyond small area applications. It is gaining a market share for large panel displays. An example is the increasing popularity for LCD screens for use in laptop computers, desktop computer monitors and even television screens. Unfortunately, the complex and expensive fabrication of large panel LCD's is somewhat limiting this growth, but improvements in the production process and LCD design are made continuously.

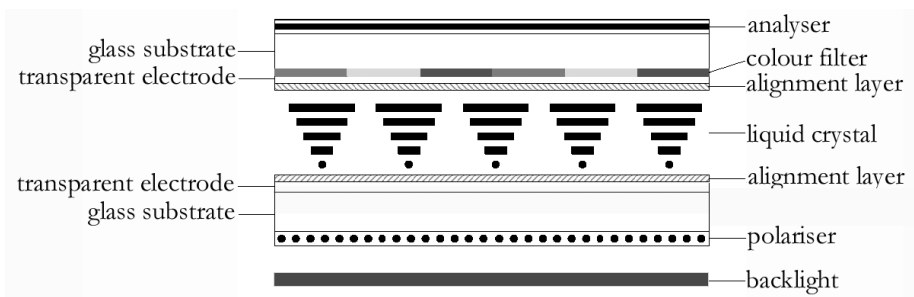


Figure 4.1. Cross-section of an LCD<sup>9</sup>

A TN LCD is made of several functional layers (see figure 4.1)<sup>1,5,10-13</sup>. The LCD is illuminated using a backlight, which is usually a cold cathode fluorescent (CCF) lamp or a light emitting diode (LED). The outermost layers of the cell are a polariser and an analyser, which are placed perpendicular to each other. Glass plates with a thickness of 1 mm are used as the substrates, on which the functional layers are present, although polymer substrates are nowadays used as well. On the substrates a transparent electrode, usually indium tin oxide (ITO), is present. A colour filter array made up of red, blue and green is present on the top substrate. Alignment layers, usually rubbed polyimides<sup>14,15</sup>, coated on both substrates are in direct contact with the liquid crystal (LC), which is sandwiched between the two plates. In a TN configuration the liquid crystals are aligned such that they make a twist over exactly 90

degrees over the thickness of the LC layer<sup>1,16</sup>. A small amount of chiral dopant is added to direct the handedness of the twist and to avoid the formation of multiple domains with opposite twist. The thickness of the LC layer (usually between 4 and 6  $\mu\text{m}$ ) is defined by the use of spherical or cylindrical spacer particles. Each pixel can be electrically addressed to generate a white and black state and a number of grey scales.

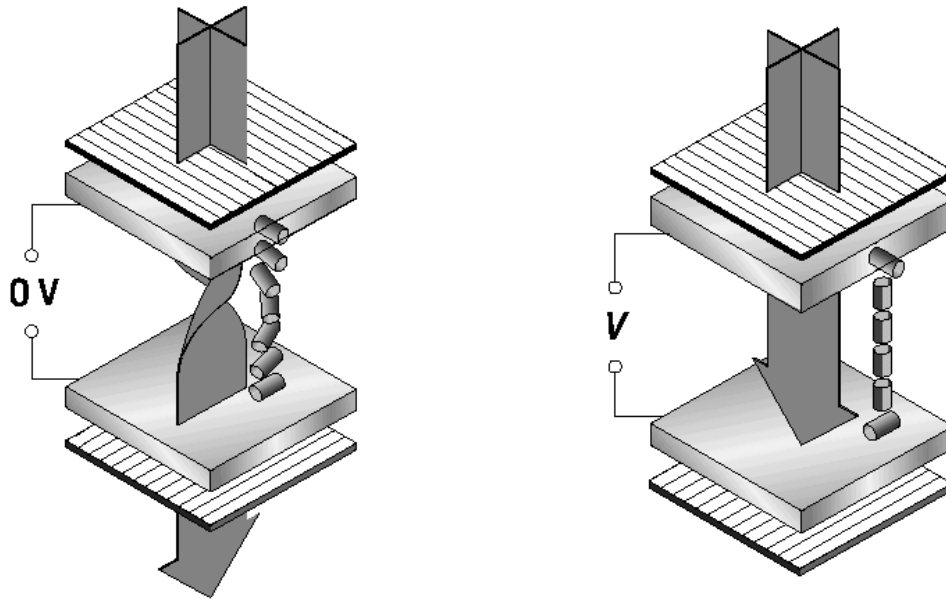


Figure 4.2 TN LCD operation (left: transmissive state; right: dark state)<sup>9</sup>

The operation of a TN LCD is relatively straightforward<sup>1,5,10-13</sup> (see figure 4.2). The cell is placed between two crossed polarisers. The first polariser blocks one of the two polarisation directions of the incoming light. The other polarisation direction is transmitted and enters the cell. Simply stated, the polarisation direction closely follows the director profile of the liquid crystal and is therefore rotated over  $90^\circ$ . The analyser transmits the light and the cell appears transparent. When a voltage is applied over the cell, the liquid molecules orient themselves in the direction of the electric field (Fréedericksz transition)<sup>17</sup>, which is perpendicular to the orientation layers, the so-called homeotropic configuration. As light enters the cell in this case, the polarisation direction is not altered and the second polariser blocks the light. The cell appears dark in this case. After the voltage is removed, the liquid crystal returns to its originally twisted state by the combined action of the surface anchoring and the elastic forces. With this process it is possible to electrically switch between a transparent and a dark state. The actual processes occurring in the cell are more complex than stated above. The rotation of the polarisation direction is more accurately described when the ellipticity of the light is taken into account (see paragraph 3.2). In reality, the

electric response of the liquid crystal is also not as straightforward as mentioned above. Liquid crystals have a dielectric anisotropy ( $\Delta\epsilon$ ):

$$\Delta\epsilon = \epsilon_{\parallel} - \epsilon_{\perp} \quad (4.1)$$

$\epsilon_{\parallel}$  and  $\epsilon_{\perp}$  are the dielectric permittivity for a low-frequency electric field parallel and perpendicular to the director of the liquid crystal. If  $\Delta\epsilon$  is positive, the liquid crystals align themselves parallel to the direction of an applied electric field vector. Liquid crystal molecules in the centre of the cell gap between two alignment layers with strong anchoring will switch to a homeotropic alignment. However, the molecules at the substrate retain their planar alignment (figure 4.3). This induces a mechanical stress into the LC layer, which increases the deformation free energy (equation 3.2).

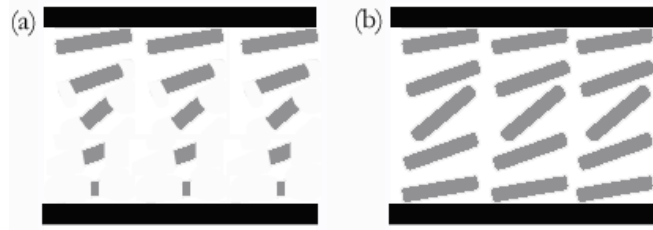


Figure 4.3 Deformation of the liquid crystal layer during electric switching; (a) TN configuration, (b) planar configuration

The dielectric force needs to be larger than the energetic losses due to the mechanical stress to be able to switch a cell<sup>5,13,17</sup>. For  $90^\circ$  twisted cells with a  $0^\circ$  pretilt angle the threshold voltage depends on the elastic constants for splay ( $K_1$ ), twist ( $K_2$ ) and bend ( $K_3$ ), the twist angle  $\phi_t$ , the dielectric constant  $\epsilon_0$  and the dielectric anisotropy  $\Delta\epsilon$ <sup>1,18,19</sup>:

$$V_{\text{threshold}} = \sqrt{\frac{\pi^2 K_1 + \phi_t^2 (K_3 - 2K_2)}{\epsilon_0 \Delta\epsilon}} \quad (4.2)$$

The voltage threshold is determined by measuring the transmission dependence of the voltage. Under an applied voltage, the tilt angle increases. In the centre of the cell, this effect is the strongest. Due to the modulation of the director, the ellipticity of the light changes and the outgoing light does not appear linearly polarised anymore. The resulting loss of transmission depends on the applied voltage. The LC molecules at the boundaries have a less disturbing influence than those in planar cells. This is due to the fact that the molecules at

the boundary are aligned perpendicular to each other, which compensates the retardation. The transmitted intensity as a function of the (corrected) thickness ( $d\Delta n/\lambda$ ) for a  $90^\circ$  twisted cell is (same as in the previous chapter, equation 3.8)<sup>5,20,21</sup>:

$$T_{90^\circ \text{ twisted}} = \frac{I}{I_0} = 1 - \frac{\sin^2\left(\frac{1}{2}\pi\sqrt{1+u^2}\right)}{1+u^2}$$

$$u = \frac{d\Delta n}{\lambda} \quad (4.3)$$

Twisted cells undergo the Fréedericksz transition at a lower threshold voltage than homogeneously planar cells. Extra energy stored in the twist deformation is available for twisted cells<sup>22,23</sup>. The threshold voltage for homogeneously planar cells is only dependent on the splay elastic constant and the dielectric constant and dielectric anisotropy:

$$V_{\text{threshold}} = \pi \sqrt{\frac{K_1}{\epsilon_0 \Delta\epsilon}} \quad (4.4)$$

For planar uniaxial cells, the highest contrast between a non-switched and fully switched state is measured when the cell is placed between crossed polarisers under an angle of  $45^\circ$  to the optical axes of the polarisers<sup>5,24</sup>. When an electric field is placed over the cell, the optical retardation of the LC layer is lowered and the transmitted intensity through the crossed polarisers decreases. The LC molecules in contact with the alignment layers retain their planar orientation, which results in a lower transmitted intensity. Planar uniaxial cells are usually not suitable for practical applications, at the common low switching voltages. This is due to the low contrast between the switched-off and switched-on state and the fact that the alignment of the LC molecules at the boundaries do not compensate each other. Also, the wavelength dependence for uniaxially aligned LC layers in the non-switched state is much larger than for TN cells, because only a  $\frac{1}{2}\lambda$  retardation can be achieved for a wavelength. The transmitted intensity as a function of  $d\Delta n/\lambda$  for planar cell is (same as equation 3.9)<sup>5,20,21</sup>:

$$T_{\text{planar}} = \frac{I}{I_0} = \sin^2\left(\frac{\pi d\Delta n}{\lambda}\right) \quad (4.5)$$

If a pretilt angle is present, the Fréedericksz transition occurs smoother and the threshold voltage is somewhat lowered. The pretilt has a more important function however, as is shown in figure 4.4 (for clarity a planar cell is shown). When a voltage is applied, a cell with a  $0^\circ$  pretilt angle can switch in two directions, creating a visible transition or disclination, which reduces the optical quality of the cell. A cell with non-zero pretilt angle only switches in one direction and no multi-domain formation occurs.

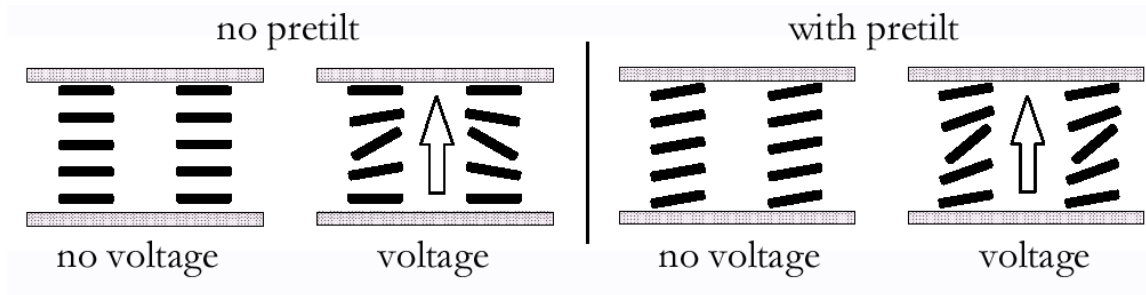


Figure 4.4 Electric switching of cells with and without a pretilt angle<sup>9</sup>

The actual cell properties, such as brightness, switching time and voltage and viewing angle characteristics, depend on many more variables. As a general rule a voltage of a few volts is enough to switch these types of cells with an adequately high contrast between the dark and transparent states, with a response time in the order of tens of microseconds.

#### 4.2.2 Personalised security features

Credit cards, valuable documents and other items that are sensitive to counterfeit usually contain security features that prevents or hinders copying<sup>25,26</sup>. To stay ahead of counterfeiters, these security features are constantly upgraded or new types are developed. To be successful, three levels of security need to be present: (1) the user or owner must clearly see and understand the security feature; (2) instances, such as banks or shops, should be able to perform a quick and simple authenticity verification; (3) the issuer of the card or document, e.g. a credit card company or national bank, should be able to do an extensive check on the authenticity and should have unique rights and/or possibilities to manufacture the security elements. The security element itself also has several requirements<sup>25-27</sup>: they should be difficult to copy or manufacture and preferably they should be integrated and non-removable from the protected document or card.

Security features based on laser-melted TN LCD systems are an interesting potential application<sup>27</sup> that complies with all of the above security requirements and levels. Rather than using low molecular mass liquid crystals, which are sensitive to flow, pressure and

temperature changes, liquid-crystalline networks are used. They can be aligned at the laser-patterned substrates in their monomeric state. After photo-initiated crosslinking, their patterned orientation is permanently fixed. The information thus stored in the polymer network is hidden under ambient light conditions, but can be made visible by the use of polarisers ('lock-and-key principle'). In addition to the requirements and security levels mentioned earlier, it is possible to individualise or personalise these security features by patterning a barcode, numbers or even images such as photos, signatures or fingerprints. This type of security features is not an electro-optical switch, since the liquid crystal is fixed and there is no electrical switching involved, but they are described in this chapter because of their similarity to TN displays. By using polymer dispersed LC (PDLC) systems, it should be possible to construct a switchable system.

#### 4.2.3 Cholesteric texture liquid crystal displays

The highest contribution to the energy consumption of liquid crystal displays originates from the illumination device, such as cold CCF lamps or LED's. Since a common TN LCD has a very low light efficiency due to light absorbing layers, such as polarisers and colour filters<sup>28</sup>, the illumination device needs to be quite powerful. The result is that the display consumes much energy, reducing the battery life within portable devices and increasing the energy costs. In general, the solution to use ambient light to reveal image display in LCD's is commonly sought in reflective type LCD's<sup>28-31</sup>, such as reflective mirror containing TN or super-twisted nematic (STN) LCD's or transfective LCD's containing a semi-transparent mirror. Reflective display cells can also be constructed based on cholesteric liquid crystals<sup>32-36</sup>. Their operation is quite different from the more common twisted nematic LCD's. Cholesteric LCD's often operate on the principle of bistability, which means that there are two stable liquid crystal configurations between which can be switched by electric pulses or by thermal treatment.

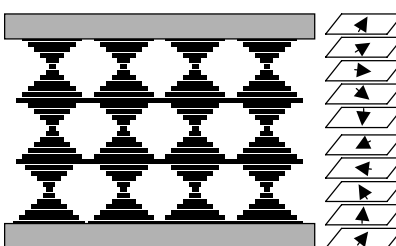


Figure 4.5 Cholesteric liquid crystal director orientation

In the cholesteric liquid crystal phase, the chiral liquid crystals self-organise into a helical structure. Alternatively, additives, such as chiral dopants, are used to induce the



helical twist in a nematic host. The cholesteric phase can be represented as a series of stacked planes in which there is nematic orientational order, but with each successive plane the director is slightly rotated with respect to the previous plane<sup>37</sup> (see figure 4.5). Cholesteric helices with their helical axis perpendicular to the observation plane reflect light with a same wavelength as the pitch of the helix<sup>38,39</sup>:

$$\lambda = \bar{n} \cdot p \quad (4.6)$$

In this equation,  $p$  is the helical pitch (twice the periodicity) and  $\bar{n}$  is the average refractive index. When a light beam contains the wavelength in the range of the cholesteric pitch enters the helix, it is split into two circularly polarised parts. One part of the circularly polarised components matches the twist direction of the helix and is reflected; the rest is transmitted. The wavelength range that is reflected ( $\Delta\lambda$ ) is given by:

$$\Delta\lambda = p\Delta n \quad (4.7)$$

The non-reflected wavelengths are transmitted or show polarised waveguiding. Usually,  $\Delta\lambda$  is in the order of magnitude of 50 - 100 nm<sup>38</sup>.

Cholesteric liquid crystals can orient themselves in three phases upon electrical switching<sup>39-42</sup>: the planar configuration, the homeotropic configuration and the focal-conic configuration (see figure 4.6). The planar and the focal-conic configurations are the zero-field stable phases. In the planar configuration (also known as grandjean texture), the helices are, on average, aligned with their axis perpendicular to the surface. This is the reflective configuration. The planar configuration is zero-field stable at room temperature. In the other zero-field stable configuration, the focal-conic state, the helices are not aligned perpendicular to the surface, but the directors of axes of the helices are randomly distributed. A cell with a cholesteric liquid crystal in the focal conic state is weakly forward scattering. Usually, the back of the electrode is painted black and the cell appears dark in this state. The focal-conic configuration is obtained when a voltage pulse (usually of approximately 20 V) is applied to the planar configuration. The homeotropic state is usually obtained when the voltage is (normally) switched to approximately 35 V (either from the planar or focal-conic states). The helical structure is lost and the liquid crystals align themselves in the direction of the electric field, perpendicular to the surface. This state is not zero-field stable and when the voltage is switched off, it relaxes into the planar state. Therefore, this state can be used to switch back

from the focal-conic state to the planar state. During the transition from the homeotropic to planar configuration, a fourth state is briefly formed, the transient planar configuration, which has a periodic structure and causes reflection, but at a different wavelength than the planar configuration<sup>40</sup>.

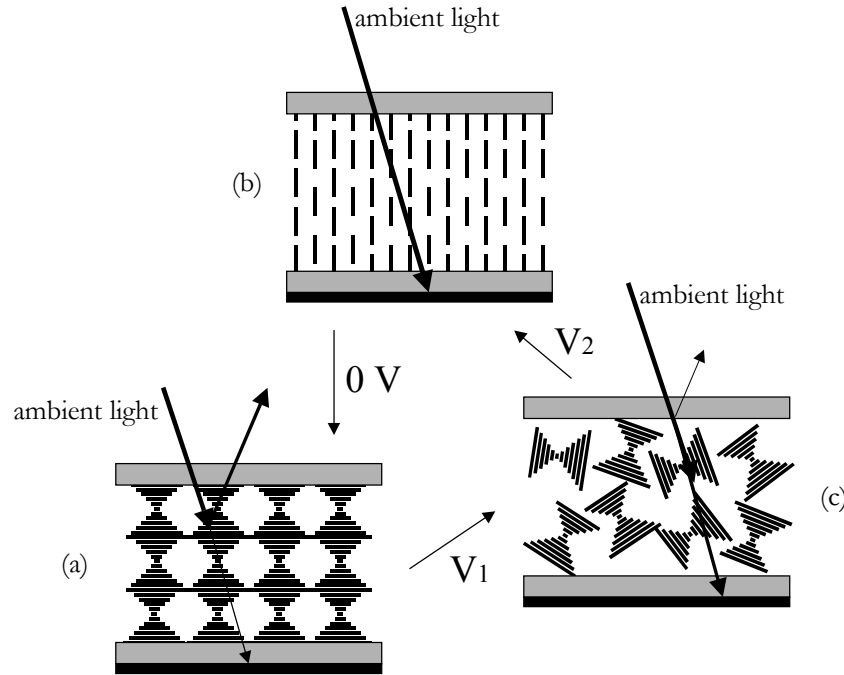


Figure 4.6 Cholesteric LC configurations (including the black layer at the back); (a) planar, (b) homeotropic, (c) focal-conic

With cholesteric LCD's, usually abbreviated as ChLCD or CTLC (cholesteric texture LCD), it is possible to switch between a coloured and a black state (if the back substrate is made black). A colour display can be constructed by pixelation<sup>35,36</sup> or if three cholesteric cells are stacked on top of each other, with each stack having one of the building block colours<sup>43</sup>. The set-up of a simple CTLC cell is very similar to that of TN cells. A common CTLC cell is constructed as follows: the top substrate (glass or polymer) is coated with ITO (transparent electrode) and a homeotropic polyimide, the back substrate is composed of a glass (or polymer) substrate with a black coating at its back and ITO and homeotropically aligning polyimide at the surface towards the LC material. In the cell gap between the layers, a cholesteric liquid crystal is present. Boundary conditions are not critical for the cholesteric ordering of the LC and the homeotropically aligning polyimide is primarily there to increase the viewing angle (by disturbing the perfect structure of the planar configuration) and to induce or enforce the bistability. The black coating is necessary to be able to switch between a bright state (planar configuration) and a dark state.

CTLC's show high contrast and large viewing angles and long storage time without power<sup>41,42</sup> and grey scales have been shown<sup>44</sup>. CTLC's are an interesting candidate for use in flexible displays because the cell gap is less critical than for TN or STN devices. Therefore, there have been several attempts to use only polymeric substrates for the construction of these optical cells. Unfortunately, there are also several drawbacks to the use of cholesterics. They often need high voltages and have a slow response for the switching between the different liquid crystal states<sup>41</sup>. When the cholesteric liquid crystal is in the planar configuration, the colour and luminance are viewing angle dependent, resulting in an angular dependence of the contrast<sup>42</sup>. Still, due to its unique characteristics (especially their bistable nature) displays based on cholesterics are a very interesting for mobile applications, which need high contrast and low power consumption.

### 4.3 Experimental

#### 4.3.1 Direct focused laser writing

Direct focused laser writing was performed with the same setup as described in chapter 2.2.2. Laser melting on rubbed polyimide coatings was performed with a writing speed of 1 mm/s and a power density of  $2.1 \times 10^{11}$  W/m<sup>2</sup>. Patterns were written with variable line spacings. Laser pyrolysis on polyimide films was performed with a power density of  $2.54 \times 10^{11}$  W/m<sup>2</sup> and a writing speed of 1 mm/s. The laser-pyrolysed patterns consisted 200  $\mu$ m wide patterns, consisting of 5 overlapping lines with a width of 60  $\mu$ m and a depth of 10  $\mu$ m, written with a line spacing of 50  $\mu$ m.

#### 4.3.2 Materials

Orientation layer polyimide AL1051 was obtained from JSR (see paragraph 2.2.1). Glass coated with indium tin oxide was obtained from Merck (type 327-735-PO). Liquid crystal material E7 was obtained from Merck. UV curable diacrylate LC monomer RM257 (figure 4.7) and UV initiator Irgacure 651 were obtained from Merck. Polyimide films with a thickness of 180  $\mu$ m (Kapton 300HN) were obtained from DuPont.

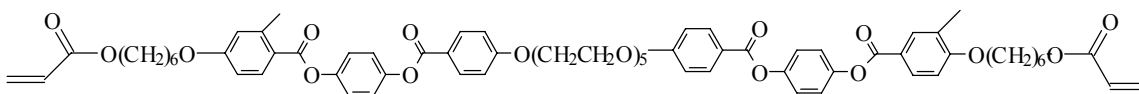


Figure 4.7 Chemical structure of cholesteric LC RM257.

The cholesteric liquid crystal that was used was a mixture of 30% BL087 and 70% BL088 (Merck). BL087 and BL088 are both mixtures of nematic compounds. BL088 also contains chiral components. Polyimide SE7511L (structure not known) was obtained from Nissan.

#### 4.3.3 Cell design

TN LCD's: Orientation was induced by uniaxial rubbing of the polyimide coated substrates with a velvet(-like) cloth. Two 3.5 x 3.5 cm plates of (patterned or non-patterned) polyimide on glass / ITO were attached to each other by application of a UV curable glue (Norland UV Sealant 91) at the edges and cured under pressure. The sealant is provided with 6  $\mu\text{m}$  cylindrical glass spacer particles, which determines the cell gap. The cells were capillary filled with LC material at 80 °C, 20 °C above the nematic – isotropic transition temperature of LC material E7.

Cells used for personalized security features were capillary filled with UV curable LC monomers mixed with 0.5 weight% UV initiator. The filling was performed at 100 °C in a UV protected environment. The LC was cured by placing it under a UV lamp for 10 minutes.

Cholesteric texture LCD's were constructed by gluing a glass/ITO or a PET/ITO substrate with a homeotropic polyimide coating on the laser-written polyimide films, using no spacers and capillary filling of the cholesteric LC. Both substrates were coated with a homeotropic polyimide layer. The cell was capillary filled with the cholesteric liquid crystal.

#### 4.3.4 Characterisation

Polarised light microscopy was performed with a Zeiss Universal, mounted with a photcamera and Zeiss Axioplan 2 mounted with a CCD camera. Contrasts between the written and non-written sections of the cell between crossed polarisers were measured using a HeNe laser (Melles Griot, model 05-LHP-991, 30 mW, 633.8 nm), an integrating sphere (Newport, model 819) and a power meter and detector (Newport, models 1815 C and 818-UV). To investigate the switching characteristics, the cells were electrically switched at varying currents and examined by polarised visual inspection. The switching curves were measured using an Autronic Display Measurement System. The reflection wavelength band of the cholesteric layer was determined by UV-VIS-NIR scanning spectroscopy (Shimadzu UV-3102 PC). This was achieved by measuring the transmission (using circularly polarised light) of a cholesteric layer sandwiched between two glass plates coated with homeotropically aligning polyimide.

## 4.4 Results and discussion

### 4.4.1 Twisted nematic liquid crystal displays

Laser-melted, rubbed polyimide orientation layers were incorporated in LCD cells. Figure 4.8 shows the effect of electrical switching on the LC alignment in a TN cell with on one side a laser-melted pattern on the rubbed polyimide orientation layer.

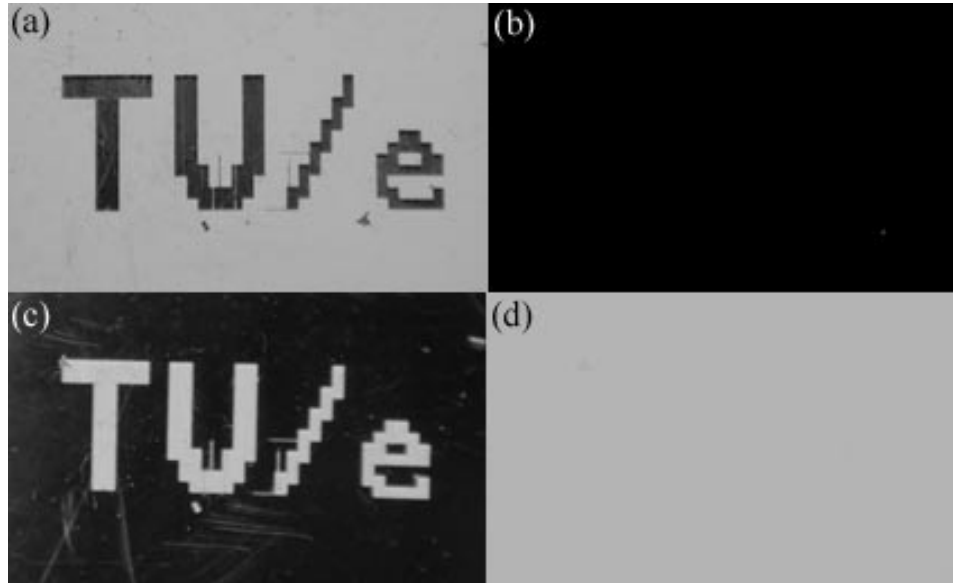


Figure 4.8 Photographs of a TN LCD cell with a laser-written pattern on one orientation layer  
 (a) crossed polarisers,  $V = 0$  V, (b) crossed polarisers,  $V = 15$  V, (c) parallel polarisers,  $V = 0$  V,  
 (d) parallel polarisers,  $V = 15$  V

Figure 4.8a and 4.8c show a cell with on one side a laser-written pattern (the TU/e logo) between crossed and parallel polarisers respectively, when no voltage is applied. Figure 4.8b shows the cell between crossed polarisers when a voltage of 15 V is applied: the LC molecules are switched to a homeotropic state in both the patterned and non-patterned sections, resulting in a completely dark cell between crossed polarisers. In figure 4.8d the result can be seen when a voltage of 15 V is applied to a cell between parallel polarisers: the cell switches to a fully transparent state. When switching the cell, there is a clear distinction between the written and non-written sections. At a voltage of 3-4 V, the non-written sections of the cell are fully switched to the homeotropic state, while the written sections are only partly switched and therefore appear lighter in colour than the surroundings. Above approximately 10-15 V, the whole cell is homogeneously switched. This is an indication that a parallel orientation is present at the laser-melted sections, because the surplus of elastic energy stored in the twisted configuration drives the liquid crystals to undergo the

Fréederiksz transition at lower voltages (see paragraph 4.2, especially equations 4.2 and 4.4)<sup>22,23</sup>. Figure 4.9 shows a schematic representation of a cell in a non-switched and a fully switched configuration.

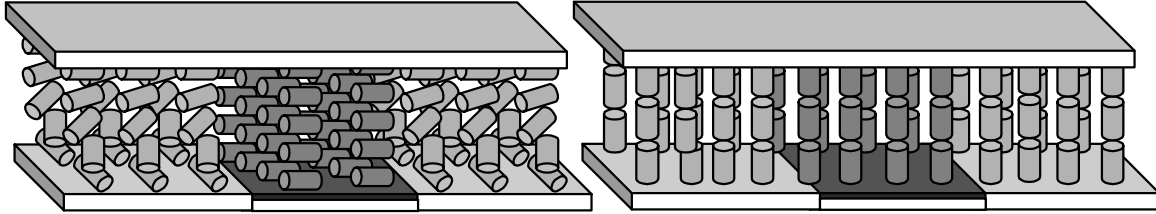


Figure 4.9 A non-switched and a fully switched one-sided laser-melted TN LCD cell

If the cell is placed between polarisers, with the optical axis of the LC parallel to the polarisers, no contrast between the on- and off-states is present for the written sections (both are dark between crossed polarisers). When the sample is placed under an angle of 45°, it is possible to observe the transition in an electrical switching experiment. The transmitted intensity for this situation is given in equation 4.5<sup>5</sup>. Figure 4.10 is the same as figure 3.14a (Gooch-Tarry curve<sup>5,20,21</sup>) and graphically represents equation 4.5 for a homogeneously planar cell with  $d = 6 \mu\text{m}$ ,  $\Delta n = 0.2246$  and  $\lambda = 550 \text{ nm}$  ( $d\Delta n/\lambda = 2.5$ ), values relevant for the systems described in this chapter. The homeotropic state has zero transmission between crossed polarisers for all values of  $d\Delta n/\lambda$ . Therefore, a cell with a  $d\Delta n/\lambda$  value for maximum transmission can switch between a dark state and a maximum transmissive state upon electrical switching.

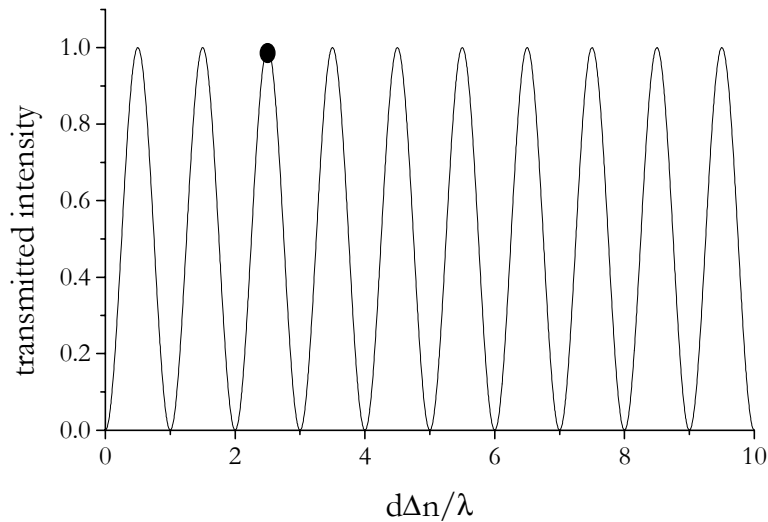


Figure 4.10 Gooch-Tarry curve for a planar cell placed 45° between crossed polarisers

For cells with  $d\Delta n/\lambda = 2.5$ , equation 4.5 results in a transmitted intensity of 1 (see black dot in figure 4.10), which indicates maximum transmission. At high voltages, the LC molecules switch to a homeotropic state. The birefringence, and therefore also  $d\Delta n/\lambda$ , is lowered to (nearly) zero. This results in a value for the transmitted intensity of 0. The switching curve was measured on the homogeneously planar sections in a one-side written TN cell placed under an angle of  $45^\circ$  between crossed polarisers. The curve was measured on a pattern consisting of several touching lines forming a larger area. The result is shown in figure 4.11. A transmittance of 100 % corresponds with the transmittance through two parallel polarisers without a cell in between. At zero voltage, the retardation of the cell causes the transmittance to be 45 %. At approximately 1.4 - 1.5 V, the transition starts and upon increasing voltage the curve shows several maximums and minimums. The number of maximums and minimums corresponds with the Gooch-Tarry curve for this configuration (figure 4.10). The pattern on which this curve was measured consists of several touching lines and the diameter of the measuring spot (approx. 0.2 mm) is larger than the width of the individual lines (approx. 50  $\mu\text{m}$ ). This results in leakage through the spaces between the lines in the pattern (which have a twisted configuration), causing the maximum transmission to periodically exceed that of the zero-voltage state.

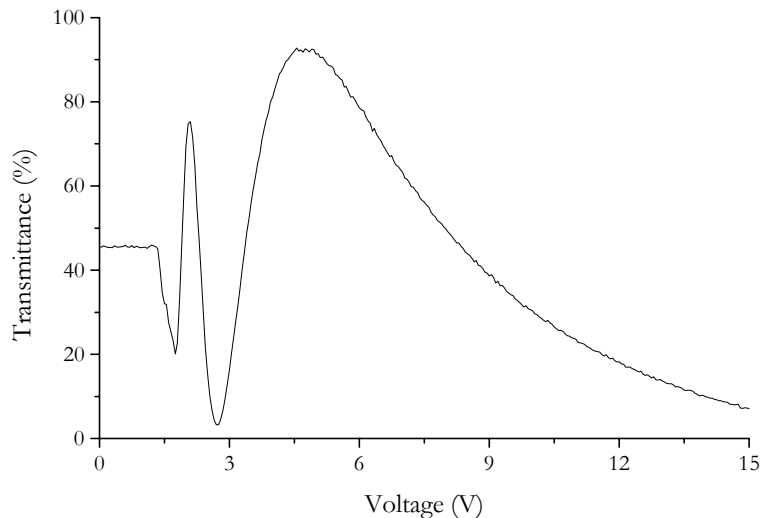


Figure 4.11 Switching curve of laser-melted pattern in a cell placed under an angle of  $45^\circ$  between crossed polarisers

The Gooch-Tarry curve for a  $90^\circ$  twisted configuration between crossed polarisers (based on equation 4.3) is given in figure 4.12. The position of the black dot indicates used value of  $d\Delta n/\lambda = 2.5$ .

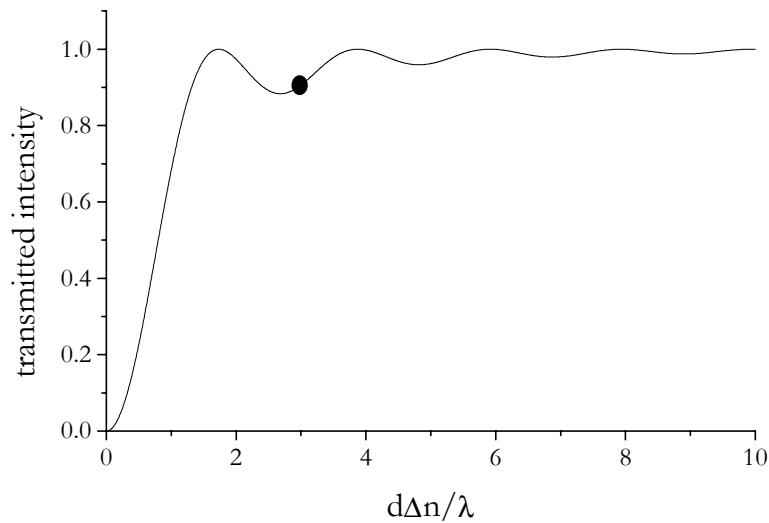


Figure 4.10 Gooch-Tarry curve for a  $90^\circ$  twisted cell between crossed polarisers

The non-irradiated sections of the cell described above have a TN configuration and a switching curve was measured on this area. Figure 4.11 shows the results of this measurement. The  $d\Delta n/\lambda$  value is in our case not optimised for the TN configuration. The reference transmittance of 100 % was measured through the cell at 0 V, therefore a transmittance of 100 % in figure 4.11 corresponds with a transmitted intensity of approximately 0.9 in figure 4.10. The switching voltage is 1.3 V, which is lower than the value found for the homogeneously planar areas, as was predicted by equations 4.2 and 4.4.

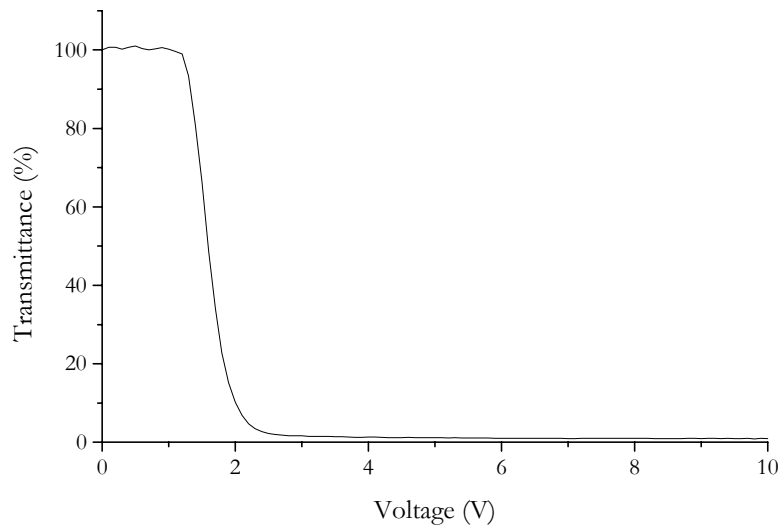


Figure 4.11 Switching curve of TN sections in a cell between crossed polarisers



The patterns can be written in any shape or size, as is shown in figure 4.12. When the lines are written with a spacing that is the same size as the line width, larger areas are the result, creating the opportunity to generate patterns with features with a minimum resolution of tens of microns. There is an excellent contrast between the homogeneously planar and the twisted areas of the optical cells constructed with rubbed polyimides with laser-melted patterns. Therefore, they can be used for purposes such as the marking, encoding or labelling of individual display cells or for switchable gratings, while still the possibility to electrically switch the cell to a fully homeotropic configuration is maintained.

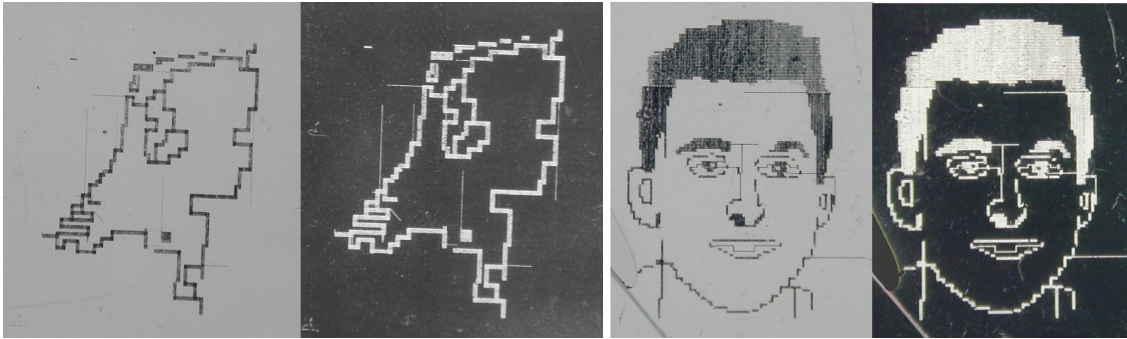


Figure 4.12 Examples of the versatile nature of the patterns that are possible to generate

#### 4.4.2 Personalised security features

Security features based on twisted nematic optical cells are an interesting application of laser-patterned rubbed polyimide orientation layers. To be applied in security features, regular liquid crystal materials cannot be used, due to the risk of leakage after damage. However, the cells need to be capillary filled to obtain the imposed orientation determined by the laser-patterned polyimide layers. Therefore, TN cells were capillary filled with a diacrylate LC monomer (see experimental) that could be cured after filling with UV light to form a solid polymeric film. The cells consisted of one laser-patterned orientation layer and a non-patterned layer perpendicular to this. After filling and curing, a fixed, non-mobile LC layer was obtained. Above the laser-written patterns, the LC layer had a homogeneously parallel orientation, while the non-patterned areas showed twisted alignment, similar to the cells with non-curable LC. Figure 4.13 shows an optical micrograph of such a cell. The minimum resolution of the patterns is several tens of microns. By writing touching or overlapping lines features up to several millimetres or more are obtained. After curing, the fixed LC layer remains stable up to, at least, 150 °C. In the system described above, the rubbed polyimide layers were coated on glass substrates, but to be applied in e.g. credit cards, polymer substrates need to be used to increase the robustness of the security feature. Security features exist in several security classes, depending on the number of fraud-

preventing items. These cells have a very high security level, since because they can be integrated in the document or credit card, they cannot easily be removed without damaging the cell. Also, they can be personalised (e.g. patterns as shown in figure 4.12 can easily be made) and external polarisers are needed to read out the pattern (lock-and-key principle).

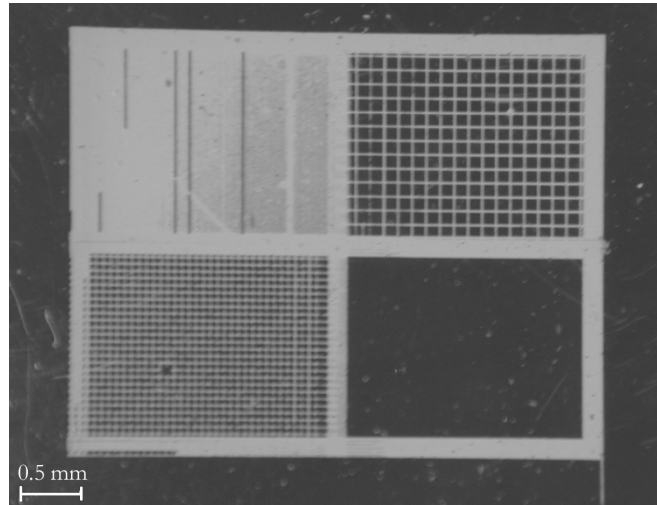


Figure 4.13 Polarised photograph of a laser-patterned TN cell, filled with a UV-curable LC

#### 4.4.3 Cholesteric texture liquid crystal displays

In chapter 2 electrically conductive laser-pyrolysed patterns in polyimide films were presented. Due to the black discoloration of the pyrolysed lines and the thick yellow coloured polyimide films, these conductive patterns are difficult to apply in transmissive optical applications. However, in cholesteric texture LCD's these drawbacks can be potentially used as an advantage. Instead of a glass/ITO back substrate, a laser-pyrolysed polyimide film is used. In this paragraph the polyimide film was laser-written with  $200\ \mu\text{m}$  patterns consisting of 5 slightly overlapping lines (see figure 4.14, similar to the patterns described in paragraph 2.3.3 for the electrical conductivity measurements), which were used as the switching electrodes.

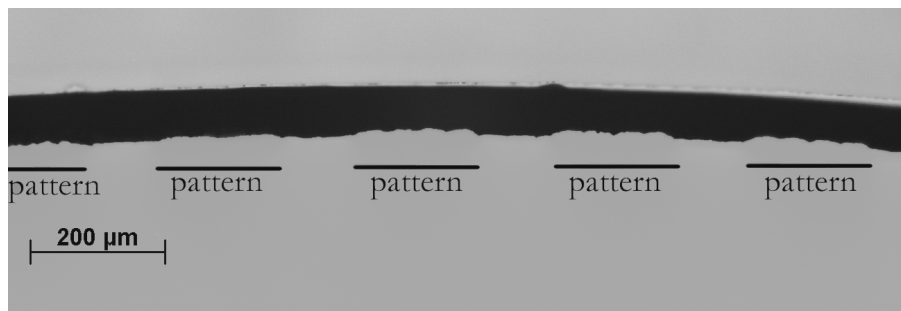


Figure 4.14 Optical micrograph of laser-pyrolysed patterns in polyimide (cross section)

If the top substrate (support, ITO and orientation layer) is glued directly on the laser-written polyimide film, the laser-pyrolysed patterns provide the cell gap for the CTLC cell (see figure 4.15). In our case, a cell gap of 10  $\mu\text{m}$  was obtained.

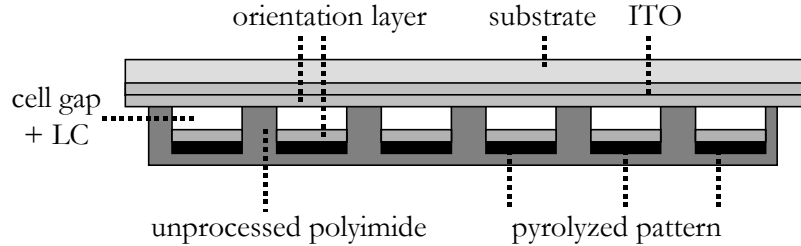


Figure 4.15 Configuration of the CTLC cells

The cells were capillary filled with a cholesteric liquid crystal (see experimental). Figure 4.16 shows a UV-VIS spectrograph of this cholesteric material sandwiched between two glass slides. The reflected wavelengths (transmittance = 0 % in figure 4.16) are in the red and far-red region.

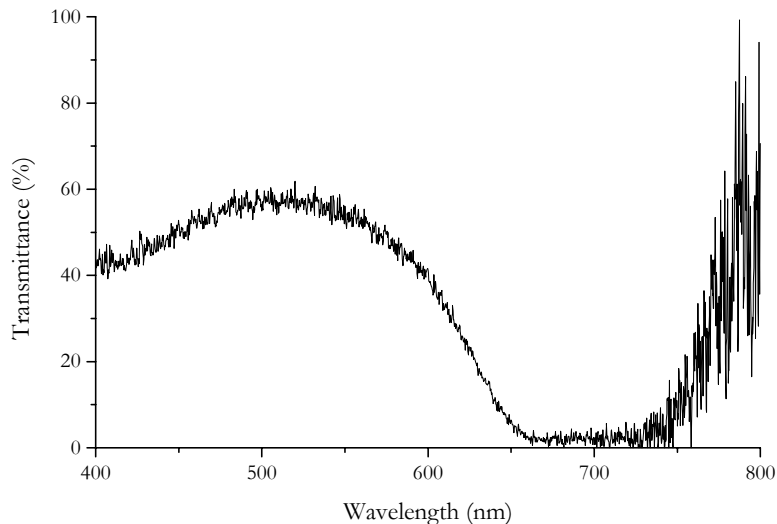


Figure 4.16 UV-VIS spectrograph of the cholesteric liquid crystal

A high switching voltage (80 V or higher) was needed to electrically switch the cells from a coloured to a dark state (see figure 4.17). The high optical absorption of the pyrolysed lines provides the black colour of the switched-on state instead of the usual black coating. The high switching voltage is caused by a relatively large, non-flat cell gap and the inhomogeneous nature of the laser-written electrical pathways. The dark state is the

homeotropic configuration; the focal conic region was not stable in these cells, probably due to the poor quality of the cells and the needed high voltages. After the voltage was removed, the liquid crystal returned to the coloured, reflective state.

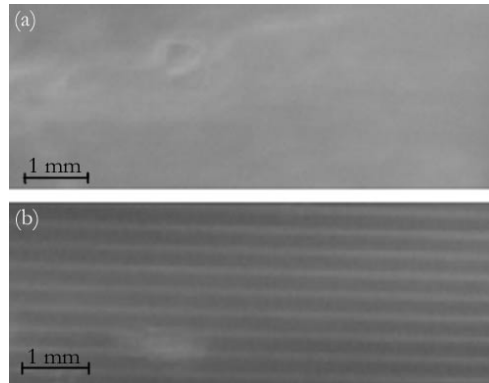


Figure 4.17 Photograph of a section of a laser-pyrolysed CTLC cell. (a) no voltage, (b) 80 V

The overall quality and mechanical stability of the constructed cells was quite poor. The polyimide had a tendency to bend during laser writing and gluing. This caused disattachment of the substrates after cell construction, enhanced by the poor adhesion from the used glue, followed by spilling of the cholesteric liquid crystal out of the laser-written structures. Combined with the already non-flat surface of the laser-pyrolysed patterns, these additional factors made it difficult to generate a homogeneous cell gap and an optically homogeneous cell. By optimising the laser writing procedure and settings and materials choice, e.g. the type of glue, substrates and liquid crystal (with a more convenient reflection band e.g. in the green region), many of these problems can be overcome. However, these initial experiments showed that the proof of principle that laser-pyrolysed patterns can be applied for the electrical switching of specific LCD's.

## 4.5 Conclusions

In this chapter we showed two examples of laser-patterned polyimides in LCD's and personalised security features. Incorporating rubbed polyimide with laser-melted patterns orientation layers in TN LCD's resulted in display cells with a high contrast between the patterned and non-patterned areas. Upon electrical switching, the whole cell switches to a homeotropic state and no distinction between the patterned and non-patterned sections is observed. These cells have a high contrast, a wide range of length scales and a relative ease of production. Therefore, potential applications include the labelling, marking or encoding of displays and cosmetic purposes. By replacing the liquid crystal by a curable LC monomer that is cured after filling, these cells can be easily adapted for use as personalised security

features. Laser-pyrolysed patterns in polyimide films can be used to electrically switch liquid crystals in cholesteric texture LCD's. The laser-pyrolysed polyimide layer can be used to replace several functional layers and materials in common CTLC cells (substrate, black colouring agent, ITO and spacers), resulting in a thinner, more flexible display.

#### 4.6 References

- [1] M. Schadt, W. Helfrich, *Appl. Phys. Lett.* **18**, 127, (1971).
- [2] M. Schadt, *Annu. Rev. Mater. Sci.* **27**, 305, (1997).
- [3] T. Scheffer, J. Nehring, *Annu. Rev. Mater. Sci.* **27**, 555, (1997).
- [4] P. J. Bos, K. R. Beran, *Mol. Cryst. Liq. Cryst.* **113**, 329, (1984).
- [5] I. C. Sage, in D. Demus, J. Goodby, G. W. Gray (Eds.): *Handbook of Liquid Crystals, Vol. 1: Fundamentals*, p. 731, Wiley-VCH Verlag GmbH, Berlin, (1998).
- [6] M. C. W. van Boxtel, R. H. C. Janssen, D. J. Broer, H. T. A. Wilderbeek, C. W. M. Bastiaansen, *Adv. Mater.* **12**, 753, (2000).
- [7] L. Bouteiller, P. LeBarny, *Liq. Cryst.* **21**, 157, (1996).
- [8] L. J. M. Schlangen, A. Pashai, H. J. Cornelissen, *J. Appl. Phys.* **87**, 3723, (2000).
- [9] image taken from: J. van Haaren, *Course Display Techniques, Basic Physics and New Developments in Liquid Crystal Displays (syllabus)*, (2001)
- [10] P. J. Collings, *Liquid Crystals - Nature's Delicate Phase of Matter*, Princeton University Press, Princeton, (1990).
- [11] A. G. Knapp, *Philips Res. bull. on Systems and Software* **8**, 1, (1992).
- [12] S. W. Depp, W. E. Howard, *Sci. Am.* **268**, 40, (1993).
- [13] J. van Haaren, in M. H. Francombe (Ed.): *Handbook of Thin Film Devices, Volume 2: Semi-Conductor Optical and Electro-Optical Devices*, Academic Press, San Diego, (2000).
- [14] H. Zocher, *Naturwissenschaften* **49**, 1015, (1925).
- [15] N. A. J. M. van Aerle, *J. Soc. Inf. Display* **2**, 41, (1994).
- [16] T. J. Scheffer, J. H. Nehring, *Appl. Phys. Lett.* **45**, 1021, (1984).
- [17] V. Fréedericksz, V. Zolina, *Trans. Faraday Soc.* **29**, 919, (1933).
- [18] F. M. Leslie, *Mol. Cryst. Liq. Cryst.* **12**, 57, (1970).
- [19] K. H. Yang, *Appl. Phys. Lett.* **43**, 171, (1983).
- [20] C. H. Gooch, H. A. Tarry, *J. Phys. D* **8**, 1575, (1975).
- [21] P. Yeh, *Optical Waves in Layered Media*, Wiley, New York, (1988).
- [22] P. A. Breddels, H. A. van Sprang, *J. Appl. Phys.* **60**, 968, (1986).
- [23] L. M. Blinov, in D. Demus, J. Goodby, G. W. Gray (Eds.): *Handbook of Liquid Crystals, Vol. 1: Fundamentals*, Wiley-VCH Verlag GmbH, Berlin, (1998).
- [24] J. van Haaren, *Course Display Techniques, Basic Physics and New Developments in Liquid Crystal Displays (syllabus)*, (2001)

- [25] R. W. Phillips, A. F. Bleikolm, *Apl. Opt.* **35**, 5529, (1996).
- [26] R. L. v. Renesse, *Optical Document Security*, Artech House, Boston, (1998).
- [27] M. Schadt, H. Seiberle, *Patent WO 9852077*, (1998).
- [28] K. Kato, K. Tanaka, M. Date, *Electron. Commun. Jpn. Pt. II-Electron.* **81**, 32, (1998).
- [29] S.-T. Wu, *SPIE* **3421**, 84, (1998).
- [30] Van Haaren, J., *Lecture Notes Eurodisplay'99*, Berlin, (1999), website: <http://www.extra.research.philips.com/password/syllabfoils.pdf>
- [31] C. L. Kuo, C. K. Wei, S. T. Wu, C. S. Wu, *Jpn. J. Appl. Phys.* **36**, 1077, (1997).
- [32] W. D. Stjohn, Z. J. Lu, J. W. Doane, B. Taheri, *J. Appl. Phys.* **80**, 115, (1996).
- [33] W. D. Stjohn, Z. J. Lu, J. W. Doane, *J. Appl. Phys.* **78**, 5253, (1995).
- [34] J. W. Doane, D. K. Yang, M. Pfeiffer, *Macromolecular Symposia* **96**, 51, (1995).
- [35] D. K. Yang, J. L. West, L. C. Chien, J. W. Doane, *J. Appl. Phys.* **76**, 1331, (1994).
- [36] D. K. Yang, J. W. Doane, Z. Yaniv, J. Glasser, *Appl. Phys. Lett.* **64**, 1905, (1994).
- [37] W. H. de Jeu, *Physical Properties of Liquid Crystalline Materials*, Gordon & Breach Science Publishers Ltd., London, (1980).
- [38] [http://www.cremes.fr/Oper\\_recherche/Polymer/LCP/Html\\_LCP/Liquid\\_Crystals\\_Physics.htm](http://www.cremes.fr/Oper_recherche/Polymer/LCP/Html_LCP/Liquid_Crystals_Physics.htm)
- [39] W. D. Stjohn, W. J. Fritz, Z. J. Lu, D. K. Yang, *Phys. Rev. E* **51**, 1191, (1995).
- [40] J. Anderson, P. Watson, J. Ruth, V. Sergan, [http://www.lci.kent.edu/boslab/people/anderson\\_j/pubs/anderson\\_j\\_fast\\_frame\\_rate\\_bct\\_ref\\_disp.pdf](http://www.lci.kent.edu/boslab/people/anderson_j/pubs/anderson_j_fast_frame_rate_bct_ref_disp.pdf)
- [41] A. V. Henzen, F. A. M. A. Paulissen, *SID 00 Digest*, 269, (2000).
- [42] S. Valyukh, A. Slobodanyuk, V. Sorokin, *SID 00 Digest*, 213, (2000).
- [43] X.-Y. Huang, A. A. Kahn, D. J. Davis, G. M. Podojil, C. M. Jones, N. M. Miller, J. W. Doane, *Proc. SPIE* **3635**, 120, (1999).
- [44] M. Xu, D. Yang, *SID 99 Digest*, 950, (1999).



## Chapter 5

### Laser Patterning in Linearly Photo-Polarisable Polymers

#### 5.1 Introduction

In chapter 3, laser processing was performed in the melting regime to pattern rubbed polyimide liquid crystal alignment layers. This was a subtractive process where the orientation-inducing properties of the rubbed polyimide were locally inactivated by the laser melting process. This chapter will focus on the photochemical patterning of liquid crystal orientation layers in an additive process. The ability to align liquid crystals is added to the polymer layer by photochemical processes in chromophores with a dichroic nature.

Patterning is performed on a group of photosensitive polymers that undergo a crosslinking reaction when illuminated with UV radiation<sup>1</sup>. If linearly polarised UV light is used, these crosslinked polymers gain liquid crystal alignment properties. These materials, called linearly photo-polarisable polymers (LPP), were developed as an alternative orientation layer material to rubbed polyimides. By introducing non-contact alignment methods to generate the LC alignment properties, LPP materials overcome some inherent drawbacks to the rubbing process (e.g. dust sensitivity and the generation of electro-static charges). The chemical structures and the aligning mechanisms of some relevant LPP materials, such as cinnamates<sup>2-5</sup>, chalcones<sup>6-9</sup> or coumarins<sup>1, 2, 6, 10, 11</sup> are given in the next paragraphs.

The photochemically induced alignment enables the formation of patterns with different alignment direction. This is, for instance, utilised in so-called multi-domain TN displays, where each pixel element of the display is sub-divided in areas with alternating alignment. This enormously improves the viewing angle characteristics of the LCD's with respect to angular dependent contrast and so-called grey-scale inversion. In literature lithographic approaches based on photo-masks involving multiple exposure steps are presented to realise patterns with different LC alignment<sup>1,2</sup>.

In this chapter, we will discuss the method of direct laser writing to generate complex and high-resolution patterns. The geometry, structure and the LC alignment properties of the written patterns are investigated.



## 5.2. Linearly photo-polarisable polymers

In the past decade, several methods have been developed for the photo-alignment of liquid crystals. Several classes photo-aligning polymers are distinguished<sup>1</sup>, such as azobenzene containing materials<sup>2-4</sup>, photo-degradation materials<sup>1,5-10</sup> and photo-crosslinkable materials<sup>11-14</sup>. We used this last class of materials, in the literature denoted as linearly photo-polarisable polymers (LPP), in this chapter and this paragraph gives an overview of the relevant crosslinkable LPP materials.

Polyvinylcinnamates and derivatives were the first photo-crosslinkable materials that were found to align liquid crystals<sup>12-15</sup>. If a liquid crystal is brought in contact with a polarised UV exposed film at these materials, an LC alignment occurs perpendicular to the direction of the electric field vector of the UV light.

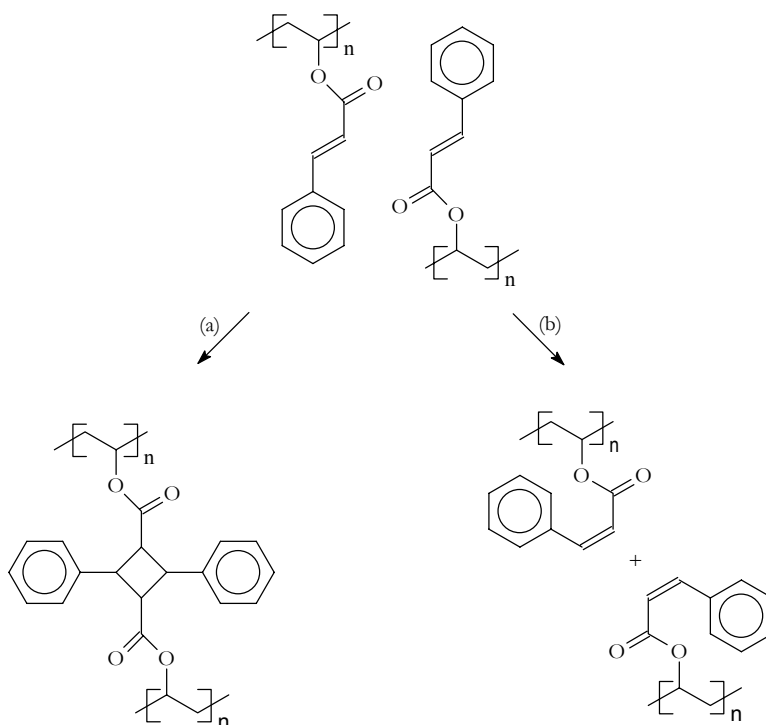


Figure 5.1 Photochemical reactions of cinnamate containing polymers. (a) photo-dimerisation, (b) photo-cis/trans isomerisation

There is some controversy about the exact nature of the effect caused by polarised UV illumination. Figure 5.1 shows the two main photochemical reactions that can occur with cinnamate containing polymers. The photo-dimerisation reaction (figure 5.1a) is

thought to cause an alignment due to the anisotropic (2+2)-cycloaddition and the resulting decrease in the number of cinnamate side chains<sup>12</sup>, although there is some controversy if the cyclo-addition reaction indeed results in an anisotropic photoproduct<sup>16</sup>. A different explanation is that a photo cis/trans isomerisation is the dominant reaction that induces the aligning properties, especially at small fluences (figure 5.1b)<sup>17</sup> and that the dimerisation reaction only supports and enhances the aligning properties.

The LC alignment perpendicular to the electric field vector of the light limits non-planar LC orientation because of symmetry reasons. For many LCD types small polar angles (pre-tilt) are desired to prevent domain formation upon switching. Therefore, LC orientation parallel to the electric field vector is desired. Besides the alignment perpendicular to the polarisation direction, there are some other drawbacks<sup>1</sup> to the use of cinnamate containing polymers, including a low anchoring energy and a poor thermal stability.

Polymers with chalcone side-chains (figure 5.2) are photo-crosslinkable materials that were developed to induce an LC alignment parallel to the polarisation direction of the UV irradiation<sup>1,11,18,19</sup>. With these LPP materials it is possible to induce a pre-tilt angle, which not only improves the quality and performance of displays, it also opens up the possibility to generate multi-domain structured orientation layers, which result in wider viewing angles.

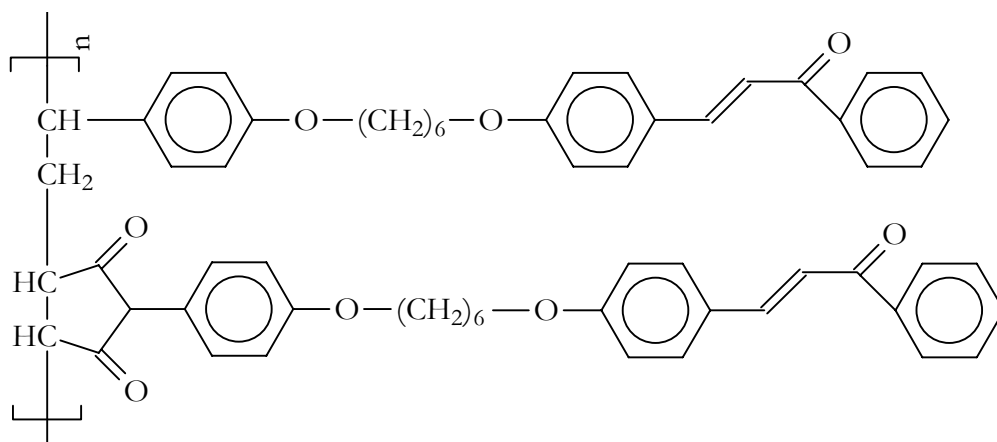


Figure 5.2 Photo-alignment polymer with chalcone side-groups and an alkyl spacer (JSR PMI-15)<sup>18</sup>;

Different spacers give different photo-sensitivity and aligning properties

A third type of photo-crosslinkable photo-alignment material that is very promising for use as an orientation layer are polymers (usually polymethacrylates) with coumarin moieties in their side-chains<sup>1,14,20-22</sup>. Similar to polymers with chalcone side-chains, these materials are used to generate homogeneous pre-tilts because it features a parallel alignment to the polarisation direction of the incident light. Other advantages are the high photo-

sensitivity, the excellent aligning properties, the high thermal stability and the photo-chemical stability after irradiation. A photo-dimerisation reaction takes place in a very similar fashion as with cinnamate based materials (see figure 5.3).

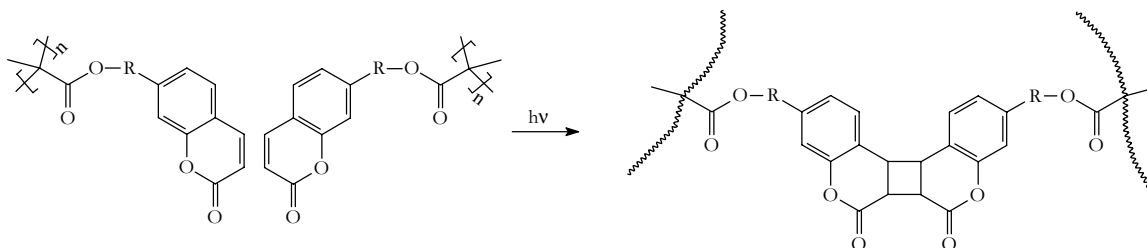


Figure 5.3 Photodimerisation of a polymethacrylate with coumarin side chains; R is an alkyl spacer

Because of steric reasons, the *cis/trans* isomerisation cannot take place with this type of materials and the aligning properties are fully due to the photodimerisation, which has a preferred orientation when irradiated with polarised UV light. By varying the angle of incident light with respect to the surface, tilt angles can in principle be generated up to several degrees and even homeotropic alignment materials have been developed<sup>14,20,21</sup>.

## 5.3 Experimental

### 5.3.1 Direct focused laser writing and interferometry

Direct focused laser writing was performed using the same setup as described in paragraph 2.2.2. The power density was set to different levels, depending on the type of orientation layer material. Interferometry was performed using a Mach-Zehnder interferometer. The frequency-stabilised beam was set to 351.1 nm and expanded to approximately 1.5 cm. The pitch (the distance between two following holographic maximums) was usually set to the maximum obtainable setting possible in the space available on the optical table, which resulted in a pitch of 2  $\mu\text{m}$ . The laser beam power density and irradiation time were varied according to the photosensitivity of the orientation layer material. An air-stabilised optical table (Newport RS4000/I2000) was used to prevent disturbances by mechanical shocks.

### 5.3.2 Materials

The LC material (Merck E7) and polyimide (JSR AL1051) were handled as described in chapter 2.2.1. Chiral dopant ZLI-088 was obtained from Merck and was used in a 0.1 wt% solution in E7 in some cases. Several UV sensitive photo-alignment orientation layers were

used. ROP-101/2CP (LPP) and ROP-106/2CP (LPP) were obtained from Rolic Ltd, JP-265CP was obtained from Vantico Ltd and PMI-15 was obtained from JSR. The chemical structures of the materials were not disclosed by the suppliers, but PMI-15 is a chalcone based material, the others are either cinnamate-based or coumarin-based materials. ROP-106/2CP (LPP) and PMI-15 are photosensitive in the 330-350 nm region, the rest has their main absorption peak around 275 nm, but do have residual absorption at 351 nm.

For clarity, the materials that are used are from here on named LPP-1 to LPP-4 instead of their commercial code. Table 1 shows the code used in this chapter and the corresponding commercial code.

code used in this chapter	commercial code	manufacturer
LPP-1	ROP-101/2CP (LPP)	Rolic
LPP-2	JP-265CP	Vantico
LPP-3	ROP-106/2CP (LPP)	Rolic
LPP-4	PMI-15	JSR

Table 5.1 Manufacturer's names of the LPP materials used in this chapter

### 5.3.3 Cell design and characterisation

The photo-alignment orientation layers were spincoated (coating thickness: 70-90 nm, measured by profilometry) onto glass or glass/ITO substrates, laser-written using a scanned focused beam or interferometry (holography) and subsequently illuminated with a polarised UV lamp ( $\lambda = 360$  nm) with the polarisation direction perpendicular to that of the laser beam. Electro-optical cells were constructed in the same fashion as described in chapter 3.3.3. Instead of two rubbed polyimide layers, one or two photo-aligned orientation layers were used. The cells were characterised using the same equipment and methods as described in chapter 3.3.4.

## 5.4 Results

### 5.4.1 LPP materials and UV sensitivity

Figure 5.4 shows the UV-VIS absorption spectra of the used LPP materials. LPP-1 and LPP-2 have their main absorption peaks around 275 nm, while LPP-3 and LPP-4 have a high absorption around 350 nm. Because the laser writing occurs at a wavelength of 351.1

nm, the latter two materials are expected to have more response resulting in shorter reaction times or require lower laser power densities.

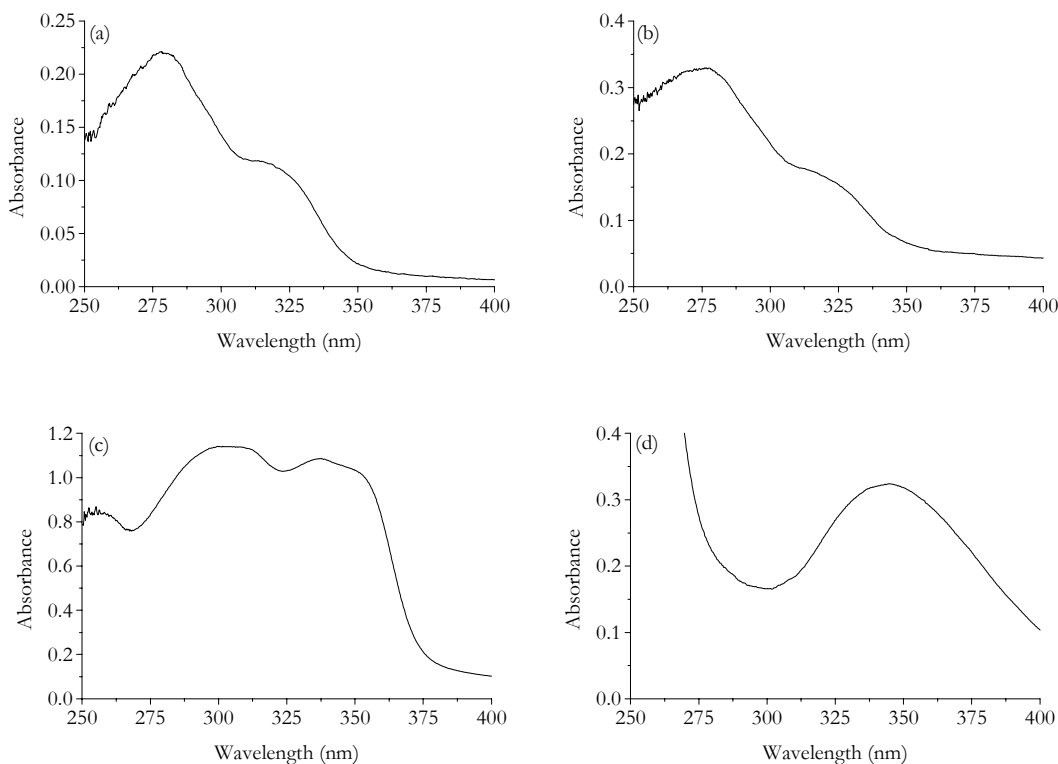


Figure 5.4 UV-VIS absorption spectra of photo-alignment orientation layers

(a) LPP-1, (b) LPP-2, (c) LPP-3, (d) LPP-4

LPP-1 and LPP-4 were both irradiated with a (non-polarised) UV lamp and at regular time intervals a UV-VIS spectrum was measured. Figures 5.5a and 5.5b show the time dependent UV-VIS transmission spectra for both materials. Due to the conversion of double bonds and the corresponding loss of conjugation during the photo-induced cross-linking reaction, the absorption bands in the 300-400 nm region disappear. Figures 5.5c and 5.5d illustrate the time dependence clearer by showing the absorption decrease at the main peaks of both materials as a function of the fluence (power per area per second). In both cases a plateau level, which indicates maximum conversion, is reached after a steep absorption decrease. A fluence of 200-300  $\text{kJ}/\text{m}^2$  is needed to reach the plateau level for LPP-1, while for LPP-4 this plateau level is reached sooner (at approximately 100  $\text{kJ}/\text{m}^2$ ), due to increased photosensitivity at near-UV wavelengths. The lamp operates at 360 nm, while the laser illumination occurs at 351.1 nm, which is closer to the absorption peaks of both materials. This should reduce the fluence to reach maximum conversion for both materials, especially for LPP-4, which has its absorption peak around 350 nm.

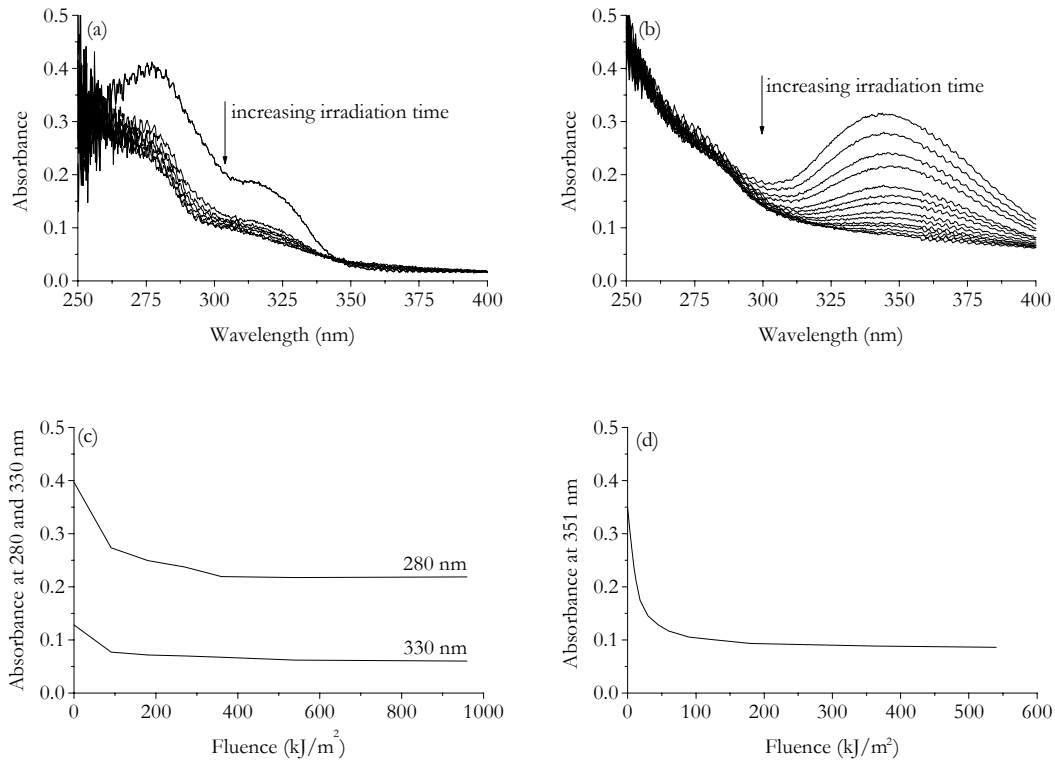


Figure 5.5 Time dependent UV-VIS absorption, (a) LPP-1, (b) LPP-4; Main absorption peak decrease as a function of the fluence, (c) absorption at 280 nm and 330 nm, LPP-1, (d) absorption at 351 nm, LPP-4

The different LPP materials are used alternatingly in this chapter. In some cases the properties of two or more different LPP materials are compared, but if there is no (apparent) influence on the type of LPP on the investigated property, they are used in an arbitrary fashion.

#### 5.4.2 Masked illumination

The common method to micro-pattern LPP materials is masked illumination. Figure 5.6 shows an LCD cell with two LPP-1 orientation layers, one of which was illuminated with polarised UV light through a mask, followed by a second (maskless) illumination with a polarised UV lamp with the polarisation direction perpendicular to the first illumination. The LPP-1 layer at the opposite glass plate of the cell was uniformly aligned with a polarised UV lamp and placed with its aligning axis perpendicular to the first irradiated sections of the opposite orientation layer. This resulted in a hybrid cell containing both homogeneously planar and 90° twisted areas (schematically shown in figure 5.7). Line patterns with different spacings ranging from 300  $\mu\text{m}$  (figures 5.6a and 5.6b) to 2  $\mu\text{m}$  (figure 5.6d) were achieved.

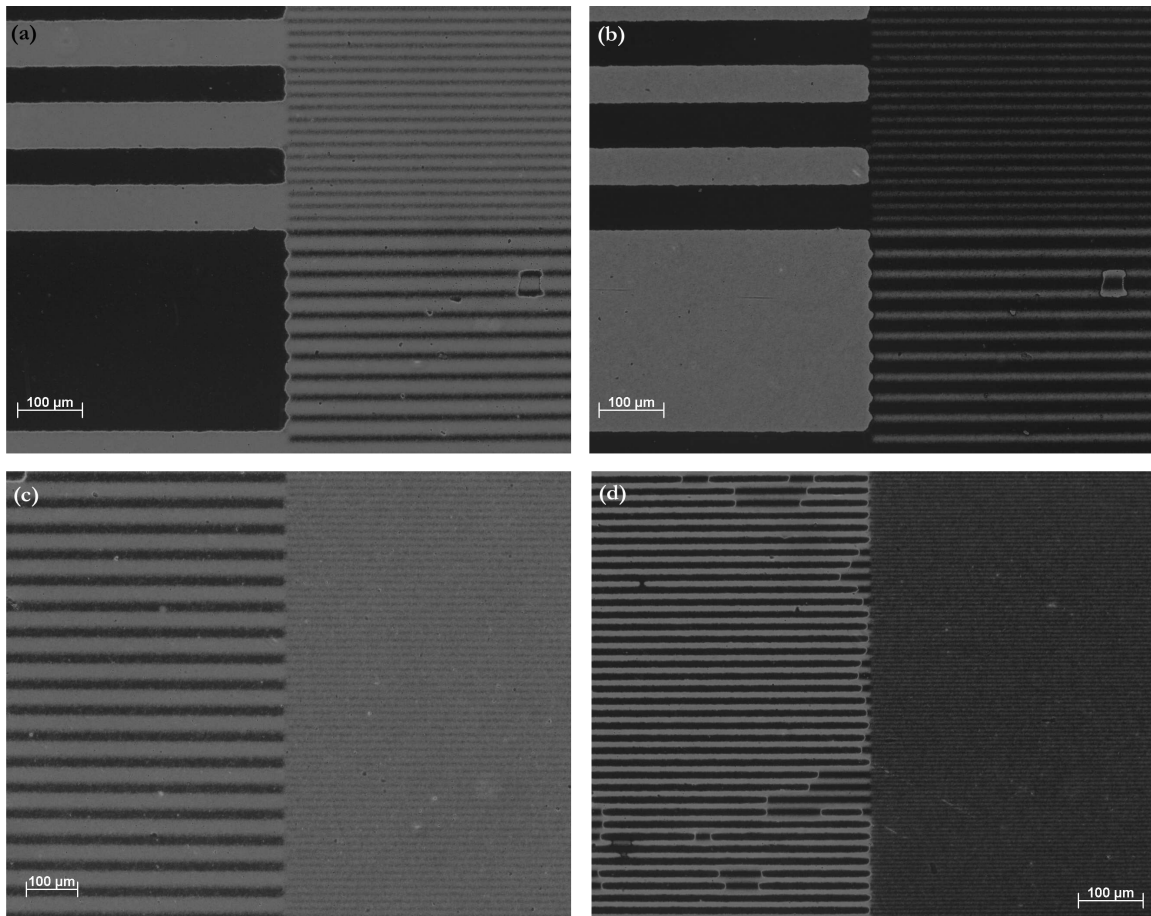


Figure 5.6 Cell with a masked illuminated LPP-1 orientation layer with several mask spacings. (a)  $300\ \mu\text{m}$ ,  $50\ \mu\text{m}$ ,  $10\ \mu\text{m}$ ,  $5\ \mu\text{m}$ , parallel polarisers, (b) same, crossed polarisers, (c)  $30\ \mu\text{m}$ ,  $5\ \mu\text{m}$ , crossed polarisers, (d)  $10\ \mu\text{m}$ ,  $2\ \mu\text{m}$ , crossed polarisers

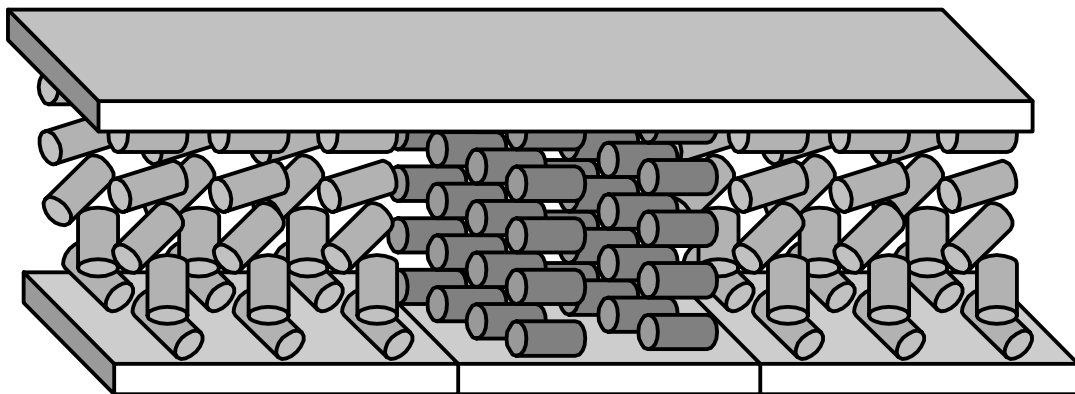


Figure 5.7 Schematic representation of a hybrid LCD cell containing one patterned LPP-1 and one non-patterned LPP-1 orientation layer (as shown in figure 5.3)

## 5.4.3 Direct focused laser writing

Lines were written on orientation layer material LPP-1 at various power densities. Scanning probe microscopy was used to study eventual relief structures, which might interfere with LC alignment caused by the laser writing. The result is shown in figure 5.8. Figures 5.8a to 5.8d show height scans of several laser-written lines with increasing power densities. Figures 5.8e and 5.8f are three-dimensional representations of figures 5.8b and 5.8d respectively. It is quite obvious that increasing the laser power density results in larger relief structures. The line in figure 5.8a, written at  $0.51 \times 10^{11} \text{ W/m}^2$  and  $1 \text{ mm/s}$ , is the only one that can be used for photo-alignment of LC's, the other lines induce surface structures, which are assumed to be too large for our purpose of surface induced liquid crystal alignment. Similar results were obtained for the other photo-alignment orientation layers.

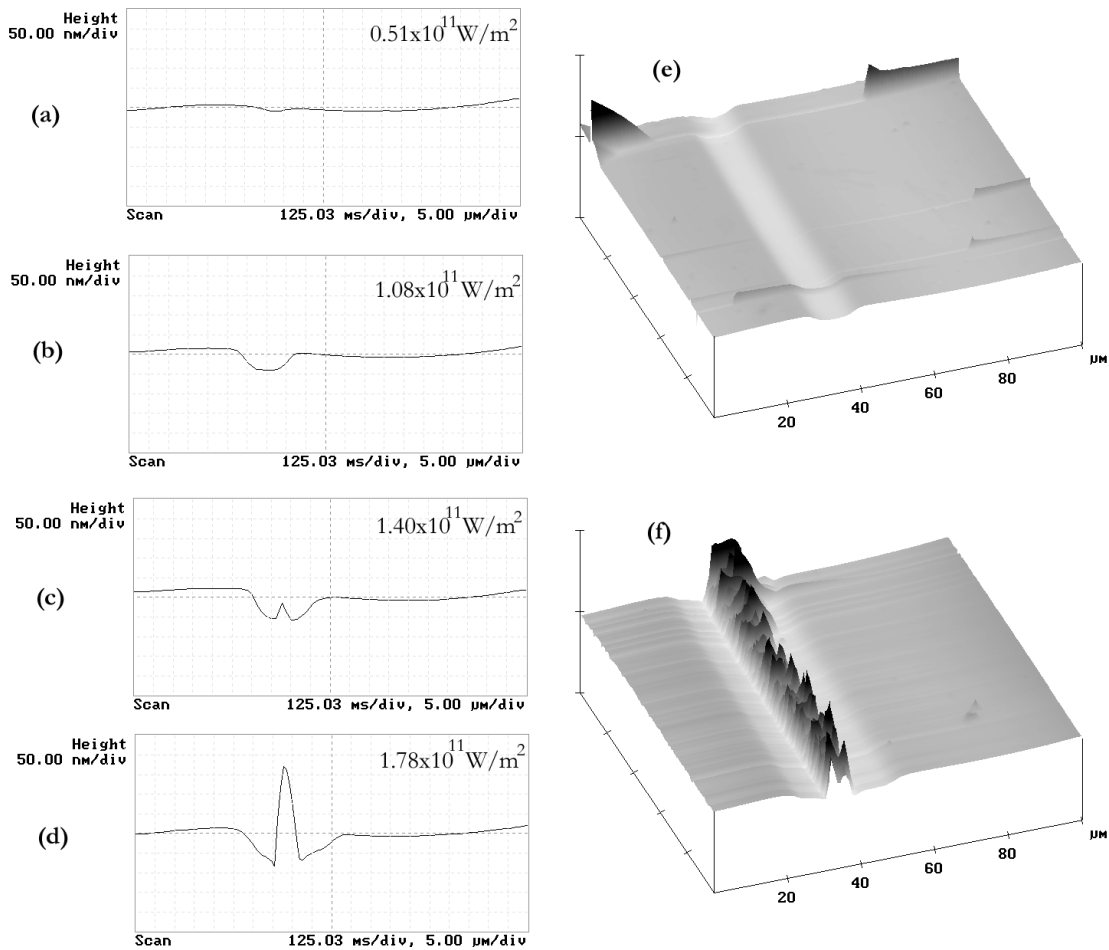


Figure 5.8 Scanning probe micrographs of laser-written LPP-1 at increasing laser power density;

(e) is a 3-D profile of (b), (f) is a 3-D profile of (d)



Figure 5.9 shows the effect of increasing laser writing power densities on LPP-4 on the LC alignment after cell construction. The orientation layers were constructed such that above the lines there should be a homogeneous planar configuration, while the non-processed areas have a twisted orientation. This was achieved by illuminating the laser-written orientation layer with a polarised UV lamp with the polarisation direction perpendicular to that of the laser-written patterns. The opposite orientation layer, a rubbed polyimide, was placed with its aligning axis perpendicular to the non-written areas of the LPP-4 layer (and therefore parallel to the laser-written sections). The  $0.51 \times 10^{11} \text{ W/m}^2$  lines are the first that are fully homogeneous over their length, the line width of these lines is  $15 \mu\text{m}$ . Increasing the power density results in homogeneous lines up to  $1.40 \times 10^{11} \text{ W/m}^2$ , which results in a line width of  $25 \mu\text{m}$ . At a laser power density of  $2.10 \times 10^{11} \text{ W/m}^2$ , the centre of the lines becomes black, which is caused by pyrolysis of the orientation layer. Overexposure causes additional orientation outside the lines at higher power densities.

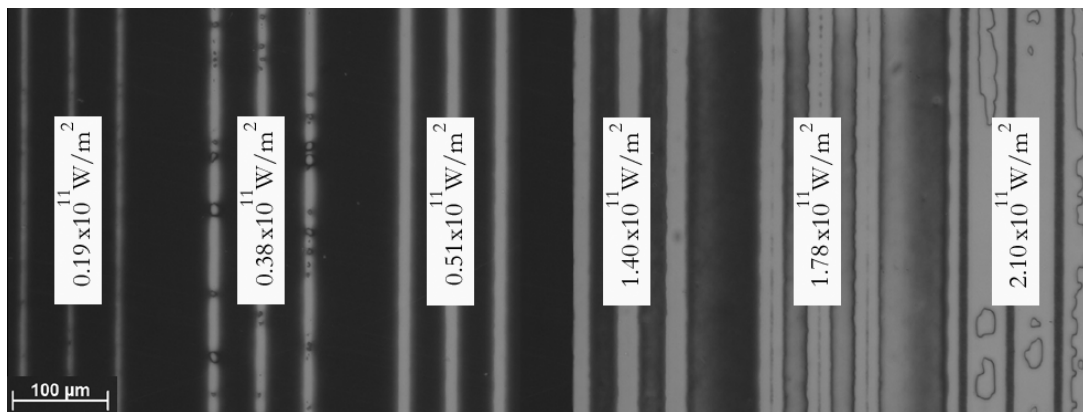


Figure 5.9 Composite polarised micrograph of a cell with LPP-4 in which lines were written with a range of laser power densities (parallel polarisers). The used laser power density is indicated next to the lines

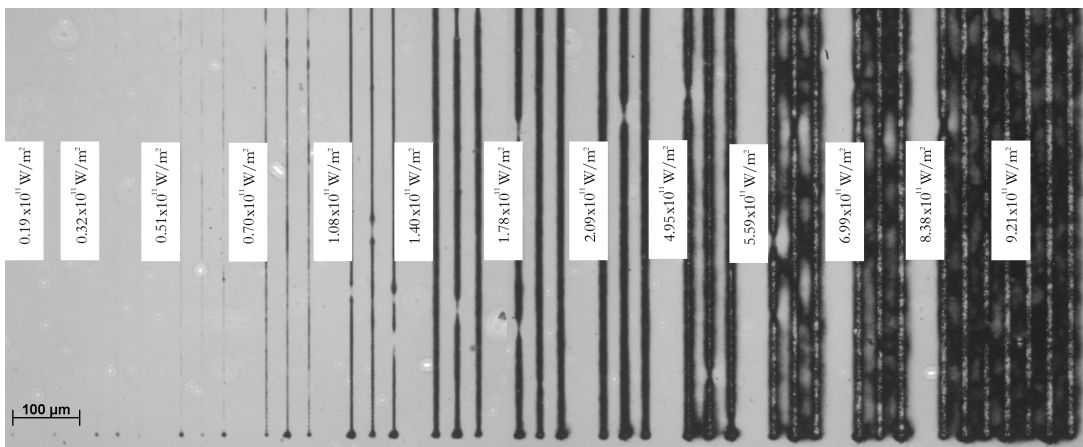


Figure 5.10 Polarised micrograph of a cell with a laser-written power density range on LPP-2 (crossed polarisers)

Figure 5.10 shows a power density range similar to that of figure 5.9 with laser-written patterns on orientation layer material LPP-2. As could be expected, due to the lower light absorption at 351 nm of LPP-2, a higher power is needed to form homogeneous patterns and at higher power densities also pyrolysis occurs.

The line width dependence on the power density is linear, as is shown in figure 5.11. This can be explained if the threshold level for orientation is very sharp. In this case the active area of the beam can be considered as a circle instead of Gaussian. The parts of the beam outside this active area do not contribute to the photo-alignment. At increased power density the circular active area is extended. No maximum line width was (yet) observed. The line widths of LPP-4 are much larger than that of LPP-2, due to the higher absorption of LPP-4 at 351 nm. For the other orientation layer materials similar power density ranges were observed and optimal laser writing parameters were derived. If the line spacing is decreased such that the LC alignment effect touch or overlap, patterns with larger dimensions up to several millimetres or even centimetres can be made.

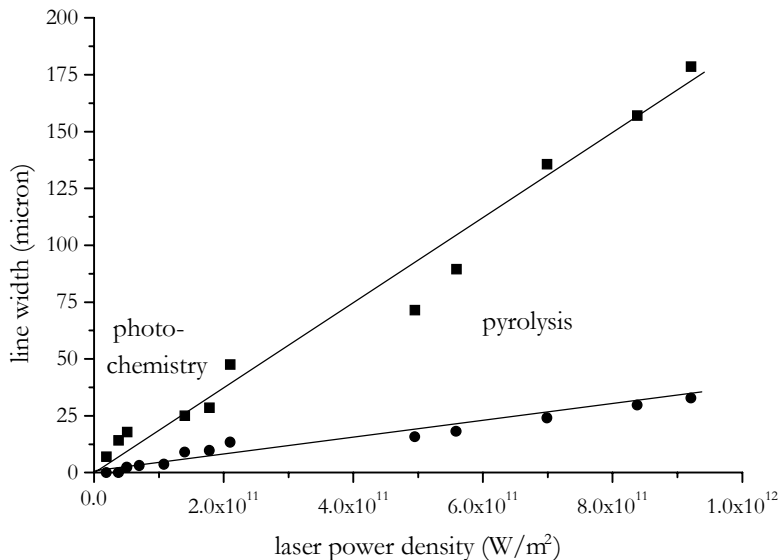


Figure 5.11 Line width dependence on the power density (writing speed = 1 m/s); (■) LPP-4, (●) LPP-2

#### 5.4.4 Complex patterns by multiple scanning directions

If a grid with horizontal and vertical lines is written, but with the same polarisation direction, an interesting pattern emerges when the grid spacing becomes sufficiently small. Figure 5.12 shows a polarised micrograph of a 100  $\mu\text{m}$  by 100  $\mu\text{m}$  grid. First the horizontal lines are written, followed by the vertical pattern. The LPP layer is subsequently irradiated with UV light with a polarisation direction perpendicular to the laser-written lines. The

opposite alignment layer induces a planar configuration and is placed with the aligning axis parallel to the laser-written lines of the laser-written layer. A circular pattern between the lines is observed. Above the lines a homogeneously planar configuration is present, while in the ‘circles’ a TN alignment is present. The Gaussian beam shape causes the generation of these circular patterns. At the places where the lines overlap, the area receives a double exposure. The sections just outside the overlapping areas, which received not enough energy to be aligned after the first pass, now receive an additional dose of energy and gain LC alignment properties. The further away from the centre of both lines, the lower the total received dose. This causes the corners of the overlapping sections to be rounded. Reducing the line spacing results in the formation of the circular features.

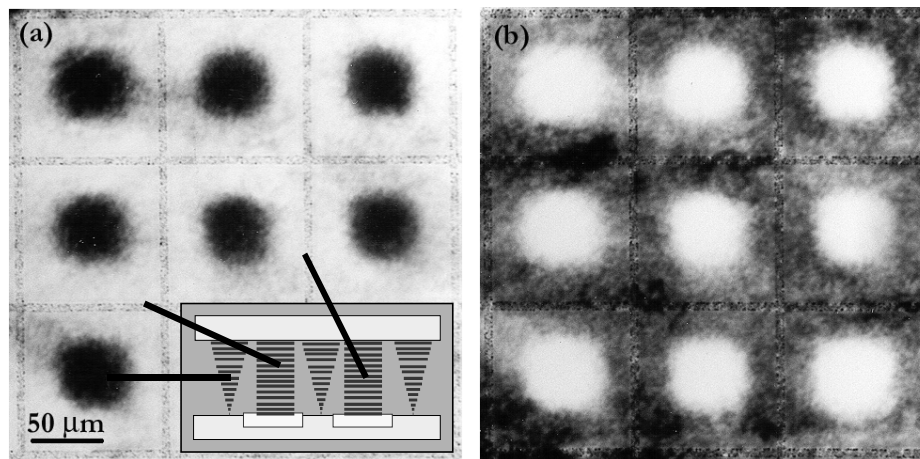


Figure 5.12 Polarised optical micrograph of a cell with a laser-written 100x100 μm grid on LPP-1; (a) parallel polarisers, (b) crossed polarisers

Another pattern was written on LPP-2 with vertical lines with a vertical polarisation direction, followed by a partly overlapping pattern of horizontal lines, written with a horizontal polarisation direction. Rotating the sample 90° in the sample holder and writing an identical pattern achieved this. The orientation layer was then illuminated with a polarised UV lamp with the polarisation direction identical to the first lines and a cell was constructed with a rubbed polyimide as the counter orientation layer with its LC aligning direction parallel to that of the first lines and the non-laser-written areas. The result is shown in figure 5.13. The vertical lines and the non-written sections show a homogeneous planar LC alignment and the horizontal lines a twisted nematic LC configuration, which is exactly as was expected. The LC orientation above the pattern that was written first (the vertical lines), was not influenced or altered by the second exposure when the horizontal lines were written. This demonstrates once again the irreversible and stable nature of alignment properties of the photo-chemically induced orientation.

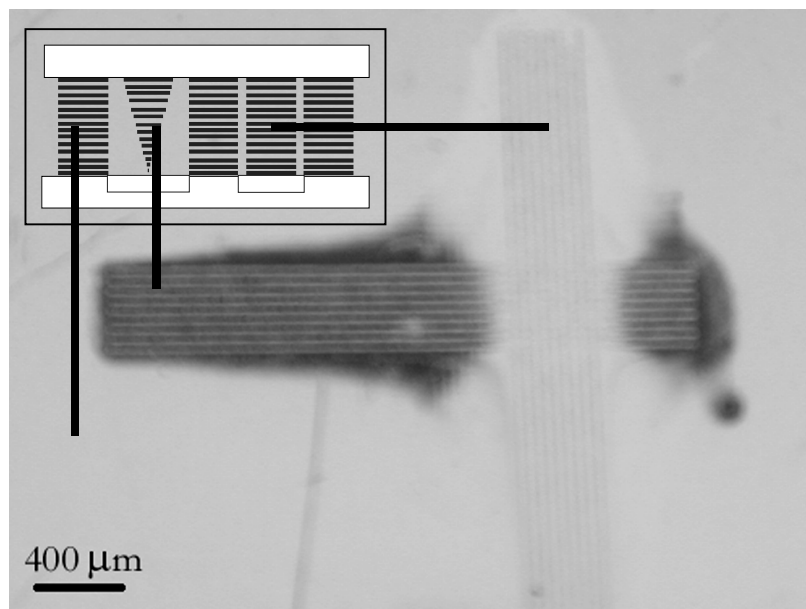


Figure 5.13 Photograph of a cell between parallel polarisers with laser-written patterns LPP-2; The horizontal lines were written with horizontally polarised light, the vertical line were laser written with vertically polarised light

#### 5.4.5 Interferometry

Interferometry was used to further reduce the resolution of the alignment patterns. Because of the narrow power window of the photo-alignment layers, it appeared to be difficult to establish constant alignment direction over large areas (see the appendix for a comprehensive description of the difficulties to overcome). Nevertheless, we succeeded in writing periodic structures ranging from 1-4 μm. At these pattern dimensions, disclinations on the boundaries between different LC alignment areas were a problem and they were indeed often observed, as is shown in figure 5.14. Patterns with smaller holographic pitches were made, but these are difficult to visualise due to the resolution of the microscope.

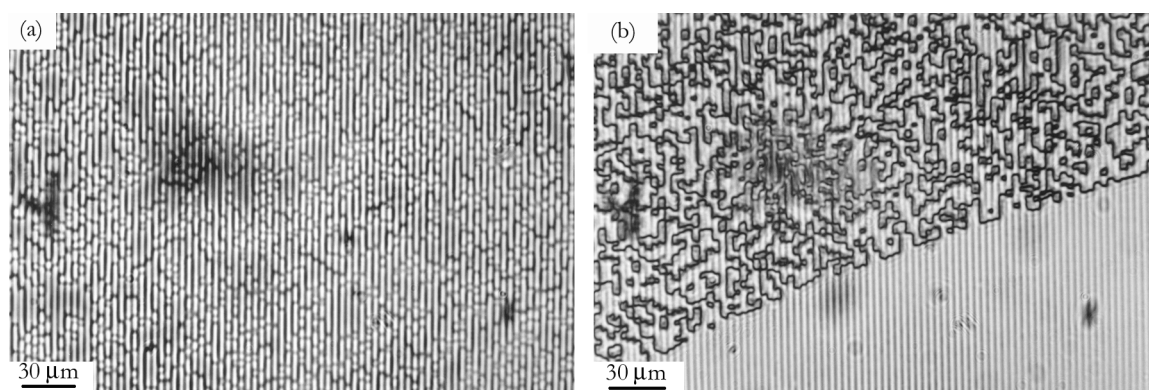


Figure 5.14 Polarised light micrograph of disclinations within a cell with holographically patterned LPP-2

Adding a small amount of chiral dopant reduced or even eliminated these disclinations. However, usually dopants were not used, since large enough sections without disclinations could generally be found in the cells to observe the holographic pattern. Figure 5.15 shows cells with a 4  $\mu\text{m}$  spaced holographic pattern in cells with LPP-2 and LPP-1 orientation layers.

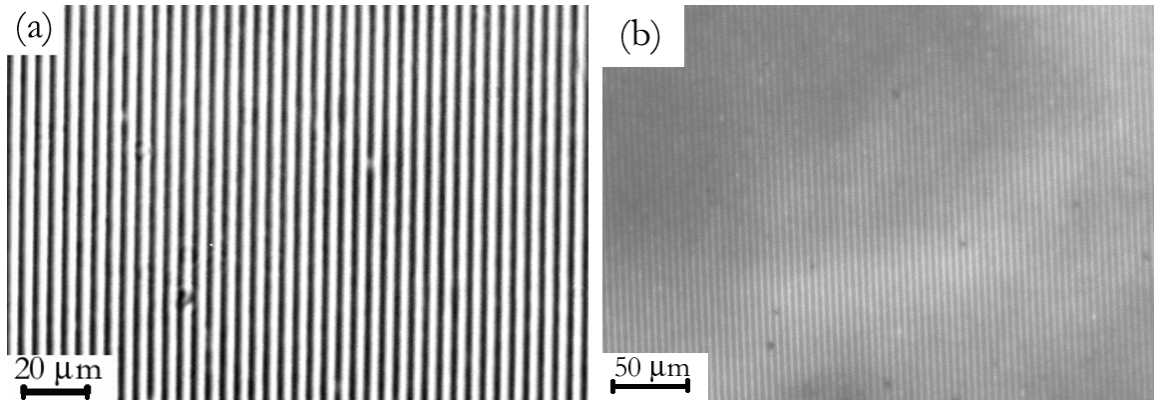


Figure 5.15 Polarised light micrographs of cells with holographically patterned photo-alignment orientation layers and without chiral dopants; (a) LPP-2, (b) LPP-1

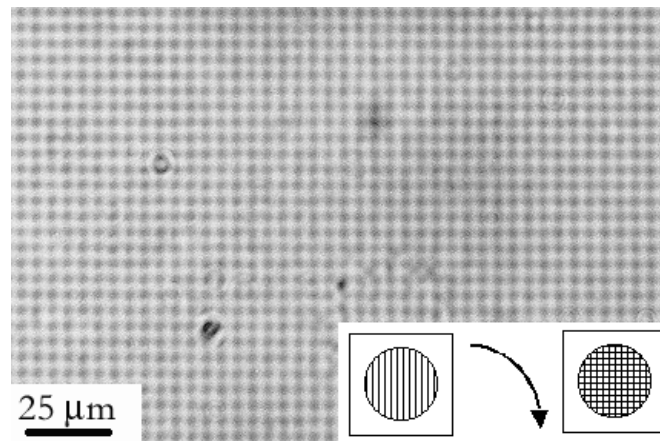


Figure 5.16 Polarised optical micrograph of a cell with double exposed LPP-2 (between parallel polarisers)

Grid structures are obtained by a double holographic exposure. After the first holographic pattern has been formed, the sample is turned  $90^\circ$  and illuminated again. A second line pattern is now formed perpendicular to the first, but with the same LC aligning direction. A post-irradiation with UV light with a polarisation direction perpendicular to that of the lines, fixed the orientation of the non-written sections. Figure 5.16 shows a micrograph of a  $4 \times 4 \mu\text{m}$  grid in a cell with double holographically exposed LPP-2 and a homogeneously planar aligning opposite orientation layer (placed with its aligning axis parallel to the laser-written lines). The transparent lines are homogeneously parallel aligned

LC, while the dark areas are the non-laser-written sections of the orientation layer. This patterning is very similar to the patterns shown in figure 5.12. The rounding of the edges is present, but due to the small dimensions not very clear in figure 5.16. Other grid dimensions or shapes are easily achieved by increasing or decreasing the holographic pitch or by placing the sample under a different angle for the second illumination.

## 5.5 Conclusions

By using direct focused laser writing and interferometry with linearly polarised UV light in the sub-melting regime, it is possible to photo-chemically pattern functional photosensitive polymers without mechanical changes to the material. These patterned polymers are applied as hybrid LC orientation layers with which optical cells are constructed with different LC alignment on a single substrate.

It was possible to use direct focused laser writing to create high contrast hybrid TN cells, but a lower resolution than approximately 5 microns is not available through this technique. Care needs to be taken that no relief structures are formed. Interferometry results in line patterns with smaller pitches. By subsequent illumination, grids and more complex structures are patterned.

With interferometry it is possible to further reduce the resolution to 1 or 2 microns, but this technique still has to be optimised for use with LPP materials before large area, high-resolution hybrid cells are formed. However, through fine-tuning the laser writing settings and material absorption parameters, it should be possible to increase the homogeneity of the patterns. The processing window in which homogeneous holographic spots are formed (see the appendix) is for LPP materials very small. Especially on LPP-3 and LPP-4, which have a high absorption at 351 nm, it proved to be very difficult to generate homogeneous patterns. The spatial distribution of the LC alignment is difficult to maintain over the width of the cell, causing shifts and mixing of the different areas (figure 5.17). This effect increases for larger cell spacings.

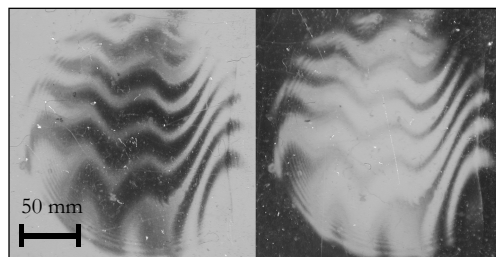


Figure 5.17 Inhomogeneous spots due to mixing and shifting of twisted and homogeneous parallel domains in holographic spots in linearly photo-polarised polymers

To investigate if increased viewing angle optical cells can be constructed using laser-patterned LPP orientation layers, further studies are needed whether the tilt angle and direction can be modulated by performing the direct focused laser writing and interferometry under an angle. These patterned orientation layers can easily be implemented in TN LCD's or personalised security features in a similar way as the laser-melted rubbed polyimide orientation layers described in chapter 4.

## 5.6 References

- [1] M. O'Neill, S. M. Kelly, *J. Phys. D - Appl. Phys.* **33**, R67, (2000).
- [2] W. M. Gibbons, P. J. Shannon, S. T. Sun, B. J. Swetlin, *Nature* **351**, 49, (1991).
- [3] K. Ichimura, Y. Suzuki, T. Seki, A. Hosoki, K. Aoki, *Langmuir* **4**, 1214, (1988).
- [4] K. Ichimura, H. Akiyama, N. Ishizuki, Y. Kawanishi, *Makromol. Chem. - Rapid Commun.* **14**, 813, (1993).
- [5] M. H. Kim, J. D. Kim, T. Fukuda, H. Matsuda, *Liq. Cryst.* **27**, 1633, (2000).
- [6] J. L. West, X. Wang, Y. Ji, J. R. Kelly, *SID 95 Digest*, 703, (1995).
- [7] D. C. Rich, E. Sichel, P. Cebe, *J. Appl. Pol. Sci.* **65**, 1151, (1997).
- [8] M. Nishikawa, J. L. West, *Jpn. J. Appl. Phys.* **38**, 5183, (1999).
- [9] M. Nishikawa, T. Kosa, J. L. West, *Jpn. J. Appl. Phys.* **38**, L334, (1999).
- [10] M. Hasegawa, Y. Taira, *J. Photopol. Sci. Technol.* **8**, 241, (1995).
- [11] M. Kimura, S. Nakata, Y. Makita, Y. Matsuki, A. Kumano, Y. Takeuchi, H. Yokoyama, *IDW'00* (Kobe, Japan), 53, (2000).
- [12] M. Schadt, K. Schmitt, V. Kozinkov, V. Chigrinov, *Jpn. J. Appl. Phys.* **31**, 2155, (1992).
- [13] A. Dyadyusha, V. Kozinkov, T. Marusii, Y. Reznikov, V. Reshetnyak, A. Khizhnyak, *Ukr. Fiz. Zh.* **36**, 1059, (1992).
- [14] M. Schadt, H. Seiberle, A. Schuster, *Nature* **381**, 212, (1996).
- [15] K. Rajesh, S. Masuda, R. Yamaguchi, S. Sato, *Jpn. J. Appl. Phys.* **36**, 4404, (1997).
- [16] P. O. Jackson, R. Karapinar, M. O'Neill, P. Hindmarsh, G. J. Owen, S. M. Kelly, *Proc. SPIE* **3635**, 38, (1999).
- [17] K. Ichimura, Y. Akita, H. Akiyama, Y. Hayashi, K. Kudo, *Jpn. J. Appl. Phys.* **35**, L992, (1996).
- [18] M. Kimura, S. Nakata, Y. Makita, Y. Matsuki, A. Kumano, Y. Takeuchi, *SID 01 Digest*, 1162, (2001).
- [19] S. Nakata, M. Kimura, A. Kumano, Y. Takeuchi, *IDW'00* (Kobe, Japan), 1161, (2000).
- [20] H. Seiberle, M. Schadt, *J. SID* **8**, 67, (2000).
- [21] M. Schadt, *Annu. Rev. Mater. Sci.* **27**, 305, (1997).
- [22] M. Obi, S. Morino, K. Ichimura, *Chem. Mater.* **11**, 656, (1999).

## Chapter 6

### Laser Writing of Conductive Patterns Using Gold Nanoparticles

#### 6.1 Introduction

In chapter 2 and 3 we showed that conductive patterns were directly written in polyimide with direct focused laser writing in the pyrolysis regime and that these conductive patterns were used for the addressing of LCD's. Due to the nature of the patterns and the limited transmittivity of the polyimide films, these patterns could only be applied in a specific type of LCD. Direct writing of conductive patterns in thin, transparent rubbed polyimide films would combine LC orientation and electrical addressing of a display in one layer. Since pyrolysis of thin polyimide films results in irregularly shaped structures<sup>1</sup>, an alternate route needs to be found. In literature it was reported that the addition of conductive particles to a polymer, followed by a laser patterning step, results in conductive patterns<sup>2,3</sup>. Metallic powders are used and the particles are fused together through laser melting. Another route that was presented in literature is the use of organo-metallic particles, which are mixed with or coated on top of a polymer. By patterning these blends or coatings with techniques such as electron beam writing<sup>4-8</sup> or focused ion beam writing<sup>9</sup>, the organic components of the material are removed, resulting in purely metallic patterns. If wanted, the metallic structure can be developed by rinsing the organic material still present at the non-irradiated sections with an organic solvent (sketched in figure 6.1).

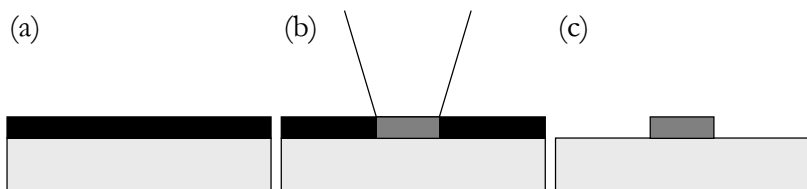


Figure 6.1 Three-step procedure to produce freestanding metallic micro-patterns by laser writing on a polymer-organometallic coating. (a) mixing/coating, (b) laser writing, (c) development

The metallic component should be able to mix or blend with the polymer and should be coatable on a substrate. Common organo-metallic solutions, e.g. palladium acetate solutions<sup>10,11</sup>, can be used, but their metal content is relatively low. This might prevent the



formation of continuous conductive patterns. Therefore, metallic nanoparticles are chosen as the organo-metallic component<sup>12</sup>. These materials consist of a metallic core with a maximum dimension ranging between 1 and 50 nanometres, on which organic molecules are chemically bonded, e.g. gold cores with thiol-containing molecules (see figure 6.2). These organic molecules prevent the metallic cores from aggregating into larger metallic structures and make the particles soluble in organic solutions. This enhances their ability to produce coatings and blends with polymers. Also, the metal content of nanoparticles is much larger than in other organo-metallic materials<sup>6,7</sup>, which reduces carbon contamination due to pyrolysis.

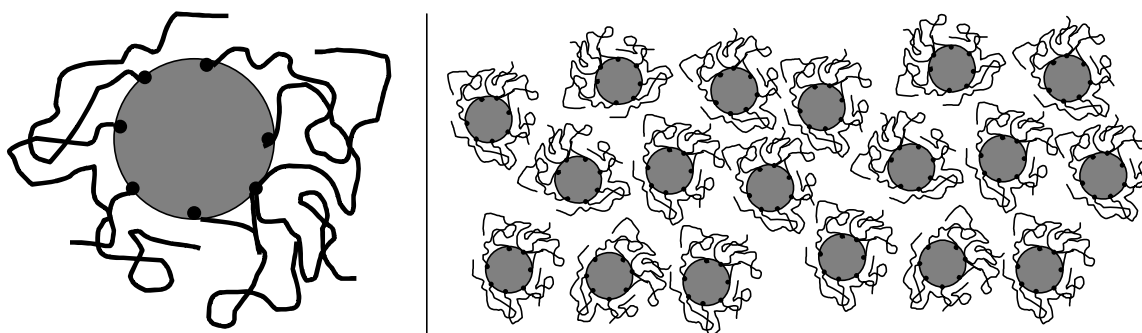


Figure 6.2 Cartoon of a single nanoparticle and a cluster of stabilised metallic nanoparticles

Due to their small, usually spherical, shape, metallic nanoparticles have a large contact area and are very sensitive to oxidation and other chemical reactions (these particles have excellent catalytic properties and this is the area in which they are mostly applied<sup>13,14</sup>). Most particles can only exist as metaloxides<sup>13,14</sup> or other chemically bonded structures, such as cadmium sulfide<sup>12</sup>. To obtain metallic nanoparticles, which are chemically more stable and that are not prone to oxidation, noble metals, such as gold or silver are used.

The direct writing experiments reported in literature made use of electron<sup>4,8</sup> or focused ion<sup>9</sup> beams to write patterns on coatings consisting of only metallic nanoparticles. With these techniques, patterns with sub-100 nm resolutions have been achieved. For larger pattern sizes, e.g. in the range from 1 to several 100  $\mu\text{m}$ , a laser is a much more versatile and convenient direct patterning tool. Mixing the nanoparticles with polymers makes the coatings mechanically more stable and opens up the possibility to use functional polymers, such as rubbed polyimides. This chapter describes the choice of a model system of a blend of a polymer with metallic nanoparticles, the nanoparticle synthesis, the coating procedure and the laser writing process. Also, we investigated if the non-irradiated organic components can be removed from the substrate through rinsing. The electrical conductivity of the

patterns is examined, followed by an evaluation of the possibilities for application of these laser-patterned coatings, along with a discussion of the possibility to adapt this system for use with functional anisotropic polymers, such as rubbed polyimides, in electro-optical applications.

## 6.2 Experimental

### 6.2.1 Materials

All chemicals were obtained from Aldrich, except sodium borohydride, which was obtained from Fluka and the toluene, which was obtained from Biosolve.

### 6.2.2 Synthesis

The recipes for the synthesis of hexanethiol, dodecanethiol and octadecanethiol stabilised gold nanoparticles are the same, with the exception of the amount of added alkanethiol. The recipe is an adaptation of one given by M. Brust *et al.* for the synthesis of dodecanethiol stabilised gold nanoparticles<sup>15</sup>.

A 30 mM solution of hydrogen tetracholoaurate (1.000 g) in water (98 ml) was added to a 50 mM solution of tetraoctylammonium bromide (0.715 g) in toluene (262 ml). This two-phase system was then vigorously stirred until the hydrogen tetracholoaurate had transferred into the toluene layer, resulting in a deep orange solution. After the stirring was stopped and the layers were fully phase-separated, 1.85 mmol alkanethiol (219 mg in the case of hexanethiol, 374 mg in the case of dodecanethiol or 866 mg in the case of octadecanethiol) was added to the toluene layer. Under vigorous stirring, over the course of approximately one hour, a 0.4 M sodium borohydride (1.237 g) solution in water (50 ml) was added to the system. After the first few drops the color of the solution turned to deep-black as the gold nanoparticles were formed. After the mixture was stirred for 3 more hours and the two phases were phase-separated again, the toluene phase was removed from the mixture. Approximately 90% of the toluene was removed in a rotary evaporator ( $T_{\text{bath}} = 40$  °C,  $p = 80$  mbar) and the remaining solution was mixed with 500 ml ethanol and kept overnight at -18 °C. The product was filtered off and washed with ethanol several times. The nanoparticles were dissolved in 20 ml toluene and precipitated in 400 ml ethanol. The ethanol was decanted and evaporated as much as possible and the nanoparticles were dried overnight in a vacuum oven at 50 °C. The product was collected and sealed in a glass container, where it remained stable for indefinite time. The yield of dodecanethiol stabilised gold nanoparticles ranged between 50% and 70%, that of octadecanethiol stabilised gold

nanoparticles ranged between 70 % and 90 %. The synthesis of hexanethiol stabilised gold nanoparticles however resulted into a very low yield (< 5 %).

### 6.2.3 Coating

The nanoparticles were dissolved in toluene and polymethyl methacrylate (PMMA) was added. PMMA with various molecular weights were used ( $M_w = 120000$  g/mol, 350000 g/mol and 996000 g/mol) at various concentrations. Coatings were made on glass substrates using three techniques: film casting, spin-coating and doctor-blading.



Figure 6.3 Photograph of filmcasted octadecanethiol stabilised nanoparticle / PMMA coatings

Film casting was done from solution under a soft nitrogen flow and resulted in inhomogeneously thick films ranging from 100-500 micron (figure 6.3). Increasing the temperature did not result in significantly improved coatings. Therefore, the film casting method was not further used.

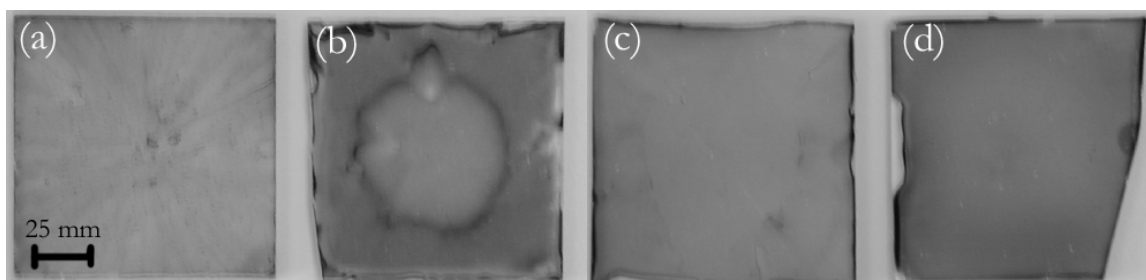


Figure 6.4 Photograph of spin-coated octadecanethiol stabilised nanoparticle / PMMA coatings. (a) too high spin speed, (b) too low spin speed, (c) 2.5 wt% nanoparticles, (d) 5 wt% nanoparticles

Spin-coating (Karl Suss RC-8) was done at various speeds, depending on the PMMA concentration of the solutions. It proved very difficult to obtain a homogeneous

nanoparticle distribution in the sample. Often radial patterns were observed after spin-coating at too low or too high spin speeds (see figure 6.4a and 6.4b). Homogeneous coatings (such as shown in figure 6.4d) were obtained with solutions with a concentration in toluene of 9.5 wt% PMMA ( $M_w=350000$  g/mol) and 5 wt% octadecanethiol stabilised gold nanoparticles and the three-step spin-coater settings as shown in table 6.1 (step 1 distributes the solution over the whole substrate, step 2 is the actual spin-coating cycle, step 3 is a drying cycle). A film thickness of 100-200 nm was obtained. Lowering the nanoparticle concentration resulted in less strongly coloured substrates (figure 6.4c), but more discontinuities also often occurred. Increasing the nanoparticle concentration resulted in more clustering of the nanoparticles.

step #	acceleration (rpm/s)	speed (rpm)	time (s)	cover
1	500	500	30	open
2	500	2000	60	closed
3	500	1000	15	open

Table 6.1 Optimal octadecanethiol stabilised gold nanoparticles/PMMA/toluene spin-coating settings

Doctor-blading was done using an Erikson Coatmaster model 509/MC-I and resulted in thicker (several  $\mu\text{m}$ ) and more homogeneous coatings than with both film casting and spin-coating. A homogeneous coating was obtained if a solution in toluene of 9.7 wt% PMMA ( $M_w=350000$  g/mol) and 2.5 wt% octadecanethiol stabilised nanoparticles was doctor-bladed with a 7.5  $\mu\text{m}$  blade and a speed of 10 mm/s. The coatings were dried at 100 °C to remove all the toluene. The film thickness was approximately 5 micron was obtained. Similar settings were used for dodecanethiol stabilised gold nanoparticles.

#### 6.2.4 Direct focused laser writing

Laser writing was performed with the same set-up as described in chapter 2.2.2. Laser intensities and writing speeds were varied. To obtain conductive patterns, the laser power was set between  $1.27 \times 10^{11}$  W/m<sup>2</sup> and  $2.54 \times 10^{11}$  W/m<sup>2</sup> and patterns were written with a speed of 0.1 mm/s.

#### 6.2.5 Development of conductive structures

The development of the metallic structures was done by carefully moving the laser-written substrates through a toluene solution. The rinsed substrate was left in the toluene solution for approximately one hour and dried overnight in the air.

### 6.2.6 Characterisation

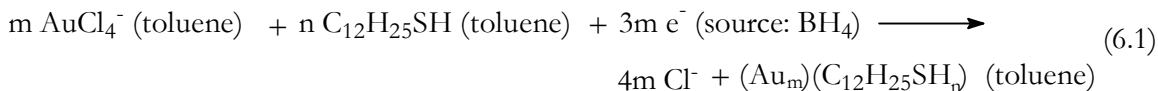
Thermogravimetric analysis (TGA) was performed using a Perkin-Elmer TGA 7. Transmission Electron Microscopy (TEM) was performed using a JAOL JEM 2000 FX. UV-VIS absorption spectra were measured using a Shimadzu UV-3102PC UV-VIS-NIR scanning spectrophotometer. Environmental Scanning Electron Microscopy (ESEM) was performed using a Philips XL30 FEG-ESEM. Light microscopy was performed using a Zeiss Universal and a Zeiss Axioplan 2. Conductivity measurements (2-point method) were performed with a Keithley 237 high voltage source measure unit. The contact was enhanced using a silver lacquer. Coating thickness was determined using a Tencor P-10 Profilometer.

## 6.3 Results

### 6.3.1 Synthesis and analysis of alkanethiol stabilised gold nanoparticles

In general, the formation of stabilised metallic nanoparticles occurs via several different approaches<sup>14</sup>, such as grinding of metals, followed by the addition of the stabilizing molecules, synthesis from metal vapors, 'wet' chemical methods from solutions and electrochemical reactions. Often, these synthesis methods are quite complex and/or result in low yields. However, high yields of alkanethiol stabilised gold nanoparticles are synthesised relatively straightforward via a one-flask, two-phase liquid-liquid synthesis<sup>15</sup>. These alkanethiol stabilised gold nanoparticles have high solubility in common organic solvents such as xylenes and toluene and high absorption in UV wavelengths.

Several alkanethiol stabilised gold nanoparticles were synthesised (with 1-hexadecanethiol, 1-dodecanethiol and 1-octadecanethiol as the stabilizing ligands) to find the material with the best properties for use in blends with polymers. They were synthesised using a modification of the two-phase liquid-liquid method described by M. Brust *et al.*<sup>15</sup> (see experimental). This method was chosen because it is quick, relatively straightforward and results in a good nanoparticle yield with the required properties. The reaction takes place in a two-phase water-organic (toluene) system. Using phase-transfer agent tetraoctylammonium-bromide,  $\text{AuCl}_4^-$  is transferred from the water phase to the toluene phase, where the alkanethiol is present. Using aqueous sodium borohydride, the  $\text{AuCl}_4^-$  is reduced and the alkanethiol is simultaneously bonded to the forming gold clusters. The gold nanoparticles stay dissolved in the toluene layer. The nanoparticle forming reaction that takes place is given in reaction equation 6.1<sup>15</sup>.



To enhance the yield, the alkanethiol is added in slight excess. After removal of the particles from the solvent and purification, the deep black alkanethiol stabilised nanoparticles can be kept at room temperature for an unlimited time (no degradation was observed on any sample, even after several years).

The hexanethiol and dodecanethiol stabilised gold nanoparticles were obtained in low yield and were viscous, sticky wax-like materials. The octadecanethiol stabilised nanoparticles were synthesised with a high yield and were obtained as a well-defined loose powder. We therefore concentrated our further research mainly on the octadecanethiol stabilised gold nanoparticles.

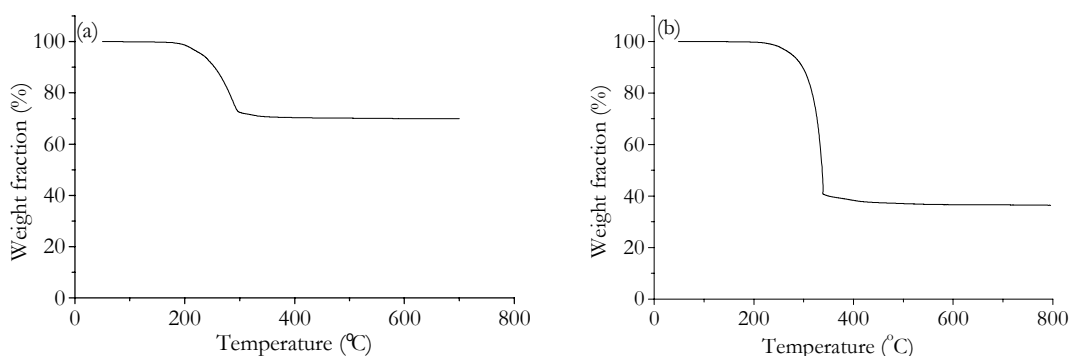


Figure 6.5 Thermo-gravimetric analysis plots for (a) dodecanethiol stabilised gold nanoparticles and (b) octadecanethiol stabilised gold nanoparticles

The gold content of the nanoparticles was determined using thermo-gravimetric analysis (TGA). Figure 6.5 shows typical results for dodecanethiol stabilised gold nanoparticles and octadecanethiol stabilised gold nanoparticles. The organic parts of the nanoparticles were removed between 200 °C and 330 °C. After the sample was removed from the TGA, a yellow colored solid material remained behind. This is pure gold that agglomerated into a metallic powder. The gold weight fraction of the dodecanethiol stabilised gold nanoparticles was 70 %; that of the octadecanethiol stabilised gold nanoparticles was 40 %.

We calculated the gold – alkanethiol ratios for both types of nanoparticles. The molar gold – dodecanethiol ratio is 2.4 : 1. This indicates that the gold particles are stabilised by a less than equimolar amount of dodecanethiol stabilisers. The molar gold – octadecanethiol ratio is 1 : 1.03, which is an almost equimolar amount. These results might

explain the lower yield of the dodecanthiol stabilised gold nanoparticles, since a large part of the added dodecanethiol was not used to stabilise the gold particles. The very low yield of hexanethiol stabilised gold nanoparticles is explained in the same way if this effect is even worse for shorter-length thiols. Unfortunately, not enough hexanethiol stabilised gold nanoparticles was available for a thermogravimetric analysis.

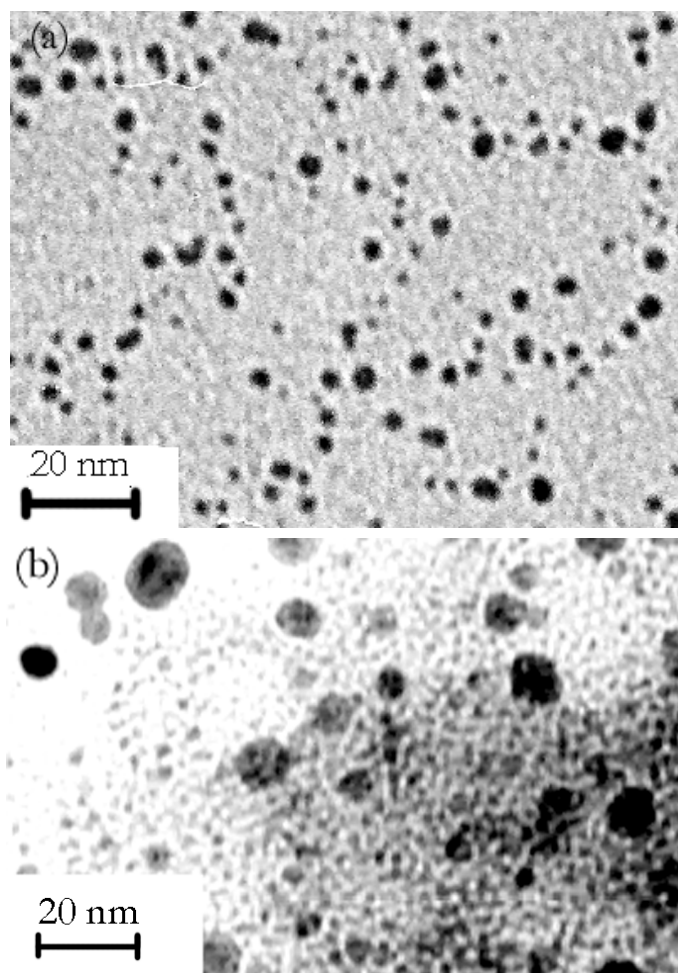


Figure 6.6 Transmission electron micrographs of (a) dodecanethiol stabilised gold nanoparticles, (b) octadecanethiol stabilised gold nanoparticles

The size of the nanoparticles was determined using transmission electron microscopy (TEM). Figure 6.6 shows a transmission electron micrograph of dodecanethiol and octadecanethiol stabilised gold nanoparticles. Only the gold cores are visualised by TEM and therefore only the core diameter is determined through this technique. There seems to be a large particle diameter distribution, but this is mainly caused by clustering of the particles. The average diameter of the dodecanethiol stabilised gold nanoparticles is approximately  $2.5 \pm 0.3$  nm, the average diameter of the octadecanethiol stabilised gold nanoparticles is

approximately  $1.5 \pm 0.3$  nm. The diameter was determined from the smallest particles visible in the micrographs to minimise the influence of clustered particles. The number of gold atoms per nanoparticle (based on closest spherical packing and a gold atom diameter of 0.3 nm) is for dodecanethiol stabilised gold nanoparticles approximately 300, while for octadecanethiol stabilised gold nanoparticles this is approximately 65. Table 6.2 shows an overview of the different properties and values determined above.

	hexanethiol	dodecanethiol	octadecanethiol
Yield	< 5 %	50 - 70 %	70 - 90 %
Molar Au content	-	70 %	40 %
Molar ratio Au : alkanethiol	-	2.4 : 1	1.03 : 1
Nanoparticle core diameter	-	2.5 nm	1.5 nm
Au atoms per nanoparticle	-	~ 300	~ 65

Table 6.2 Yield, molar Au content, molar ratio Au : thiol, nanoparticle diameter and number of Au atoms per nanoparticle for gold nanoparticle with three different alkanethiol stabilisers, determined by TGA and TEM

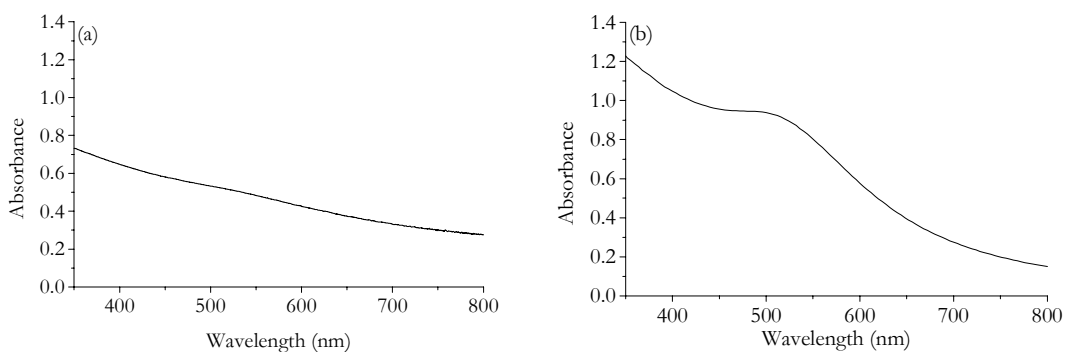


Figure 6.7 UV-VIS spectrum of (a) a doctor-bladed octadecanethiol stabilised gold nanoparticle / PMMA coating and (b) a 0.04 wt% octadecanethiol stabilised gold nanoparticle solution in toluene

The UV-VIS spectrum of a gold nanoparticle coating, mixed with PMMA for mechanical stability and to prevent excessive clustering (figure 6.7a), shows a broad absorption band, which gradually increases into the UV region. These broad peaks are common for metallic nanoparticles, although if the size distribution is narrower, individual peaks become more pronounced. This is achieved by lowering the nanoparticle content in the coatings or by using an extremely dilute solution. Figure 6.7 illustrates this, the peak at 520 nm is much more pronounced for the dilute solution (figure 6.7b) than for the doctor-bladed film (figure 6.7a).



The band at 520 nm is the plasmon absorption band, resulting from the collective oscillation of electrons in the gold particles<sup>16</sup> and is typically observed for colloidal gold nanoparticle solutions<sup>17</sup>. This band is broadened due to a large size distribution, scattering and because for small particles (< 2 nm), the average free path of the electrons exceeds the particle size, lowering the effective optical conductivity<sup>16</sup>. The UV-VIS spectra show that at 351 nm, the operating wavelength of the argon ion laser, there should be sufficient absorption to pattern these coatings.

### 6.3.2 Gold nanoparticle coatings

It was found that it was impossible to produce a stable and homogeneous coating using pure alkanethiol stabilised gold nanoparticle solutions in toluene. The nanoparticles formed large powder-like clusters and could easily be wiped or blown from the glass substrates. Since the nanoparticles have to be mixed with a polymer for our purposes, some of these problems are easily overcome. A polymer can supply structural stability and enhanced adhesion to the substrate to prevent material removal from the substrate. Also, due to a reduction in nanoparticle mobility, clustering of the particles is prevented to a large extent. And, of course, the objective of this chapter is to generate conductive structures in (functional) polymers. Initially, polyimide was chosen as the polymeric component, but unfortunately there was not a solvent that could sufficiently dissolve both the alkanethiol stabilised gold nanoparticles and the polyimides. Therefore, poly(methyl methacrylate), PMMA, was chosen as the polymeric component as a model material to investigate if the principle of laser writing on this type of hybrid organic-inorganic blends can indeed result in electrically conductive structures. PMMA is both miscible with the nanoparticles, as well as soluble in toluene.

Three coating techniques were used: film casting, spin-coating and doctor-blading. Film casting resulted in very inhomogeneous coatings with varying thickness (100 – 500  $\mu\text{m}$ ). Spin-coating resulted in flat, thin coatings with a sub-micron thickness (100 - 200 nm), depending on the PMMA concentration and the spin-coating cycle program). Doctor-blading resulted in thicker (several  $\mu\text{m}$ ) and more homogeneous coatings than with both film casting and spin-coating. Also, larger areas were coated using this technique, making it the preferable method for coating application.

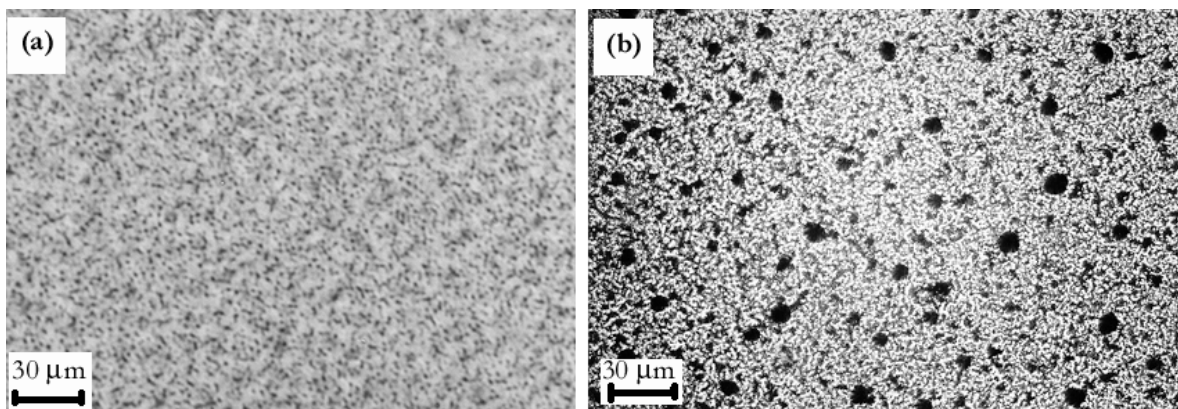


Figure 6.8 Optical micrograph of a doctor-bladed dodecanethiol stabilised nanoparticle / PMMA coating  
(a) 2.5 wt% nanoparticles, (b) 10 wt% nanoparticles

While the doctor-bladed coatings were the most homogeneous, when examined with an optical microscope, still small (several  $\mu\text{m}$ ) agglomerates of clustered nanoparticles were observed within the PMMA matrix (figure 6.8). Larger nanoparticle concentrations resulted in larger agglomerates and a broader cluster size distribution. Between the agglomerates, smaller clusters, below the resolution of the microscope, are also present.

### 6.3.3 Thermal decomposition

The TGA plots (figure 6.5) show that at temperatures between 200 °C and 330 °C, all organic stabilisers are removed from the nanoparticles. This is a temperature rise that should easily be reached with direct focused laser writing, since the absorption at 351 nm is sufficiently high for laser processing (figure 6.7). The TGA experiments were carried out on pure nanoparticles in powder form. To investigate if a coated nanoparticle / PMMA mixture also degrades to gold above these temperatures, some doctor-bladed octadecanethiol stabilised gold nanoparticle / PMMA coatings were placed under a  $\text{N}_2$  atmosphere in an oven at 500 °C for 30 minutes. After removal of the substrates from the oven, yellow coloured clusters with a wide distribution in size were obtained (figure 6.9). These clusters were easily wiped off the substrate, indicating that all organic material, including the PMMA, was removed and only gold remained on the surface. Non-stabilised gold particles fuse together into larger metallic agglomerates. The average size of the agglomerates depended on the nanoparticle concentration in the used solutions. Higher concentrations resulted in larger agglomerates.

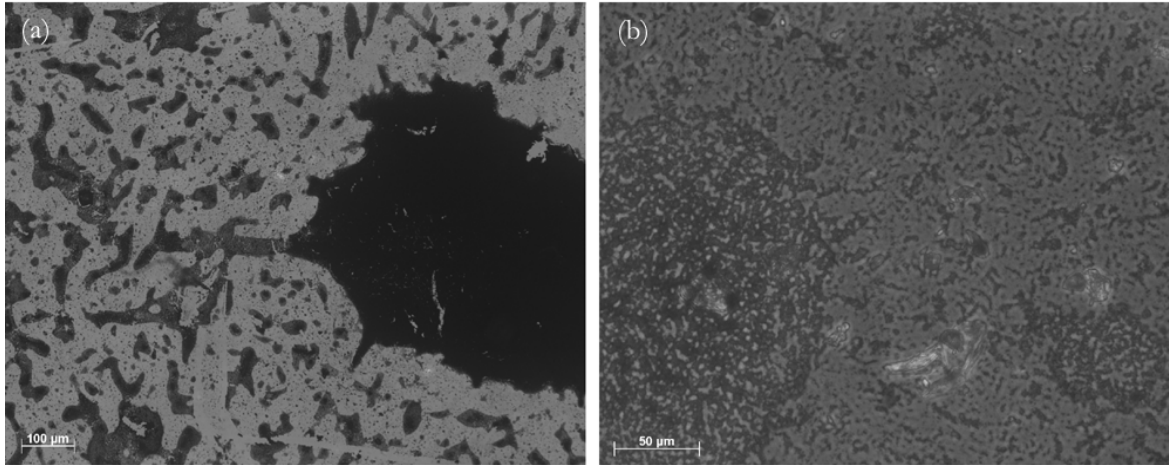


Figure 6.9 Optical micrographs of a doctor-bladed PMMA/octadecanethiol stabilised gold nanoparticle coating, heated for 30 minutes at 500 °C (N<sub>2</sub> atmosphere)

#### 6.3.4 Direct focused laser writing

With the focused beam of the Ar<sup>+</sup> laser lines were written in a 5 µm thick, doctor-bladed octadecanethiol stabilised gold nanoparticle/PMMA coating. The line width was determined as a function of the laser power density (figure 6.10). There is a threshold laser power of 0.7 W/m<sup>2</sup> below which no continuous lines are formed.

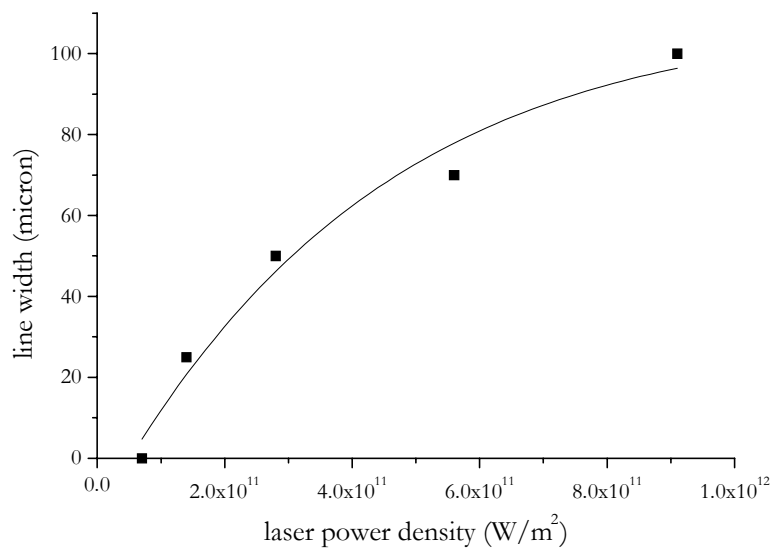


Figure 6.10 Line width dependence on the power density for a doctor-bladed laser-written octadecanethiol stabilised gold nanoparticles/PMMA coating (writing speed 1 mm/s)

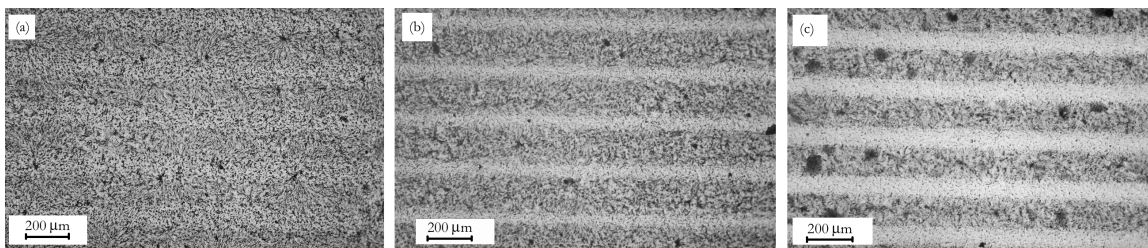


Figure 6.11 Optical micrographs of a laser-written octadecanethiol stabilised gold nanoparticles/PMMA coating at various power densities (writing speed 1 mm/s); (a)  $0.7 \times 10^{11} \text{ W/m}^2$ , (b)  $1.4 \times 10^{11} \text{ W/m}^2$ , (c)  $2.8 \times 10^{11} \text{ W/m}^2$

Figure 6.11 shows optical micrographs of patterns formed on a doctor-bladed coating at relatively low power densities (writing speed = 1 mm/s). At  $0.7 \times 10^{11} \text{ W/m}^2$  no fully metallised patterns are formed, but the laser trace is visible on the micrograph since some material was removed. At higher intensities ( $1.4 \times 10^{11} \text{ W/m}^2$ ,  $2.8 \times 10^{11} \text{ W/m}^2$ ) the metallisation has progressed further, although it is likely that the polymeric matrix still remains largely intact. Figure 6.12 shows lines written at higher power densities above a second threshold, at  $5.6 \times 10^{11} \text{ W/m}^2$ , the remaining gold starts to agglomerate into spherical particles (figure 6.12a). The black discoloration might indicate some carbon contamination due to degradation of the PMMA (e.g. by processes such as pyrolysis, head-to-head-linkage, unzipping and random chain scission)<sup>18,19</sup>. Increasing the power density more ( $9.1 \times 10^{11} \text{ W/m}^2$ ) results in full ablation, clearing the centre of the lines of all organic material, (figure 6.12b). Degraded PMMA and agglomerated gold particles are still present at the edge of the lines, due to the lower power density on the outside of the Gaussian laser beam and material diffusion towards the edges.

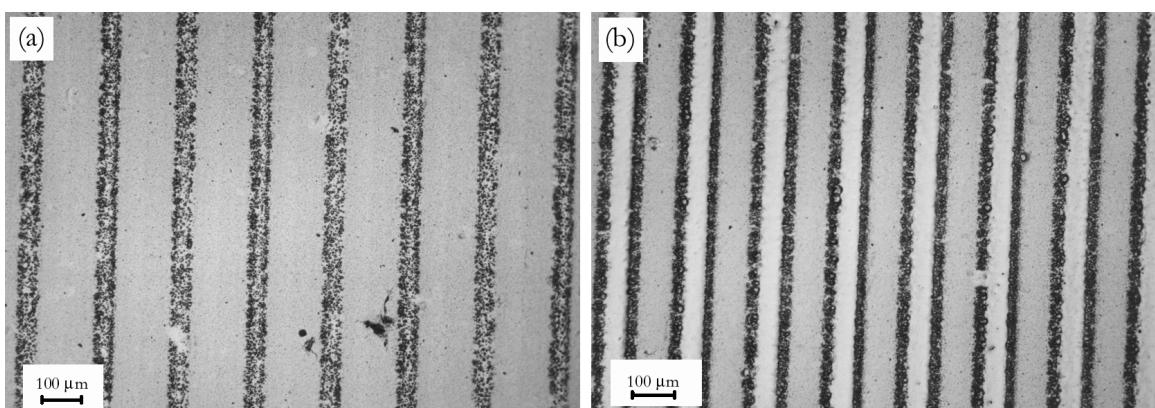


Figure 6.12 Optical micrographs of a laser-written octadecanethiol stabilised gold nanoparticles/PMMA coating at various intensities (writing speed 1 mm/s); (a)  $5.6 \times 10^{11} \text{ W/m}^2$ , (b)  $9.1 \times 10^{11} \text{ W/m}^2$

The clustering of gold particles due to laser irradiation observed in figure 6.12 was previously reported in literature<sup>17</sup>. Larger agglomerates were formed by fusion (through melting) from pulsed laser irradiation of colloidal thionicotinamide stabilised gold nanoparticles in solution. If a nanoparticle coating with sufficient gold content is irradiated with the right settings, it is possible to induce fusing over the whole length and width of the laser-melted patterns and to form a continuous electrical path, as is shown later in this chapter.

The line width dependence on the laser writing speed, at constant power density ( $1.4 \times 10^{11} \text{ W/m}^2$ ), is shown in figure 6.13. As anticipated, decreasing the writing speed increases the line width. At higher writing speeds, the lines become inhomogeneous.

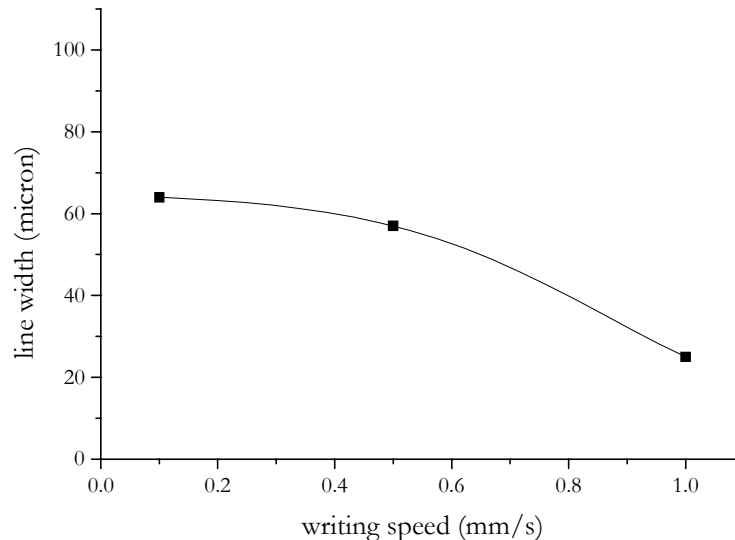


Figure 6.13 Line width dependence on the writing speed for a doctor-bladed laser-written octadecanethiol stabilised gold nanoparticles/PMMA coating (power density:  $1.4 \times 10^{11} \text{ W/m}^2$ )

Figure 6.14 shows an optical micrograph of lines written with several writing speeds and a power density of  $1.4 \times 10^{11} \text{ W/m}^2$ . No full ablation was observed in these lines, even at low writing speeds, indicating that lowering the speed is a better way to control the line width than increasing the laser power density.

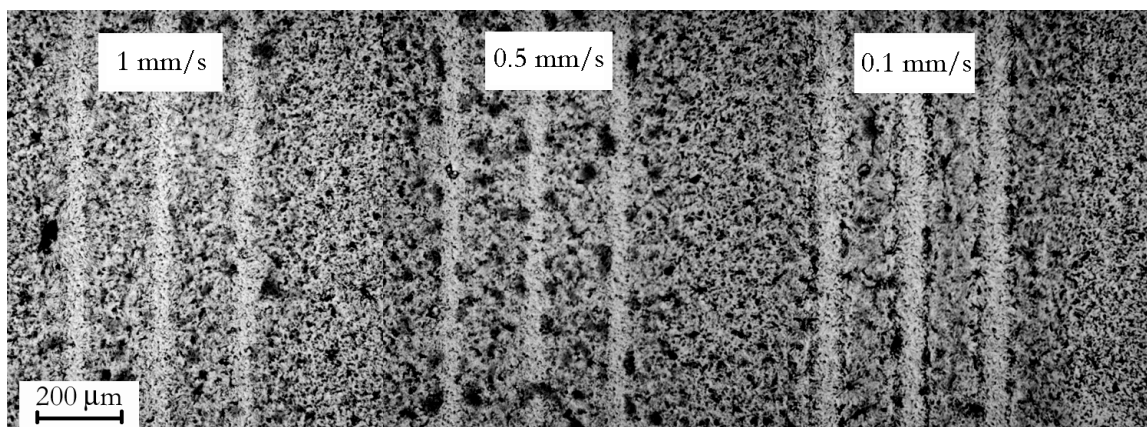


Figure 6.14 Composite optical micrograph of a laser-written octadecanethiol stabilised gold nanoparticles / PMMA coating at various speeds and a power density of  $1.4 \times 10^{11} \text{ W/m}^2$

The ESEM images in figure 6.15 show a line with a continuous metallic path over the length of the line. The pattern was written at a writing speed of 1 mm/s and a power density of  $7.0 \times 10^{11} \text{ W/m}^2$ . The 5 mm long, 300  $\mu\text{m}$  wide line consists of 6 parallel lines (each with a width of 75  $\mu\text{m}$ ) that were written with a 50  $\mu\text{m}$  spacing. Patterns written with a line spacing of 50  $\mu\text{m}$  or less resulted in touching lines. All these patterns showed continuous metallic structures similar to figure 6.15.

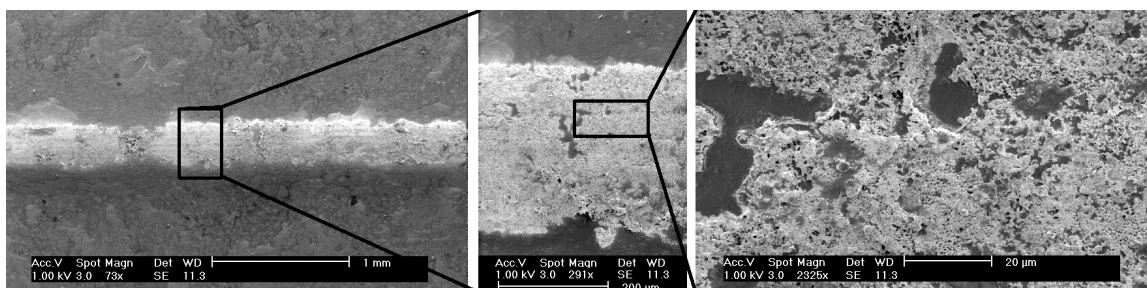


Figure 6.15 ESEM close-ups of a continuous pattern, laser-written on a doctor-bladed dodecanethiol stabilised gold nanoparticle / PMMA coating (from 2.5 wt% nanoparticles solution in toluene / PMMA)

It was observed that a single line (or a pattern with line spacings larger than 75  $\mu\text{m}$ , the line width of a single line) does not show a continuous metallic path. This results in structures very similar to figure 6.12a with separated gold particles, except if the lines were written at extremely low writing speeds (0.01 mm/s). This indicates that a single laser trace only removes the organic parts of the coating, while a second trace, which overlaps with the first line, fuses the particles together to form a continuous metallic pattern (see figure 6.16). There should be a large enough, well-distributed gold content to achieve this. Small patterns are obtained when the lines are written with smaller line spacings or even fully overlapping

lines. However, due to the Gaussian nature of the beam the centre of these lines receives a high dose of laser energy and full removal of all material occurs in some cases.

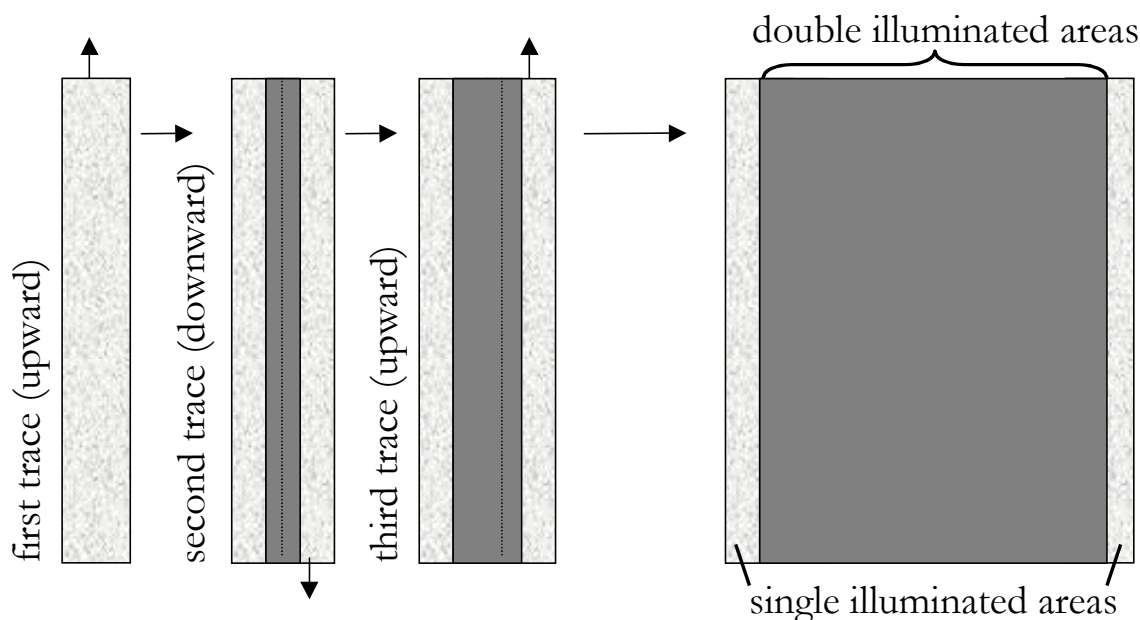


Figure 6.16 Cartoon of metallic pattern generation through partly overlapping subsequent laser traces (arrows indicate the laser writing direction, the light grey areas indicate non-fused gold, the darker areas the fused gold and the dotted lines give the borders of the separate laser traces).

Even though a continuous path is present, the density of the gold over the length of the line is not homogeneous. The line itself is very porous, due to volume reduction because of the removal of PMMA and organic stabiliser. With doctor-bladed octadecanethiol stabilised gold nanoparticles similar results as with dodecanethiol stabilisers were obtained. Figure 6.17 shows fractions of a large (13 x 7.5 mm) metallised area written on a coating made from a 5 wt% nanoparticle / 5 wt% PMMA solution in toluene. While most of the area is homogeneously covered with metallic lines, there are several defects in the pattern (see figure 6.17b). These are due to the fact that the metallic layer is easily scratched or peeled off when handled. Within the defects between the metallised sections linear structures, consisting of small gold clusters are present. Adding a coating over the patterns should protect these patterns for future applications.

Spin-coated samples did not result in continuous lines. This is due to the fact that the coatings are an order of magnitude thinner than the doctor-bladed coatings and therefore also contain a fraction of the amount of gold available to form the lines. Increasing the gold fraction results in a less homogeneous gold distribution in the coatings, creating large gaps between the clusters.

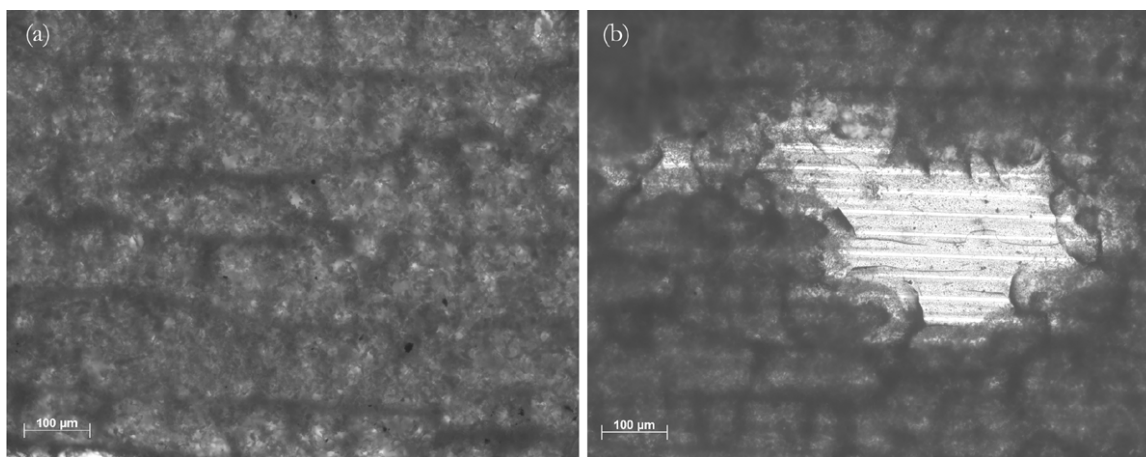


Figure 6.17 Optical micrograph of metallised structures written on a octadecanethiol stabilised gold nanoparticle / PMMA coating

The laser-written lines were developed by removing the non-exposed nanoparticles by gentle rinsing in a toluene solution. The laser-metallised patterns should extend throughout the whole coating thickness, because if there still is a layer of non-processed gold nanoparticles between the substrate and the gold layer, the pattern is washed away together with the non-processed areas. Figure 6.18 shows a micrograph of a rinsed laser written octadecanethiol stabilised gold nanoparticle/PMMA coating. The patterns were formed by a double trace of the laser.

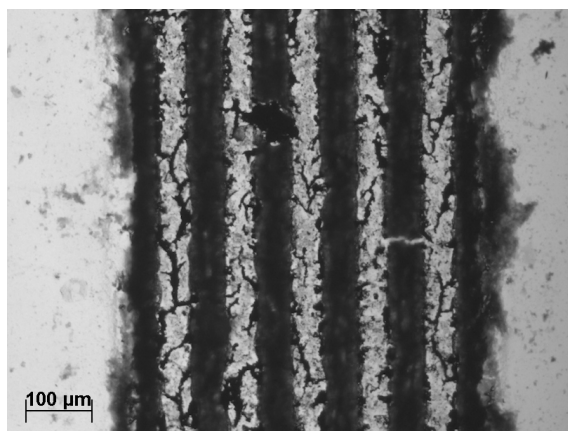


Figure 6.18 Rinsed laser-written octadecanethiol stabilised gold nanoparticle/PMMA coating

### 6.3.5 Electrical conductivity

Qualitative, simple two-point conductivity measurements were performed on lines that appeared continuous in ESEM and optical microscopy to investigate if the patterns showed any conductivity. These lines showed conductivity, ranging from  $0.001\text{-}0.1 \Omega^{-1}\text{cm}^{-1}$ .



There was a large scatter in the results, due to the porous nature of the patterns and the lines were easily damaged by handling and applying the contacts. Both patterns on rinsed and on non-rinsed samples showed conductivity. This seems to eliminate the need for rinsing, especially since the rinsing enhanced the probability of damage to the patterns. A reason to still rinse the written samples is that the recovered gold nanoparticles can be recycled, reducing the cost and time to produce the coatings or to generate a transparent substrate, since the coatings are highly coloured.

## 6.4 Discussion

Although it was impossible to accurately determine the conductivity, it was shown that it was possible to generate electrically conductive structures in the model system of coatings containing PMMA and alkanethiol stabilised gold nanoparticles. Due to the fragile nature of the lines, the patterns should be coated with a protective layer to prevent damage. Non-rinsed samples are deeply coloured and are therefore not suitable for use in most transmissive LCD's. Rinsed samples are optically more transparent, although the remaining gold lines have a yellow colour, but reducing the line width should decrease this problem. It would be interesting to examine if it is possible to adapt patterning process for use with rubbed polyimides or other orientation layer materials (e.g. LPP's), to integrate the addressing of LCD's with the orientation layer. However, it might be a challenge to find a nanoparticle/orientation layer system, which is both miscible and colourless. A solution is to coat rinsed patterns with an orientation layer, which not only protects the patterns from mechanical damage, but also integrates them directly into the cell. First experiments with spin-coating a thin polyimide layer over the patterns showed promise that this indeed was possible.

## 6.5 Conclusions

We used direct focused laser writing in the (organic) ablation regime to show that conductive patterns were written on a model system consisting of hybrid coatings with PMMA and alkanethiol stabilised gold nanoparticles. The ablation process only removes the organic components of these coatings, leaving behind patterns, consisting of pure gold particles. These are fused together through a second laser scan, resulting in conductive pathways.

The synthesis of the nanoparticles was optimised to generate good yields of gold nanoparticles, stabilised with dodecanethiol or octadecanethiol. Hexanethiol stabilised particles resulted in too low yields to be of practical use. Coatings of gold nanoparticles with

PMMA on glass were made using three techniques, of which film casting proved non-favourable, due to large inhomogeneities in coating thickness and gold nanoparticle distribution. Spin-coating and doctor-blading resulted in good quality coatings on which laser writing was performed. Conductive, continuous patterns (with a conductivity, ranging from 0.001-0.1  $\Omega^{-1}\text{cm}^{-1}$ ) were laser-written on both dodecanethiol and octadecanethiol stabilised gold nanoparticle coatings if the lines were written at low speeds. Conductive metallised patterns were formed in a two-step writing process. A first pass of the laser beam removed all organic material; a second pass fused the pure gold clusters to form a continuous path if there was sufficient gold available. Doctor-bladed coatings provided enough gold, while spin-coated samples, which are much thinner and therefore contain less gold, did not result in any continuous patterns. Rinsing the samples removed the non-laser-written parts of the coatings (and some of the PMMA), while the lines remained conductive. Due to the high sensitivity to mechanical damage and the porous nature of the metallised lines, the scatter in the measured conductivity values was relatively large. A protective (PMMA, polyimide or other polymer) coating might increase the mechanical stability of the patterns. The used system is not easily adapted for use in optical applications and should be only considered as a model system to prove the principle of this laser writing process.

## 6.6 References

- [1] This thesis, Chapter 2
- [2] M. Eckart, *Patent US 4496607*, (1985).
- [3] Ramos, R.A., Chartash, K.E., Suh, N.P., *Patent US 4159414*, (1979).
- [4] M. T. Reetz, M. Winter, G. Dumpich, J. Lohau, S. Friedrichowski, *J. Am. Chem. Soc.* **119**, 4539, (1997).
- [5] J. Lohau, S. Friedrichowski, G. Dumpich, E. F. Wassermann, *J. Vac. Sci. Technol. B* **16**, 77, (1998).
- [6] T. R. Bedson, R. E. Palmer, J. P. Wilcoxon, *Microelec. Eng.* **57-8**, 837, (2001).
- [7] T. R. Bedson, R. E. Palmer, J. P. Wilcoxon, *Appl. Phys. Lett.* **78**, 2061, (2001).
- [8] T. R. Bedson, R. E. Palmer, T. E. Jenkins, D. J. Hayton, J. P. Wilcoxon, *Appl. Phys. Lett.* **78**, 1921, (2001).
- [9] P. Hoffmann, G. Benassayag, J. Gierak, J. Flicstein, M. Maarstumm, H. Vandenberg, *J. Appl. Phys.* **74**, 7588, (1993).
- [10] L. R. Harriott, K. D. Cummings, M. E. Gross, W. L. Brown, *Appl. Phys. Lett.* **49**, 1661, (1986).
- [11] T. J. Stark, T. M. Mayer, D. P. Griffis, P. E. Russell, *J. Vac. Sci. Technol. B* **9**, 3475, (1991).
- [12] A. N. Shipway, E. Katz, I. Willner, *Chemphyschem* **1**, 18, (2000).
- [13] M. T. Reetz, S. A. Quaiser, M. Winter, J. A. Becker, R. Schafer, U. Stimming, A. Marmann, R. Vogel, T. Konno, *Angew. Chem., Int. Ed. Engl.* **35**, 2092, (1996).
- [14] H. Bonnemant, R. M. Richards, *Eur. J. Inorg. Chem.*, 2455, (2001).

- 
- [15] M. Brust, M. Walker, D. Bethell, D. J. Schiffrin, R. Whyman, *J. Chem. Soc. Chem. Commun.* , 801, (1994).
- [16] R. H. Doremus, P. Rao, *J. Mater. Res.* **11**, 2834, (1996).
- [17] H. Fujiwara, S. Yanagida, P. V. Kamat, *J. Phys. Chem. B* **103**, 2589, (1999).
- [18] Y. Kasiwagi, A. Inaba, J. E. Brown, K. Halada, T. Kitayama, E. Masuda, *Macromolecules* **19**, 2160, (1986).
- [19] A.P.Nising, T.M. Zeilmann, T. Meyer, website: [http://dcwww.epfl.ch/lgrc/\\_site\\_meyer/Research/files/Thomas-Hambourg.%2001.pdf](http://dcwww.epfl.ch/lgrc/_site_meyer/Research/files/Thomas-Hambourg.%2001.pdf)

## Technology Assessment

Micro-structuring of polymers is typically performed with replication techniques, but the direct writing of these structures is gaining more importance. Instead of just using polymers as a carrier material for the structures, it is also possible to pattern polymeric materials with an added (electro-)optical functionality. In this thesis, we used lasers to directly write patterns in (anisotropic) functional polymers to form novel, unique microstructures that influence the electrical or optical properties of the polymeric material itself or of the material that is brought in direct contact with this polymer. Direct laser patterning offers a wide range of possibilities with respect to chemical or physical changes it can induce in polymers, e.g. based on photochemical reactions or melting and relaxation, respectively. We have studied various options to form novel patterns with different length scales, ranging from micrometers to millimetres, and with different functionalities, making use of a large degree of design freedom in substrates and components. Typical applications of the technologies that we have developed are personalised security features and electro-optical switches, which can be used in flat panel displays based on twisted-nematic and cholesteric texture liquid crystal effects..

The processing regime in which the laser writing was performed (photochemistry, heating, melting, pyrolysis or ablation) determined the geometry and properties of the patterns. The main topics as described in this thesis can be divided into two main parts: generating novel optical effects by laser patterning liquid crystal orientation layers and producing electrical pathways inside LCD's directly on one of the polymeric substrates to reduce the number of layers within a cell.

By laser patterning orientation layers, the LC alignment properties are locally removed (laser melting in polyimides) or added (photo-orientation of linearly photo-polarisable polymers). Liquid crystal cells with these laser-melted polyimides showed hybrid LC alignment with homogeneously planar areas surrounded by twisted nematic areas. These cells can easily be adapted for use in personalised security features for e.g. credit cards. When integrated in a credit card or a document, these features provide a high level of protection against counterfeit. Due to the complex manufacturing equipment, they are difficult to copy, and are non-removable without damaging the object. Unique personalised images can be

constructed as well as high volume images and they make use of an external system (polarisers) to be detected ('lock-and-key principle'). Patterned orientation layers can also be implemented in TN LCD's. Upon electrical switching, the hybrid LC configuration switches to a homeotropic configuration, turning the pattern from visible in the unaddressed state to invisible in the addressed state or visa versa. This effect can be used to produce switchable icons or gratings, which for instance can be utilised for the labelling, marking or encoding of individual display elements. With direct focused laser writing, the design freedom is very large and complex images or patterns can be generated. However, the resolution should be decreased further to be able to generate complex patterns within a single display pixel. Holographic exposure results in higher resolution patterns, but this process is prone to disturbances and it is very difficult to obtain patterns of homogeneous quality, which still remains an issue that needs to be resolved.

Direct writing of electrically conductive patterns in functional polymers was examined for two systems: laser writing of polyimides in the pyrolysis regime and laser writing in the (organic) ablation regime of hybrid coatings consisting of polymer/inorganic blends with a polymeric carrier and organically stabilized metallic nanoparticles.

Pyrolysis of polyimide resulted in electrically conductive carbonised or graphitised micro-patterns. Writing these patterns directly in polyimide orientation layers would combine the electrical pathways and the orientation layer into one material, but unfortunately laser pyrolysis of thin polyimide coatings results in highly irregular structures. However, laser pyrolysis on thicker polyimide films resulted in well-defined patterns down to a length scale of several microns. The strong yellow color of the films and the black discoloration of the pyrolysed lines make these patterns in general unfit for use in optical systems, but in a specific case, cholesteric texture displays, one may benefit from the combined property of high electrical conductivity and light absorption. Using laser-pyrolysed polyimide substrates we replaced several functional layers in this type of display (e.g. the support polymer, the transparent electrode, the spacers and the black coating) to construct a thin, flexible reflective display system. An issue still to be resolved in our approach is the curvature that is formed in our substrates during the writing process. In a second approach conductive patterns on thin polymeric films were generated by mixing metallic nanoparticles with a polymer. Through ablation of the organic parts of the blend, a metallic pattern remained at the laser-exposed sections that was highly conductive. An issue still to be resolved here is the mechanical instability of the patterns. Protecting the patterns with a top layer improved the resistance against damage, but has its restrictions with respect to contacting. We performed our study so far on a model system with a non-functional isotropic polymer. It would be of utmost interest to write the conductive patterns in a system consisting of metallic

nanoparticles mixed with (anisotropic) functional polymers, e.g. polyimide orientation layers to once more combine alignment and electrical addressing of liquid crystals in one material.

It is envisioned that the use of laser-patterned conductive patterns in polymers can also be applied in other electric- and electronic applications, such as printed circuit boards, cost-effective simple integrated circuits, xerography, shielding of sensitive components against electro-magnetic induction, etc.

Summarising, the systems described in this thesis showed that direct focused laser writing and holography are interesting techniques to generate functional patterns on different length scales and with different morphological and structural properties in (anisotropic) functional polymers. Making use of the several available processing regimes opens up a way to pattern unique (electro-)optical properties into functional polymer systems that are difficult or impossible to achieve using traditional techniques. However, most systems need to be optimized or developed further to be interesting for larger scale use. The serial nature of the direct writing techniques might limit its industrial use, but this is compensated by the possibility to induce unique features and properties with an enormous design freedom unavailable through other techniques.



# Appendix

## Laser Patterning

### A.1 Laser principles

Since the earliest types of lasers were developed in the late 1950's<sup>1</sup>, the potential to apply them as a tool for a wide variation of purposes, including micro-patterning, was immediately recognised.

The word 'laser' is an acronym, which stands for 'Light Amplification by Stimulated Emission of Radiation'. A laser generates a high power, collimated and monochromatic light source, which has both spatial and frequency coherence<sup>2</sup>. Even though Albert Einstein already predicted lasers on mathematical quantum-mechanical grounds, in the early 20<sup>th</sup> century<sup>3</sup>, it took until 1960 before a working prototype was produced<sup>4</sup>.

A laser operates on the principle of continuously bringing electrons to an excited state (pumping) and by stimulated emission of electrons returning to their ground state induced by photons with the wavelength of the band gap. This releases another photon, resulting in a self-reinforcing photon stream. When the lasing material, the active medium, is placed between two mirrors (the optical cavity), the photons will enter the active medium numerous times, resulting in an extremely powerful coherent light beam. The wavelength of this beam is equal to the distance between the ground state and the excited state of the active medium. The beam itself exits the laser cavity by making one of the mirrors (the outcoupling mirror) partially transparent. When there are several excited states available, multiple wavelengths are generated by the active medium. The desired wavelength is selectively coupled out using prisms or wavelength selective mirrors.

A wide variety of lasers was developed in the second half of the 20<sup>th</sup> century. The medium consists of organic and inorganic solids, liquids, plasmas or gases. Pumping is done electrically, chemically or by radiation. The emission is in the wavelength range from deep UV to far infrared. A distinction is made between pulsed lasers and lasers that generate a continuous beam (continuous wave lasers). The beam itself can have a multitude of shapes and operation modes. And, lasers with intensities ranging from milliwatts to megawatts exist. This variety shows that there should be a laser for virtually any process that makes use of light.



## A.2 Direct focused laser writing

With direct focused laser writing a laser beam is focused onto a material through a lens or lens system<sup>5</sup>. When the sample is moved through the focal point of the lens, the localised laser intensity can be applied to write patterns. The highest practical resolution is approximately 1  $\mu\text{m}$ . This technique is a very powerful patterning tool and has many advantages. There is a huge flexibility in the design of patterns, the intensity of the laser beam can easily be controlled and processing is possible in all thermal regimes and the experimental set-up is relatively simple. Some disadvantages include that there are many variables that determine the pattern dimension and quality (such as the type of lens, the scanning speed, the laser intensity, etc.), making it laborious to find the optimal settings. Also, since many lenses that focus a beam to very small dimensions have a very small depth of focus and working distance, this results in a practical set-up that is very complex to operate. Substrates need to be sufficiently flat, else the surface of the material will move in and out of focus when the sample is moved through the focused beam, which results in inhomogeneous or discontinuous patterns. When a laser beam is focused through a lens, the energy is concentrated on a very small area, usually a few microns in diameter.

Figure A.1 shows the most important parameters used in the equations in this paragraph:  $w_L$  is the initial beam diameter before focusing,  $f$  is the focal distance,  $L$  is the focal depth,  $w_0$  is the beam waist diameter in the focal point,  $I$  is the intensity,  $r$  is the radial distance from the beam centre.  $1/e$  and  $1/e^2$  are definition points for beam diameter.

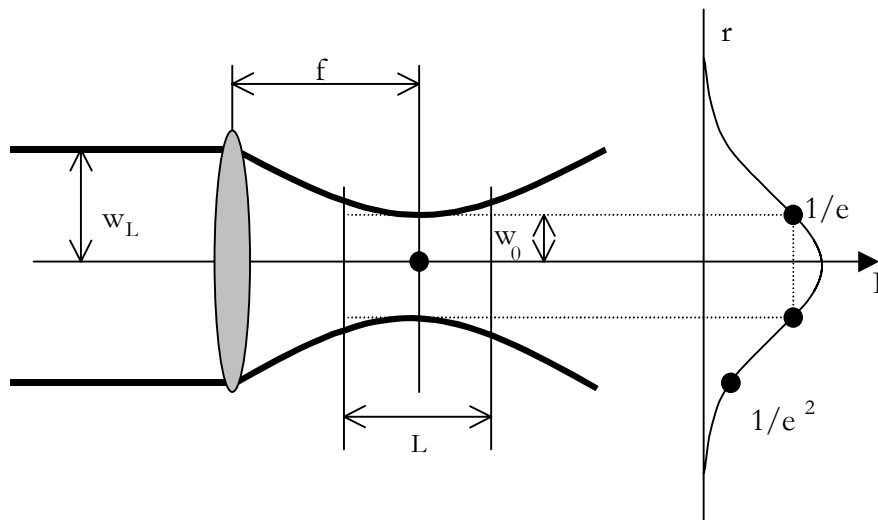


Figure A.1 Important parameters for determining beam characteristics

The radial intensity distribution of a Gaussian beam is given by:

$$I(r) = I_0 e^{-r^2} \quad (\text{A.1})$$

The focused spot size for a laser beam is an important value that can be calculated with the following equation<sup>5-8</sup>:

$$w_0 = \frac{f\lambda}{\pi(2w_L)} \quad (\text{A.2})$$

This equation is valid for the  $1/e$  intensity level, for the  $1/e^2$  intensity level this equation has to be multiplied by a factor  $\sqrt{2}$ . The depth of focus  $L$  is given by:

$$L = \frac{4f^2\lambda}{\pi(2w_L)^2} \quad (\text{A.3})$$

The parameters for the Argon Ion laser and single lens system used in this thesis are:  $f = 50$  mm,  $\lambda = 351$  nm and  $w_L = 0.95$  mm. The resulting values that are calculated from these parameters are:  $w_0 = 2.9$   $\mu\text{m}$  ( $1/e$  intensity level) or  $w_0 = 4.1$   $\mu\text{m}$  ( $1/e^2$  intensity level) and  $L = 0.3$   $\mu\text{m}$ . The theoretical focused spotsize is  $2w_0$  and therefore is  $5.8$   $\mu\text{m}$ , for the  $1/e$  case and  $8.2$   $\mu\text{m}$  for the  $1/e^2$  case. Since these equations are only valid in ideal cases and do not take into account inhomogeneities within the optics and beam, noise, the divergence of the beam and the fact that the laser beam does not cover the whole lens area, the actual spotsize is somewhat larger. We estimated that the practical focused spotdiameter is  $10$   $\mu\text{m}$ . The focal depth of  $0.3$   $\mu\text{m}$  shows that focusing should be very accurate and that the sample needs to be very flat and placed very straight to be able to guarantee constant focus quality over laser-written lines. If care is not taken, the result of laser writing will be inhomogeneous or discontinuous patterns.

The actual energy delivered to a sample is a combination of beam, lens and substrate material properties. Complex Gaussian optics and temperature distribution equations help with estimating the temperature increase in an irradiated material. In a reference beam fixed with the substrate, the temperature increase at the origin ( $\Delta T$ ), for a moving Gaussian laser spot over a substrate for surface absorption and temperature independent material parameters, can be calculated using<sup>5</sup>:

$$\Delta T = \frac{2\theta_c}{\pi} \int_0^{\infty} \frac{dt'}{1+4t'} \exp\left(-\frac{v^2(t-t')^2}{1+4t'}\right) \quad (\text{A.4})$$

In this equation,  $t$  is the dimensionless time,  $t'$  is an integration parameter,  $v$  is the dimensionless scanning speed of the beam and  $\theta_c$  is the temperature increase [K] at the centre for a stationary Gaussian beam and is given by:

$$\theta_c = \frac{\sqrt{\pi} I_a w_0}{2\kappa} \approx 0.89 \frac{I_a w_0}{\kappa} \quad (\text{A.5})$$

In this equation,  $I_a$  is the absorbed laser power density [W/m<sup>2</sup>],  $w_0$  the radius of the focused spot [m] (see equation A.2) and  $\kappa$  the thermal conductivity [W/mK]. The temperature increase equation (A.4) can only be solved analytically when all boundary conditions and material parameters are known. Some general conclusions can be drawn from this equation<sup>5</sup>. For high scanning speeds, the heat diffusion lags behind the beam centre and the temperature decreases significantly with increasing speed. At low scanning speeds, the decrease in centre temperature is very small. The temperature profile perpendicular to the scanning direction ('into the material') has a similar Gaussian shape as the beam, except when the thickness of the film is insufficiently large to fully form the profile. The Gaussian profile is broadened at decreasing scanning speed. The energy flux of a moving Gaussian beam into the material,  $J$ , is given by:

$$J = \frac{\text{powerdensity} \times \text{spotdiameter}}{\text{volume}} = \frac{I_a \frac{1}{3} \pi w_0^3}{h 2 w_0 v} = \frac{I_a \pi w_0^2}{6 h v} \quad (\text{A.6})$$

The volume (per time unit) is the product of the height (film thickness or maximum thermal penetration depth) ( $h$ ), the beam spot diameter ( $2w_0$ ) and the scan speed ( $v$ ).

Summarizing, the temperature increase and the thermal profile are determined by the scanning speed, the intensity, substrate thickness and material parameters, such as the thermal diffusivity.

### A.3 Interferometry and holography

Holography is a patterning technique in which both the intensity, as well as the amplitude of a laser light path reflected from an object, is recorded in a substrate (similar to photography, but there only the intensity is recorded)<sup>2</sup>. By illuminating the holographically

patterned substrate, the object can be made visible in a three-dimensional way. Figure A.2 shows a holographic set-up. A holographically sensitive substrate is irradiated with two beams (the reference beam and the object beam), which interfere in the sections where they overlap<sup>7,9,10</sup>. When both beams have the same spatial and frequency coherence, constructive and destructive interference occurs. Interferometry is a special type of holography, in which there is no object present and two laser beams are made to interfere with each other. The resulting interference pattern can be recorded on a material surface or even in the bulk of the material. Figure A.2 shows the difference in set up between holographic recording and interferometric patterning.

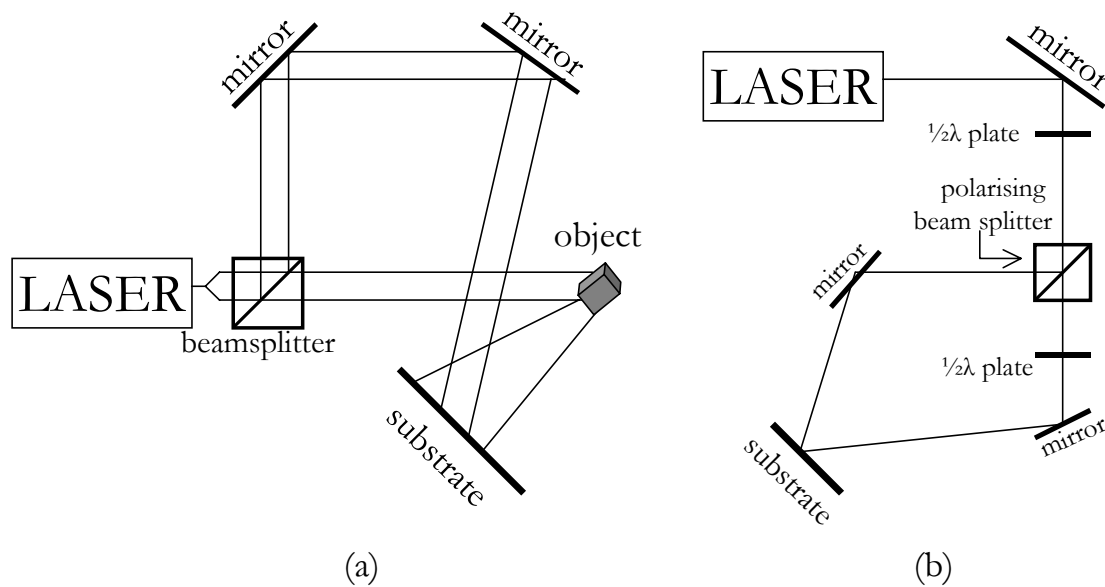


Figure A.2 (a) Holographic recording, (b) Interferometric Patterning (Mach-Zehnder interferometer)

The intensity of two interfering beams in air can be described with the following equation:

$$I(x) = I_1 + I_2 + 2\sqrt{I_1 I_2} \cos\left(\frac{4\pi}{\lambda} x \sin \alpha\right) \quad (\text{A.7})$$

$I_1$  and  $I_2$  are the intensities of the interfering beams,  $x$  is the spatial position perpendicular to the resulting line pattern,  $\lambda$  is the wavelength and  $\alpha$  is the half angle between the 2 beams ( $|\theta_1 - \theta_2|$ , see figure A.3). The result is a regular series of constructive and destructive interference over the overlapping area of the two beams, which is visible as dark and light

fringes. The periodicity or pitch ( $d$ ) of the interference pattern (the distance between the fringes) is:

$$d = \frac{\lambda}{2 \sin(0.5|\theta_1 - \theta_2|)} \quad (\text{A.8})$$

When the beams are made to interfere further away from the mirrors (and thus decreasing the angle between the beams), the pitch increases. Interferometry can be used to pattern sub-micron sized lines with a theoretic minimum pattern spacing of half the wavelength of the used light.

The holographic or interferometric information can be stored as an (amplitude and/or phase) grating in several photo-sensitive materials<sup>11,12</sup>, e.g. silver halide photographic solutions, dichromated gelatin, ferroelectric crystals and photopolymer systems. A distinction is made between thick (volume, 3-D) and thin (surface, 2-D) holograms, depending on the penetration depth and the thickness of the holographic substrate.

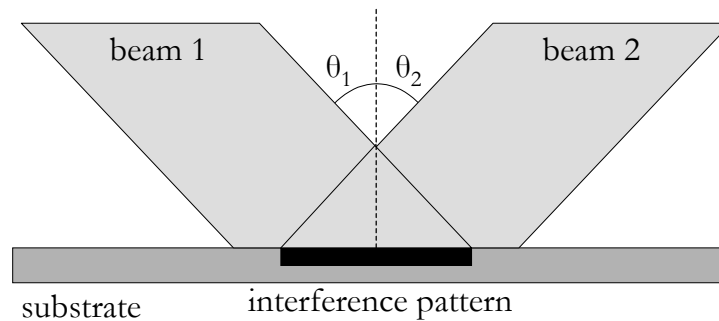


Figure A.3 Holographic illumination

To read out a hologram or interferogram, the reference beam enters the hologram and is partly diffracted into the direction of the original object beam. This results in a reconstruction of the object beam and the object is in this way be three-dimensionally visualised. A distinction is made between reflection and transmission holograms. With transmission holograms the object beam is reconstructed at the opposite side, while in a reflection hologram this occurs at the same side as the incident reference beam. A transmission hologram is produced as shown in figure A.3, a reflection hologram can be constructed when the reference and object beams are incident from opposite sides of the holographic substrate and the grating is formed in the bulk of the material.

The interferometer used in this thesis is a Mach-Zehnder interferometer, which is schematically shown in figure A.2b. This type of interferometer has a relatively easy set-up and can be easily adjusted to change the holographic pitch, while still a high accuracy is maintained. Before the beam enters the Mach-Zehnder interferometer, the spot diameter is increased from 1.9 mm to approximately 1.5 cm and cleaned through a pinhole and a series of lenses. A strong feature of holography is the possibility to pattern in the bulk of the material by placing the sample under an angle between the beams and have the beams interference pattern form inside the material instead of on the surface.

Unfortunately, holography is practically quite sensitive for disturbances, which is especially a problem when long irradiation times are necessary. Also, the laser beam needs to be of very homogeneously high quality and have a well-defined spot. Usually, extensive beam stabilizing equipment and optics are needed to clean up the beam. Also, to pattern larger areas the laser beam needs to be expanded, which not only requires more optics, but an expanded beam intrinsically means a lower energy level per irradiated surface area. Because of this, the laser needs to operate at higher intensities and/or irradiation times will vastly increase.

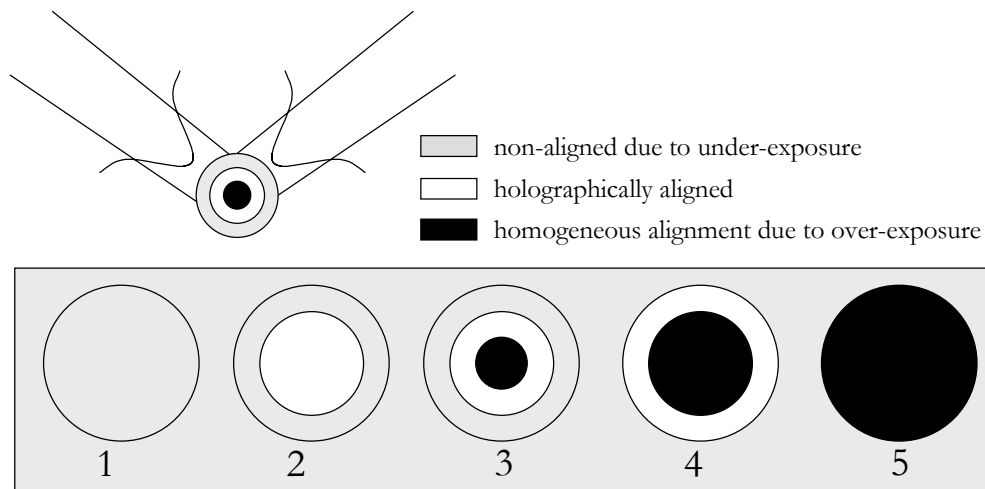


Figure A.4 Alignment variations due to the Gaussian shape of the interfering laser beams

As mentioned above, holographic or interferometric patterning is very sensitive to mechanical and other disturbances, but also other factors can cause problems in forming well-defined, homogeneous holographic or interferometric patterns. An inherent problem is the Gaussian distribution of the laser beam, as is illustrated in figure A.4. Low power leads to spot 1 in the figure, with no alignment whatsoever over the spot area. High power leads to an overexposed area, such as in spot 5, in which the overall intensity is so high that the photochemical crosslinking reaction takes place around the interferometric minimums as

well. Spots 2 to 4 have holographic patterns, but only in sections. Spot 2 is the most desirable situation, especially if the radius of the holographically aligned area is extended as far as possible. A broad ‘holographic power window’ is needed that would envelop almost the complete Gaussian power distribution of the spot. The actual spots will not have sharp borders as depicted in figure A.4..

Figure A.5 shows the time-dependent (over-)development of the holographic spot. The width of the lines formed by the holographic maximums increases over time during illumination, eventually covering up the whole area. For some materials, the ‘holographic window’ in which a good quality spot can be obtained is very small.

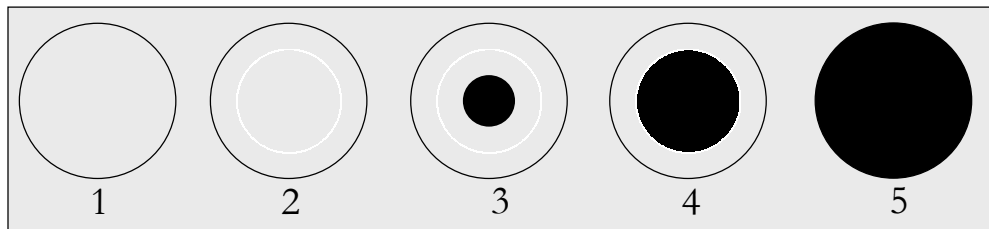


Figure A.5 Development of the holographic spot from initial illumination to complete overexposure

Despite the practical challenges that can occur with holography or interferometry, it remains a powerful technique to generate (sub-)micron sized structures in a wide variety of materials.

#### A.4 References

- [1] A. L. Schawlow, C. H. Townes, *Phys. Rev.* **112**, 1940, (1958).
- [2] W. E. Kock, *Lasers and Holography - An Introduction to Coherent Optics, Second, Enlarged Edition*, Dover Publications Inc., New York, (1981).
- [3] A. Einstein, *Phys. Z.* **18**, 121, (1917).
- [4] T. H. Maiman, *Nature* **187**, 493, (1960).
- [5] D. Bäuerle, *Laser Processing and Chemistry, second edition*, Springer, Berlin, (1996).
- [6] S. S. Charschan, *Guide To Laser Materials Processing*, CRC Press, Boca Raton, (1993).
- [7] F. L. Pedrotti, L. S. Pedrotti, *Introduction To Optics, 2nd edition*, Prentice-Hall, inc., New Jersey, (1993).
- [8] W. M. Steen, *Laser Material Processing*, Springer-Verlag, London, (1998).
- [9] E. Hecht, *Optics, 2nd edition*, Addison-Wesley, Reading, (1987).
- [10] K. K. Shvarts, *The Physics of Optical Recording*, Springer-Verlag, Berlin, (1993).
- [11] L. Solymar, D. J. Cooke, *Volume Holography and Volume Gratings*, Academic Press, London, (1981).
- [12] H. J. B. Jagt, *Polymeric Polarisation Optics for Energy Efficient Liquid Crystal Display Illumination (PhD thesis)*, Technische Universiteit Eindhoven, Eindhoven, (2001).

# Dankwoord

Vaak hoor je mensen zeggen dat hun studieperiode de beste tijd van hun leven was. Dat zijn dus duidelijk mensen die geen promotie-onderzoek hebben uitgevoerd. Ondanks de tegenslagen die bijna vanzelfsprekend samengaan met promoveren, kan ik op dit moment terugkijken op vier ontzettend leerzame, interessante, gezellige en prettige jaren. Het gevoel van vrijheid en (bijna) ongekende mogelijkheden is iets wat absoluut samengaat met promoveren. Een promotie-onderzoek is niet alleen goed voor je wetenschappelijke ontwikkeling, maar absoluut ook voor je menselijke en persoonlijke kwaliteiten. In dit dankwoord wil ik daarom een aantal mensen bedanken voor hun hulp en steun tijdens mijn promotieperiode.

Ten eerste wil ik natuurlijk mijn directe begeleiders, dr. Cees Bastiaansen en prof. Dick Broer, bedanken. Cees, de ‘even-bijpraat’ meetings resulteerden vaak in nieuwe richtingen in het onderzoek en lieten me vaak op een andere manier tegen het project aankijken. Jouw speurtocht naar de ‘rode draad’ heeft er voor gezorgd dat dit proefschrift meer is dan een losse verzameling hoofdstukken, maar dat ze samen een groter geheel zijn gaan vormen. Dick, jouw enthousiasme en wetenschappelijke inbreng werkte altijd motiverend en ik ging vaak met veel nieuwe ideeën je kamer uit. Ook jouw contacten binnen Philips en daarbuiten hebben mij erg veel geholpen doordat die mij toegang gaven tot nieuwe materialen en specifieke meettechnieken.

De volgende die ik graag wil bedanken is prof. Lemstra, die de mogelijkheid heeft geboden het promotie-onderzoek binnen SKT te laten plaatsvinden. De indrukwekkende reis naar India, die begon als een idee van u, is iets wat ik absoluut niet snel zal vergeten. Vervolgens wil ik prof. Picken en prof. de Jeu bedanken voor hun kritische blik op mijn proefschrift als lid van de leescommissie. Francesco Picchioni wil ik ook bedanken voor zijn grondige blik op de laatste versie.

Het is natuurlijk onmogelijk om een onderzoek als dit volledig in je eentje uit te voeren en gelukkig heb ik het genoeg gehad om gebruik te kunnen maken van de expertise en interesse van verschillende mensen binnen en buiten de TU/e. Dr. Martin Schadt and Rolic: thank you for the LPP materials and the interest you showed in this project. Al heeft het niet direct geleid tot een praktische samenwerking, de momenten van overleg met de DPI contactpersonen van Océ, en dan voornamelijk Susanne Heun en Sjoerd van de Geijn,



heb ik altijd als bijzonder prettig ervaren. Peter Cirkel, Giovanni Nisato en Cindy Nieuwkerk van Philips Research wil ik graag bedanken voor de hulp, de materialen en het overleg bij verschillende projecten. Johan Bosman en Ivar Boerefijn van Philips CFT wil ik bedanken voor de mogelijkheid om andere lasersystemen te zien en te gebruiken. Arjan Schuurman van TNO wil ik bedanken voor de mogelijkheid om enkele laserexperimenten uit te voeren, voordat we zelf onze laser hadden. Kornel Hoekerd, eveneens van TNO, wil ik bedanken voor de laagdiktemetingen. Een aantal mensen van de SKT groep hebben mij geholpen bij verschillende experimenten: Geong-Man Kim, (AFM), David Trimbach (AFM), Pit Teunisen (Autronic), Joachim Loos (AFM, TEM) en Pauline Schmidt (ESEM). En ik heb het voorrecht gehad om een aantal researchstudenten te begeleiden. Sander, Twan, Alexander en Sven: onderdelen van jullie werk zullen jullie voor een groot deel terugvinden in de verschillende hoofdstukken van dit proefschrift. Om prettig onderzoek te kunnen doen, is natuurlijk ook de sfeer van enorm van belang en gelukkig was die prima in orde binnen de PICT/SKT groep. Met een aantal mensen heb ik de afgelopen jaren een bijzonder prettig en gezellig contact gehad. Een aantal mensen wil ik graag even speciaal noemen. Ten eerste natuurlijk Henri en Marysia, het was meer dan prettig om kamergenoten te hebben met wie ik niet alleen op, maar ook buiten de TU bijzonder goed kon opschieten! De wekelijkse squash-uurtjes met jullie waren fanatiek en gezellig tegelijkertijd. Het internationale karakter van onze groep heb ik als bijzonder prettig beschouwd en dat komt tot uiting in de volgende rij mensen die ik allemaal bedank voor de genoten gezelligheid in de pauzes of als ik weer eens binnen kwam lopen: Ankur en Sreepad (aapkaa bahut bahut dhanyavaad!); Vid (hvala lepa, na zdravje!); Francesco en Domenico (grazie mille, sono un fantasma!); Isabelle (merci beaucoup!); Carlos (muchas gracias!); Frank, Fons, David en Pit (bedankt)! Iedereen zal onmiddellijk de bijzondere omslag van dit proefschrift zijn opgevallen. Dit ontwerp is gemaakt door Henk Hofstede. Henk, ontzettend bedankt; niet alleen voor dit prachtige ontwerp, maar ook voor de prachtige Nits muziek die me bij concerten of gewoon vanaf CD ontzettend veel plezier en afleiding hebben gebracht.

Ten slotte zijn er natuurlijk een aantal mensen die ik bijzonder wil bedanken. Angelien, de afgelopen maanden zijn door jou extra bijzonder geworden. Dankzij jouw motivatie en steun is het schrijven van dit proefschrift is een stuk soepeler gegaan. Pap, Mam en Arjan, ontzettend bedankt om er altijd er voor me te zijn, jullie steun, vertrouwen, belangstelling en natuurlijk de gezelligheid als ik weer terug in Hulshorst ben!

Dennis

## Curriculum Vitae

The author of this thesis was born in Nunspeet on July 5, 1973. After finishing the VWO (Lambert Franckens College, Elburg), he started his study Chemical Engineering at the University of Twente. In October 1997 he graduated from this university by completing his graduation project, entitled 'Poly(ferrocenyl silane) Block Copolymers', in the group 'Materials and Technology of Polymers' of prof. G.J. Vancso.

In February 1998 he started his PhD-study in the group 'Polymer Chemistry' of prof. P.J. Lemstra. The work was carried out in the sub-group 'Polymers for Information and Communication technology' of dr. C.W.M. Bastiaansen and prof. D.J. Broer. The results are described in this thesis.

During his PhD-study, the author completed all five modules of the course 'Registered Polymer Technologist' ('Register Polymeerkundige', RPK) organized by the 'National Graduate School of Polymer Science and Technology' ('Polymeertechnologie Nederland', PTN).

# Stellingen

Behorende bij het proefschrift

## Direct Laser Writing and Structuring of Functional Polymers for Electro-Optical Switches

van

Dennis Versteeg

1. Het beïnvloeden van vloeibare kristaloriëntatielagen door middel van lasersmelten is een nieuwe, veelbelovende aanvulling op bestaande technieken om vloeibare kristallen patroonmatig te ordenen.

*- Dit proefschrift, hoofdstukken 3 en 4*

2. De zwarte verkleuring veroorzaakt door laserpyrolyse is voor specifieke optische toepassingen eerder voordeel dan een ongewenst bijeffect.

*- Dit proefschrift, hoofdstuk 4, paragraaf 4.4.3*

3. De reductie in waterige omgeving van  $\text{H}[\text{AuCl}_4]$  door middel van natriumborohydride of natriumcitraat is de meest eenvoudige manier om goud nanoparticles snel en succesvol te synthetiseren.

*- A. Shipway, E. Katz, I. Willner, 'Nanoparticle arrays on surfaces for electronic, optical and sensor Applications' (review), ChemPhysChem 1, 18 (2000)*

*- H. Bönemann, R.M. Richards, 'Nanoscale metal particles – synthetic and potential applications' (review), Eur. J. Inorg. Chem., 2455 (2001)*

4. Niet-contact technieken voor oriëntatie van vloeibare kristallen zullen uiteindelijk de LCD-technologie domineren. Een te vroege introductie, terwijl er nog veel problemen op te lossen zijn (o.a. lage verankeringsenergie, image sticking, degradatie) heeft de echte industrialisering met vele jaren vertraagd.

5. Het gebruik van zachte, elastische siliconenrubber-stempels bij micro-contact printing bevordert de nauwkeurigheid van reproductie vanwege het intieme contact van de stempel met het substraat, maar limiteert tegelijkertijd deze nauwkeurigheid weer vanwege elastische deformaties van de stempel tijdens het printen.
6. Lithografie met behulp van zelf-organiserende moleculaire systemen levert periodieke structuren met nanometerdimensies op. Het nut hiervan kan echter betwijfeld worden, aangezien voor de meest interessante toepassingen voor nanolithografie (zoals (sub-) microelektronica) de benodigde structuren meer complex zijn.

- K.E. Gonsalves *et.al.*, 'Organic-inorganic nanocomposites: unique resists for nanolithography' (review), *Adv. Mater.* 13, 703 (2001)

- A.H. Gabor *et.al.*, 'Synthesis and lithographic characterization of block copolymer resists consisting of both poly(styrene) blocks and hydrosiloxane-modified poly(diene) blocks', *Chem. Mater.* 6, 927 (1994)

7. Het gebruik van elektronisch papier zal het plezier van het doorbladeren van een tijdschrift sterk doen verminderen.
8. De negatieve effecten van de afname van het aantal Nederlandse promovendi worden volledig gecompenseerd door de culturele verrijking ingebracht door het toenemende aantal buitenlandse AiO's.
9. SF – TW = R  
(Het verschil tussen science fiction en technologische werkelijkheid is research).
10. "A mind is like a parachute; it doesn't work when it's not open." (*Frank Zappa*)  
Veel wetenschappers prefereren echter de vrije val en stellen het moment van openen zo lang mogelijk uit.
11. Het uitoefenen van fysiek geweld op een computer helpt meestal niet, maar lucht wel op.
12. De film van het boek is altijd slechter dan het boek zelf.  
Het boek van de film is altijd slechter dan de film zelf.